# Eigendeformation-Based Reduced Order Homogenization for Failure Analysis of Heterogeneous Materials

Caglar Oskay* and Jacob Fish
*Scientific Computation Research Center*
*Rensselaer Polytechnic Institute*
*Troy, NY, 12180*

**Abstract**

The manuscript presents a novel model reduction approach for periodic heterogeneous media, which combines the multiple scale asymptotic (MSA) expansion method with the transformation field analysis (TFA) to reduce the computational cost of a direct homogenization approach without significantly compromising on solution accuracy. The evolution of failure in micro-phases and interfaces is modeled using eigendeformation. Adaptive model improvement strategy incorporating a hierarchical sequence of computational homogenization models is employed to control the accuracy of the model. We present the model formulation and the computational details along with verification (with respect to direct homogenization) and validation (with respect to physical experiments) studies.

## 1 Introduction

The importance of composite materials for high-performance applications that require high specific strength and/or stiffness, low electrical conductivity, transparency to radio emissions, and resistance to corrosion has been recognized more than half a century ago. Yet the supporting modeling and simulation tools used in practice are often ranging from the rule of mixtures dating back to the Renaissance era to various effective medium models of Eshelby [1], Hashin [2], Mori and Tanaka [3], self-consistent approaches of Hill [4] and Christensen [5] among many others. The emerging computational homogenization methods based on the mathematical homogenization theory pioneered by Babuska [6], Bensoussan [7], Suquet [8], Sanchez-Palencia [9], Guedes and Kikuchi [10] and Terada and Kikuchi [11] had so far very little or no impact on practitioners. This can be attributed to the following reasons:

1. Material characterization and calibration to experimental data are often available on the macroscale only;
2. Lack of accuracy in the vicinity of high gradient regions; and
3. Computational cost.

The first barrier is concerned with scale-specific measurements of in-situ properties, uncertainty quantification and indirect calibration by inverse methods [12]. The second barrier is concerned with the principal limitations of the homogenization approach: periodicity and uniformity of macroscale fields. Various hierarchical techniques [13, 14] and higher order homogenization techniques [15] have been developed to extend the range of validity of $O(1)$ computational homogenization approaches. The present manuscript does not address the first two barriers, but rather focuses on the last one.

*currently at Civil and Environmental Engineering Department, Vanderbilt University, Nashville, TN 37235.

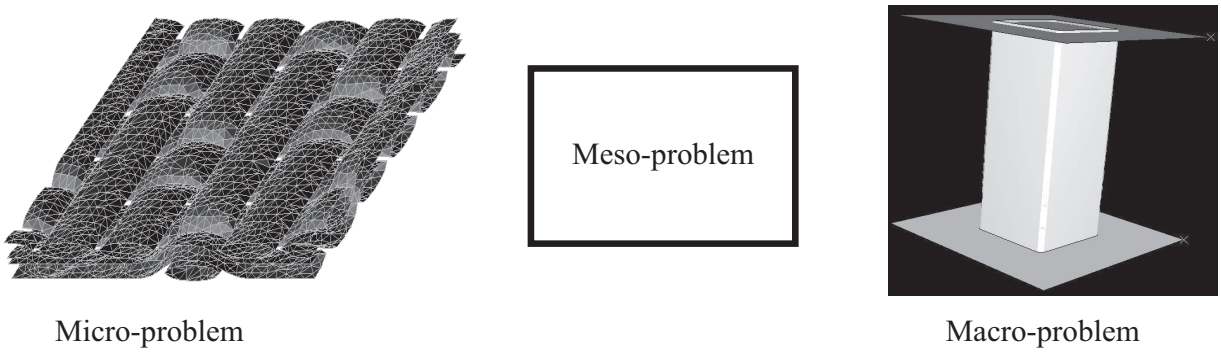


Figure 1: Linking micromechanical and macromechanical problems through a mesomechanical model.

The third barrier is purely computational. The computational complexity of solving a two-scale nonlinear problem is tremendous. To illustrate the computational complexity involved, consider a macro-problem with $N_{\text{cells}}$ Gauss points, $n$ load increments in the macroscale, and $I_{\text{coarse}}$ and $I_{\text{fine}}$ average iterations in the macro- and micro- scales, respectively. The total number of linear solves of a micro-problem is $N_{\text{cells}} \cdot n \cdot I_{\text{coarse}} \cdot I_{\text{fine}}$ - a formidable computational cost if the number of unit cells and degrees-of-freedom in a unit cell is substantial. This tyranny of scales can be effectively addressed by a combination of parallel methods and by introducing an intermediate mesomechanical model as shown in Figure 1. While parallelization in space is very natural since unit cell problems are fully parallelizable in space (see for instance Feyel and Chaboche [16]), parallelization in time remains an outstanding issue. Some promising results on parallelization in time have been obtained by utilizing waveform relaxation scheme [17] and space-time variational multigrid method [18].

Development of mesomechanical models for periodic heterogeneous continua has been an active research area in the past decade. Perhaps, one of the oldest mesomechanical approaches is based on purely kinematical Taylor's hypothesis (closely related to Cauchy-Born rule) which assumes a uniform deformation in the fine scale; it satisfies compatibility but fails to account for equilibrium across microconstituents boundaries. A major progress in mesomechanical modeling (obviously at the expense of computational cost) has been made by utilizing boundary element method [19], the Voronoi cell method [20], the spectral method [21], the transformation field analysis [22, 23], the Fast Fourier Transforms [24, 25], the network approximation method [26] and the mathematical homogenization with eigenstrains [27, 28, 29, 30, 31] based on the Transformation Field Analysis (TFA) [32]. Despite significant progress, the need for flexible low-cost mesomechanical approach, which can be easily adapted to meet accuracy needs, still remains.

The Transformation Field Analysis synonymous with the pioneering work of Dvorak and Benveniste [32], has its roots in early works of Laws [33], Willis [34] and Dvorak [35]. It is based on a brilliant idea that allows precomputing certain information (localization operators, concentration tensors, transformation influence functions) in the preprocessing phase prior to nonlinear analysis, which consequently can be carried out with a small subset of unknowns. By this approach the effect of eigenstrains, representing inelastic strains, thermal strains or phase transformation strains, is accounted for by solving a linear elasticity problem and is linearly superimposed with the deformation induced by uniform overall strain. The salient feature of TFA based approaches is that unit cell equilibrium equations, which have to be satisfied $N_{\text{cells}} \cdot n \cdot I_{\text{coarse}} \cdot I_{\text{fine}}$ times in the direct homogenization approach (see earlier discussion) are satisfied a priori, in the preprocessing stage.

In this manuscript we develop an adaptive mesomechanical approach which is based on the generalization of the mathematical homogenization theory with eigenstrains [25, 26, 27, 31] in the following two respects:

i. it accounts for interface failure in addition to failure of microconstituents; interface failure is

modeled using so-called eigendisplacements - a concept similar to eigenstrains used for modeling of inelastic deformation of phases; eigenstrains and eigendisplacements are collectively called eigendeformation.

ii. it is equipped with an adaptive model improvement capability; it incorporates a hierarchical sequence of computational homogenization models where the most inexpensive member of the sequence represents simultaneous failure of each microphase (inclusion, matrix and interface), whereas the most comprehensive model of the hierarchical sequence coincides with a direct homogenization approach (see for instance [11]);

The paper is organized as follows: The fundamental properties of the response fields and definitions of the spatial scales along with the governing equations are provided in Section 2. Section 3 outlines the formulation of the generalized mathematical homogenization with eigendeformation that decomposes the original boundary value problem into micro- and macro-scale problems. Derivation of reduced order model, nonlocal damage evolution law, and model improvement strategies are discussed in Section 4. Section 5 focuses on the implementation details of the reduced order model including stress update, consistent tangent operator and extension to large macroscopic deformation. Verification and validation studies are given in Section 6. A summary and a glimpse on future work conclude the manuscript.

# 2 Problem setting and governing equations

Consider a heterogeneous body formed by the repetition of a locally periodic microstructure occupying an open, bounded domain, $\Omega \subset \mathbb{R}^{n_{sd}}$, with $n_{sd}$ being the number of space dimensions, as shown in Fig. 2. The microstructure (unit cell) is composed of two or more different materials and is denoted by $\Theta \subset \mathbb{R}^{n_{sd}}$. The size of the unit cell is taken to be small compared to the dimensions of the macroscopic domain $\Omega$. The ratio between the size of the unit cell and the macroscopic domain is denoted by a small positive constant, $\zeta$. Under loads, the response of the heterogeneous body rapidly oscillates in space due to the fluctuations in the material properties within the unit cell. In other words, response fields are functions of the macroscale coordinate system, $\mathbf{x}$, as well as the microscale coordinate system, $\mathbf{y} \equiv \mathbf{x}/\zeta$, which may be regarded as a stretched position vector within the microstructure. Schematically, this is denoted by

$$f^{\zeta}(\mathbf{x}) = f(\mathbf{x}, \mathbf{y}(\mathbf{x})) \tag{2.1}$$

where, $f$ denotes response fields; and superscript $\zeta$ indicates the dependence of the response field on the microstructural heterogeneities. The macroscopic spatial derivative of $f^{\zeta}$ may be calculated by the chain rule

$$f^{\zeta}_{,x_i}(\mathbf{x}) = f_{,x_i}(\mathbf{x}, \mathbf{y}) + \frac{1}{\zeta} f_{,y_i}(\mathbf{x}, \mathbf{y}) \tag{2.2}$$

where, a comma followed by a subscript variable $x_i$ or $y_i$ denotes a partial derivative with respect to the components of the macroscopic and microscopic position vectors, respectively.

All response fields are assumed to be locally periodic throughout the deformation process

$$f(\mathbf{x}, \mathbf{y}) = f(\mathbf{x}, \mathbf{y} + \mathbf{k}\hat{\mathbf{y}}) \tag{2.3}$$

where, $\hat{\mathbf{y}}$ denotes the periods of the microstructure; and $\mathbf{k}$ is a $n_{sd} \times n_{sd}$ diagonal matrix with integer components.

In this manuscript, a damage process within the microconstituents and interfaces is modeled using continuous damage mechanics (CDM) although the methodology developed is applicable to other inelastic models. A history-dependent damage parameter, $\omega^{\zeta}_{\text{ph}}$, is introduced to represent the state of damage in the micro-phases (inclusion and matrix). Similarly, the adhesion between the microconstituents is modeled using CDM, in which the interface damage parameter, $\omega^{\zeta}_{\text{int}}$, represents the state of

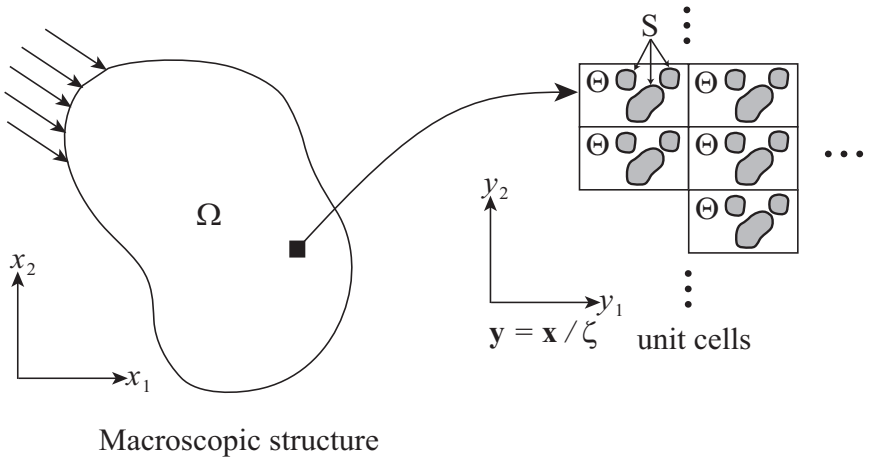


Figure 2: Macro- and microscopic structures.

adhesion. A simple Coulomb type friction model is considered to account for tractions introduced due to surface roughness along the debonded surfaces. Unilateral contact conditions are imposed along the interfaces to prevent interpenetration of microconstituents upon compressive loading. Similar interface model has been previously employed by Raous *et al.* [36] to characterize the behavior of fibrous ceramic composites.

In Sections 2 to 5 we derive the formulation for small deformation problems. Extension to large macro-deformation is given in Section 5.3. We consider the following governing equations on $\mathbf{x} \in \Omega$ and $t \in [0, t_{\mathrm{o}}]$

$$\sigma^{\zeta}_{ij,j}(\mathbf{x},t) + b^{\zeta}_{i}(\mathbf{x},t) = \rho^{\zeta}(\mathbf{x},t)\,\ddot{u}^{\zeta}_{i}(\mathbf{x},t) \tag{2.4}$$

$$\sigma^{\zeta}_{ij}(\mathbf{x},t) = \left[1-\omega^{\zeta}_{\mathrm{ph}}(\mathbf{x},t)\right] L^{\zeta}_{ijkl}(\mathbf{x})\,\epsilon^{\zeta}_{kl}(\mathbf{x},t) \tag{2.5}$$

$$\epsilon^{\zeta}_{ij}(\mathbf{x},t) = u^{\zeta}_{(i,j)}(\mathbf{x},t) \equiv \frac{1}{2}\left(\frac{\partial u^{\zeta}_{i}}{\partial x_j} + \frac{\partial u^{\zeta}_{j}}{\partial x_i}\right) \tag{2.6}$$

$$\omega^{\zeta}_{\mathrm{ph}}(\mathbf{x},t) = \omega^{\zeta}_{\mathrm{ph}}\left(\sigma^{\zeta}_{ij}, \epsilon^{\zeta}_{ij}, \mathbf{s}^{\zeta}_{\mathrm{ph}}\right) \tag{2.7}$$

where, $u^{\zeta}_{i}$ denotes displacements; $\sigma^{\zeta}_{ij}$ the Cauchy stress; $\epsilon^{\zeta}_{ij}$ the strain; $\omega^{\zeta}_{\mathrm{ph}} \in [0,1]$ with $\omega^{\zeta}_{\mathrm{ph}} = 0$ corresponding to the state of no damage, and $\omega^{\zeta}_{\mathrm{ph}} = 1$ denoting a complete loss of load carrying capacity; $b^{\zeta}_{i}$ the body force; $\rho^{\zeta}(\mathbf{x},t)$ the density; $t$ the temporal coordinate; $\Omega$ and $[0,t_{\mathrm{o}}]$ the spatial and temporal problem domains, respectively; superposed single and double dot correspond to material time derivative of orders one and two, respectively; and $L^{\zeta}_{ijkl}$ the tensor of elastic moduli obeying the conditions of symmetry

$$L^{\zeta}_{ijkl} = L^{\zeta}_{jikl} = L^{\zeta}_{ijlk} = L^{\zeta}_{klij} \tag{2.8}$$

and positivity

$$\exists C_0 > 0; \quad L^{\zeta}_{ijkl}\xi_{ij}\xi_{kl} \geq C_0\xi_{ij}\xi_{kl} \quad \forall \xi_{ij} = \xi_{ji} \tag{2.9}$$

The evolution equation of $\omega^{\zeta}_{\mathrm{ph}}$ is given in a functional form (Eq. 2.7) as a function of strain, stress and additional state variables $\mathbf{s}^{\zeta}_{\mathrm{ph}}$ (see [37]for various damage evolution equations).

The initial and boundary conditions are assumed to be a function of the macroscale coordinates

only

$$u_i^\zeta(\mathbf{x},t) = \hat{u}_i(\mathbf{x}); \quad \mathbf{x}\in\Omega; \quad t=0 \tag{2.10}$$

$$\dot{u}_i^\zeta(\mathbf{x},t) = \hat{v}_i(\mathbf{x}); \quad \mathbf{x}\in\Omega; \quad t=0 \tag{2.11}$$

$$u_i^\zeta(\mathbf{x},t) = \bar{u}_i(\mathbf{x},t); \quad \mathbf{x}\in\Gamma_u; \quad t\in[0,t_\mathrm{o}] \tag{2.12}$$

$$\sigma_{ij}^\zeta(\mathbf{x},t)\,n_j = \bar{t}_i(\mathbf{x},t); \quad \mathbf{x}\in\Gamma_t; \quad t\in[0,t_\mathrm{o}] \tag{2.13}$$

in which, $\hat{u}_i$ and $\hat{v}_i$ are the initial displacement and velocity fields, respectively; $\bar{u}_i$ and $\bar{t}_i$ are the prescribed displacements and tractions on the boundaries $\Gamma_u$ and $\Gamma_t$, respectively, where $\Gamma=\Gamma_u\cup\Gamma_t$ and $\Gamma_u\cap\Gamma_t=\emptyset$, and; $n_i$ is the unit normal to $\Gamma_t$.

Let $S^\zeta$ denote the interface between the microconstituents which is the union of the interfaces in the unit cells

$$S^\zeta = \bigcup_{\alpha=1}^{\text{all cells}} S_\alpha \tag{2.14}$$

The momentum balance along the interface is given by

$$\sigma_{ij}^\zeta n_j\Big|_{S_+^\zeta} + \sigma_{ij}^\zeta n_j\Big|_{S_-^\zeta} = t_i^\zeta(\mathbf{x},t)\Big|_{S_+^\zeta} + t_i^\zeta(\mathbf{x},t)\Big|_{S_-^\zeta} = 0 \tag{2.15}$$

where, $t_i^\zeta$ is the traction along the interface; and $S_+^\zeta$ and $S_-^\zeta$ denote the two sides of the interface. Damage progression may lead to a discontinuity of the displacements along the interface due to decohesion denoted as

$$\delta_i^\zeta(\mathbf{x},t) \equiv [\![u_i^\zeta(\mathbf{x},t)]\!] = u_i^\zeta\Big|_{S_-^\zeta} - u_i^\zeta\Big|_{S_+^\zeta} \tag{2.16}$$

where, $\delta_i^\zeta$ is the displacement jump along the microconstituent interfaces; and $[\![\cdot]\!]$ is the jump operator. The unilateral contact conditions with adhesion on $S^\zeta$ are then given as

$$t^{N\zeta}(\mathbf{x},t) - \left[1-\omega_{\text{int}}^\zeta(\mathbf{x},t)\right] k_N^\zeta(\mathbf{x})\,\delta^{N\zeta}(\mathbf{x},t) \le 0; \quad \delta^{N\zeta}(\mathbf{x},t)\ge 0 \tag{2.17}$$

$$\{t^{N\zeta}(\mathbf{x},t) - \left[1-\omega_{\text{int}}^\zeta(\mathbf{x},t)\right] k_N^\zeta(\mathbf{x})\,\delta^{N\zeta}(\mathbf{x},t)\}\delta^{N\zeta}(\mathbf{x},t) = 0 \tag{2.18}$$

in which, $t^{N\zeta}$ and $\delta^{N\zeta}$ are normal components of traction and displacement jump at the interface, respectively; $\omega_{\text{int}}^\zeta\in[0,1]$ is the interface damage variable indicating the state of debonding along the interface, with undamaged state being $\omega_{\text{int}}^\zeta=0$ and $k_N^\zeta$ being the interface stiffness along the normal direction. In the tangential directions, a Coulomb type friction model is considered in addition to adhesion

$$t_\rho^{T\zeta}(\mathbf{x},t) = t_\rho^{Ta\zeta}(\mathbf{x},t) + t_\rho^{Tf\zeta}(\mathbf{x},t) \tag{2.19}$$

$$t_\rho^{Ta\zeta}(\mathbf{x},t) - \left[1-\omega_{\text{int}}^\zeta(\mathbf{x},t)\right] k_T^\zeta(\mathbf{x})\,\delta_\rho^{T\zeta}(\mathbf{x},t) = 0 \tag{2.20}$$

$$\left\|\mathbf{t}^{Tf\zeta}(\mathbf{x},t)\right\| \le \mu_F\left|t^{N\zeta}(\mathbf{x},t) - \left[1-\omega_{\text{int}}^\zeta(\mathbf{x},t)\right] k_N^\zeta(\mathbf{x})\,\delta^{N\zeta}(\mathbf{x},t)\right| \tag{2.21}$$

$$\left\|\mathbf{t}^{Tf\zeta}\right\| < \mu_F\left|t^{N\zeta} - \left(1-\omega_{\text{int}}^\zeta\right) k_N^\zeta\delta^{N\zeta}\right| \Rightarrow \dot{\delta}_\rho^{T\zeta} = 0 \tag{2.22}$$

$$\left\|\mathbf{t}^{Tf\zeta}\right\| = \mu_F\left|t^{N\zeta} - \left(1-\omega_{\text{int}}^\zeta\right) k_N^\zeta\delta^{N\zeta}\right| \Rightarrow \dot{\delta}_\rho^{T\zeta} = \kappa t_\rho^{Tf\zeta} \tag{2.23}$$

where, $t_\rho^{T\zeta}$ and $\delta_\rho^{T\zeta}$ are the tangential components of traction and displacement jump at the interface, respectively; boldface symbols indicate the vector form; $t_\rho^{Ta\zeta}$ and $t_\rho^{Tf\zeta}$ are tangential traction due to adhesion and Coulomb friction, respectively; $k_T$ is the interface stiffness along the tangential direction; $\mu_F$ the friction coefficient; and $\kappa\ge 0$. The subscript $\rho$ is used for three dimensional problems only

where it ranges from 1 to 2. The evolution of the interface damage, $\omega_{\text{int}}^{\zeta}$, is given in the functional form as

$$\omega_{\text{int}}^{\zeta}(\mathbf{x},t)=\omega_{\text{int}}^{\zeta}\left(t_i^{\zeta},\delta_i^{\zeta},\mathbf{s}_{\text{int}}^{\zeta}\right) \tag{2.24}$$

in which, $\mathbf{s}_{\text{int}}^{\zeta}$ denote the interface state variables. Additional details are provided in Section 4.1.

The interface model with unilateral contact, adhesion and friction conditions can be summarized as follows: In case of pure tensile loading along the interface, the normal direction behavior is governed by the adhesion conditions. When compressive normal forces are present, displacement jump in the normal direction vanish (i.e., closure) and unilateral contact conditions are employed. In the presence of tangential and tensile forces along the interface, tangential behavior is governed by the adhesion condition given by Eq. 2.20. For compressive loads, friction conditions are in effect (Eqs. 2.21-2.23) in addition to adhesion.

# 3 Generalized Mathematical Homogenization With Eigendeformation

The governing equations (Eqs. 2.4-2.24) are solved approximately using two-scale mathematical homogenization with eigendeformation. The eigendeformation includes both the phase damage (modeled by eigenstrains) and interface damage (modeled by eigendisplacements). We extend the original formulation developed in [25, 26, 27], which accounted for damage at the micro-phases only. The 2-scale asymptotic expansions of the displacement field, $u_i^{\zeta}$, phase damage, $\omega_{\text{ph}}^{\zeta}$, and interface damage, $\omega_{\text{int}}^{\zeta}$, on $\mathbf{x}\in\Omega$; $\mathbf{y}\in\Theta$ and $t\in[0,t_{\text{o}}]$ are given as

$$\begin{aligned}
u_i(\mathbf{x},\mathbf{y},t) &\approx u_i^0(\mathbf{x},t)+\zeta u_i^1(\mathbf{x},\mathbf{y},t) && (3.1)\\
\omega_{\text{ph}}(\mathbf{x},\mathbf{y},t) &\approx \omega_{\text{ph}}^0(\mathbf{x},\mathbf{y},t)+\zeta\omega_{\text{ph}}^1(\mathbf{x},\mathbf{y},t) && (3.2)\\
\omega_{\text{int}}(\mathbf{x},\mathbf{y},t) &\approx \omega_{\text{int}}^0(\mathbf{x},\mathbf{y},t)+\zeta\omega_{\text{int}}^1(\mathbf{x},\mathbf{y},t) && (3.3)
\end{aligned}$$

The strain field is obtained by substituting Eq. 3.1 into Eq. 2.6 and exploiting the chain rule given by Eq. 2.2

$$\epsilon_{ij}(\mathbf{x},\mathbf{y},t)\approx\epsilon_{ij}^0(\mathbf{x},\mathbf{y},t)+\zeta\epsilon_{ij}^1(\mathbf{x},\mathbf{y},t) \tag{3.4}$$

in which, the first and second order strain components are in the form

$$\begin{aligned}
\epsilon_{ij}^0(\mathbf{x},\mathbf{y},t) &= u_{(i,x_j)}^0(\mathbf{x},t)+u_{(i,y_j)}^1(\mathbf{x},\mathbf{y},t) && (3.5)\\
\epsilon_{ij}^1(\mathbf{x},\mathbf{y},t) &= u_{(i,x_j)}^1(\mathbf{x},\mathbf{y},t) && (3.6)
\end{aligned}$$

The average strains are defined by integrating Eq. 3.4 over the unit cell domain

$$\bar{\epsilon}_{ij}(\mathbf{x},t)=\frac{1}{|\Theta|}\int_{\Theta}\epsilon_{ij}(\mathbf{x},\mathbf{y},t)\,d\Theta=u_{(i,x_j)}^0(\mathbf{x},t)+O(\zeta) \tag{3.7}$$

where, $|\Theta|$ denotes the volume of $\Theta$.

The first and second order stress components are evaluated by substituting the asymptotic strain field decomposition given by Eq. 3.4 into the constitutive equation (Eq. 2.5) and using the asymptotic expansion of the phase damage variable (Eq. 3.2)

$$\sigma_{ij}(\mathbf{x},\mathbf{y},t)\approx\sigma_{ij}^0(\mathbf{x},\mathbf{y},t)+\zeta\sigma_{ij}^1(\mathbf{x},\mathbf{y},t) \tag{3.8}$$

Further assuming $L_{ijkl}^{\zeta}=L_{ijkl}(\mathbf{y})$ gives

$$\begin{aligned}
\sigma_{ij}^0(\mathbf{x},\mathbf{y},t) &= \left[1-\omega_{\text{ph}}^0(\mathbf{x},\mathbf{y},t)\right]L_{ijkl}(\mathbf{y})\,\epsilon_{kl}^0 && (3.9)\\
\sigma_{ij}^1(\mathbf{x},\mathbf{y},t) &= \left[1-\omega_{\text{ph}}^0(\mathbf{x},\mathbf{y},t)\right]L_{ijkl}(\mathbf{y})\,\epsilon_{kl}^1-\omega_{\text{ph}}^1(\mathbf{x},\mathbf{y},t)\,L_{ijkl}(\mathbf{y})\,\epsilon_{kl}^0 && (3.10)
\end{aligned}$$

The average stress field is obtained by integrating Eq. 3.8 over the unit cell

$$\bar{\sigma}_{ij}(\mathbf{x},t) = \frac{1}{|\Theta|}\int_{\Theta}\sigma_{ij}(\mathbf{x},\mathbf{y},t)\,d\Theta = \frac{1}{|\Theta|}\int_{\Theta}\sigma^0_{ij}(\mathbf{x},\mathbf{y},t)\,d\Theta + O(\zeta) \tag{3.11}$$

The first and second order equilibrium equations are obtained by substituting Eq. 3.8 into Eq. 2.4, making use of the chain rule (Eq. 2.2) and applying Eq. 2.1 to the body force ($b^{\zeta}_i = b_i(\mathbf{x},\mathbf{y},t)$)

$$O(\zeta^{-1}) \quad : \quad \sigma^0_{ij,y_j}(\mathbf{x},\mathbf{y},t) = 0 \tag{3.12}$$

$$O(1) \quad : \quad \sigma^0_{ij,x_j}(\mathbf{x},\mathbf{y},t) + \sigma^1_{ij,y_j}(\mathbf{x},\mathbf{y},t) + b_i(\mathbf{x},\mathbf{y},t) = \rho\ddot{u}^0_i(\mathbf{x},t) \tag{3.13}$$

Considering the $O(\zeta^{-1})$ equilibrium equation and combining it with Eqs. 3.5, 3.7 and 3.9 yields

$$\left\{L_{ijkl}(\mathbf{y})\left[\bar{\epsilon}_{kl}(\mathbf{x},t) + u^1_{(k,y_l)}(\mathbf{x},\mathbf{y},t) - \mu_{kl}(\mathbf{x},\mathbf{y},t)\right]\right\}_{,y_j} = 0 \tag{3.14}$$

where, $\mu_{ij}$ is the inelastic strain defined as

$$\mu_{ij}(\mathbf{x},\mathbf{y},t) = \omega^0_{\mathrm{ph}}(\mathbf{x},\mathbf{y},t)\left[\bar{\epsilon}_{ij}(\mathbf{x},t) + u^1_{(i,yj)}(\mathbf{x},\mathbf{y},t)\right] \tag{3.15}$$

The evolution equation of the phase damage variable, $\omega^0_{\mathrm{ph}}$, is expressed in terms of the asymptotic terms of strain, stress and state variables as

$$\omega^0_{\mathrm{ph}}(\mathbf{x},\mathbf{y},t) = \omega^0_{\mathrm{ph}}\left(\sigma^0_{ij},\epsilon^0_{ij},\mathbf{s}^0_{\mathrm{ph}}\right) \tag{3.16}$$

Integrating the $O(1)$ equilibrium equation (Eq. 3.13) and exploiting periodicity of stresses yields momentum balance of the macroscopic problem

$$\bar{\sigma}_{ij,x_j}(\mathbf{x},t) + \bar{b}_i(\mathbf{x},t) = \bar{\rho}\ddot{u}^0_i(\mathbf{x},t) \tag{3.17}$$

where, $\bar{b}_i$ and $\bar{\rho}$ are the unit cell average body force and density, respectively.

Next, we consider asymptotic expansions of interface conditions. Substituting asymptotic expansion of stress (Eq. 3.8) into Eq. 2.15 leads to the expressions for the first and second order interface tractions on $\mathbf{x}\in\Omega$; $\mathbf{y}\in S$; $t\in[0,t_{\mathrm{o}}]$

$$t_i(\mathbf{x},\mathbf{y},t) \approx t^0_i(\mathbf{x},\mathbf{y},t) + \zeta t^1_i(\mathbf{x},\mathbf{y},t) \tag{3.18}$$

$$t^0_i(\mathbf{x},\mathbf{y},t) = \sigma^0_{ij}(\mathbf{x},\mathbf{y},t)\,n_j \tag{3.19}$$

$$t^1_i(\mathbf{x},\mathbf{y},t) = \sigma^1_{ij}(\mathbf{x},\mathbf{y},t)\,n_j \tag{3.20}$$

The resulting momentum balance equations at the interface are given as

$$O(1) \quad : \quad \sigma^0_{ij}n_j\big|_{S_+} + \sigma^0_{ij}n_j\big|_{S_-} = t^0_i(\mathbf{x},\mathbf{y},t)\big|_{S_+} + t^0_i(\mathbf{x},\mathbf{y},t)\big|_{S_-} = 0 \tag{3.21}$$

$$O(\zeta) \quad : \quad \sigma^1_{ij}n_j\big|_{S_+} + \sigma^1_{ij}n_j\big|_{S_-} = t^1_i(\mathbf{x},\mathbf{y},t)\big|_{S_+} + t^1_i(\mathbf{x},\mathbf{y},t)\big|_{S_-} = 0 \tag{3.22}$$

Since the leading order displacement field, $u^0_i$, is a function of the macroscopic spatial coordinate system, $\mathbf{x}$, only, it is continuous within a unit cell. Thus, the leading order displacement discontinuity is of the order $O(\zeta)$

$$\delta_i(\mathbf{x},\mathbf{y},t) \approx \zeta\delta^1_i(\mathbf{x},\mathbf{y},t) \tag{3.23}$$

In order to ensure traction continuity along the interface, normal and tangential interface stiffness coefficients should be of the order $O(\zeta^{-1})$, i.e.,

$$k^{\zeta}_N(\mathbf{x}) = \frac{1}{\zeta}k_N(\mathbf{y})\,; \qquad k^{\zeta}_T(\mathbf{x}) = \frac{1}{\zeta}k_T(\mathbf{y}) \tag{3.24}$$

where, $k_N(\mathbf{y})$ and $k_T(\mathbf{y})$ are of order $O(1)$. The interface conditions along the normal and tangential directions may be obtained by substituting the traction and displacement jump decompositions into Eqs. 2.17-2.24. In what follows, superscripts denoting the leading order terms of the interface tractions, interface displacement jumps and damage variables are omitted for conciseness of presentation.

The $O(\zeta^{-1})$ equilibrium equation given by Eq. 3.14, contact conditions at the interface, along with the periodicity assumption of local fields and evolution equations for damage variables define the so-called *unit cell* problem. The unit cell problem is summarized in Box 1. Equation 3.17 along with macroscopic domain boundary and initial conditions given by Eqs. 2.10-2.13, and constitutive relation given by Eq. 3.9 define the so-called *macroscale problem*. The macroscale problem is summarized in Box 2. Note that inertia effects appear in the macroscale problem only; the unit cell problem is quasi-static with time corresponding to history dependence.

*Given*: material properties, $L_{ijkl}$, $k_N$, $k_T$, $\mu_F$ and macroscopic strains, $\bar{\epsilon}_{ij}$
*Find*: microscopic deformations $u_i^1 \in \bar{\Omega} \times \bar{\Theta} \times [0, t_0] \to \mathbb{R}$ which satisfy on $\mathbf{x} \in \Omega$ and $t \in [0, t_0]$

- Equilibrium:
$$\left\{ L_{ijkl}(\mathbf{y}) \left[ \bar{\epsilon}_{kl}(\mathbf{x}, t) + u^1_{(k,y_l)}(\mathbf{x}, \mathbf{y}, t) - \mu_{kl}(\mathbf{x}, \mathbf{y}, t) \right] \right\}_{,y_j} = 0; \quad \mathbf{y} \in \Theta$$

- Kinematics:
$$\mu_{ij}(\mathbf{x}, \mathbf{y}, t) = \omega_{\text{ph}}(\mathbf{x}, \mathbf{y}, t) \left[ \bar{\epsilon}_{ij}(\mathbf{x}, t) + u^1_{(i,yj)}(\mathbf{x}, \mathbf{y}, t) \right]; \quad \mathbf{y} \in \Theta$$

- Unilateral contact and adhesion conditions in the normal direction ($\mathbf{y} \in S$):
$$\begin{aligned} t^N(\mathbf{x}, \mathbf{y}, t) &- [1 - \omega_{\text{int}}(\mathbf{x}, \mathbf{y}, t)] k_N(\mathbf{y}) \delta^N(\mathbf{x}, \mathbf{y}, t) \leq 0; \quad \delta^N(\mathbf{x}, \mathbf{y}, t) \geq 0 \\ \{t^N(\mathbf{x}, \mathbf{y}, t) &- [1 - \omega_{\text{int}}(\mathbf{x}, \mathbf{y}, t)] k_N(\mathbf{y}) \delta^N(\mathbf{x}, \mathbf{y}, t)\} \delta^N(\mathbf{x}, \mathbf{y}, t) = 0 \end{aligned}$$

- Friction and adhesion conditions in the tangential direction ($\mathbf{y} \in S$):
$$\begin{aligned} t^T_\rho(\mathbf{x}, \mathbf{y}, t) &= t^{Ta}_\rho(\mathbf{x}, \mathbf{y}, t) + t^{Tf}_\rho(\mathbf{x}, \mathbf{y}, t) \\ t^{Ta}_\rho(\mathbf{x}, \mathbf{y}, t) &- [1 - \omega_{\text{int}}(\mathbf{x}, \mathbf{y}, t)] k_T(\mathbf{y}) \delta^T_\rho(\mathbf{x}, \mathbf{y}, t) = 0 \\ \left\| \mathbf{t}^{Tf} \right\|(\mathbf{x}, \mathbf{y}, t) &\leq t_{\text{crit}}(\mathbf{x}, \mathbf{y}, t) \\ \left\| \mathbf{t}^{Tf} \right\|(\mathbf{x}, \mathbf{y}, t) &< t_{\text{crit}}(\mathbf{x}, \mathbf{y}, t) \Rightarrow \dot{\delta}^T_\rho(\mathbf{x}, \mathbf{y}, t) = 0 \\ \left\| \mathbf{t}^{Tf} \right\|(\mathbf{x}, \mathbf{y}, t) &= t_{\text{crit}}(\mathbf{x}, \mathbf{y}, t) \Rightarrow \dot{\delta}^T_\rho(\mathbf{x}, \mathbf{y}, t) = \kappa t^{Tf}_\rho(\mathbf{x}, \mathbf{y}, t); \quad \kappa \geq 0 \\ t_{\text{crit}}(\mathbf{x}, \mathbf{y}, t) &= \mu_F \left| t^N(\mathbf{x}, \mathbf{y}, t) - [1 - \omega_{\text{int}}(\mathbf{x}, \mathbf{y}, t)] k_N(\mathbf{y}) \delta^N(\mathbf{x}, \mathbf{y}, t) \right| \end{aligned}$$

- $\Theta$-periodic boundaries on $\mathbf{y} \in \Gamma_\Theta$
- Evolution equations for $\omega_{\text{ph}}(\mathbf{x}, \mathbf{y}, t)$ and $\omega_{\text{int}}(\mathbf{x}, \mathbf{y}, t)$

**Box 1:** Unit cell problem based on classical mathematical homogenization.

*Given*: average body force, $\bar{b}_i$, average density, $\bar{\rho}$, initial and boundary conditions, $\hat{u}_i$, $\hat{v}_i$, $\bar{u}_i$, $\bar{t}_i$, and the solution of the unit cell problem summarized in Box 1 at time $t \in [0, t_0]$
*Find*: macroscopic deformations $u_i^0 \in \bar{\Omega} \times [0, t_0] \to \mathbb{R}$

- Momentum balance ($\mathbf{x} \in \Omega$; $t \in [0, t_0]$):

$$\bar{\sigma}_{ij,x_j}(\mathbf{x}, t) + \bar{b}_i(\mathbf{x}, t) = \bar{\rho}\ddot{u}_i^0(\mathbf{x}, t)$$

- Kinematics ($\mathbf{x} \in \Omega$; $t \in [0, t_0]$):

$$\bar{\epsilon}_{ij}(\mathbf{x}, t) = u^0_{(i,x_j)}(\mathbf{x}, t)$$

- Constitutive relation ($\mathbf{x} \in \Omega$; $t \in [0, t_0]$):

$$\bar{\sigma}_{ij}(\mathbf{x}, t) = \frac{1}{|\Theta|}\int_\Theta L_{ijkl}(\mathbf{y})\left[\bar{\epsilon}_{kl}(\mathbf{x}, t) + u^1_{(k,y_l)}(\mathbf{x}, \mathbf{y}, t) - \mu_{kl}(\mathbf{x}, \mathbf{y}, t)\right] d\Theta$$

- Initial and boundary conditions:

$$\begin{aligned}
u_i^0(\mathbf{x}, t) &= \hat{u}_i(\mathbf{x}); \quad \mathbf{x} \in \Omega; \quad t = 0 \\
\dot{u}_i^0(\mathbf{x}, t) &= \hat{v}_i(\mathbf{x}); \quad \mathbf{x} \in \Omega; \quad t = 0 \\
u_i^0(\mathbf{x}, t) &= \bar{u}_i(\mathbf{x}, t); \quad \mathbf{x} \in \Gamma_u; \quad t \in [0, t_o] \\
\sigma_{ij}^0(\mathbf{x}, t)\, n_j &= \bar{t}_i(\mathbf{x}, t); \quad \mathbf{x} \in \Gamma_t; \quad t \in [0, t_o]
\end{aligned}$$

**Box 2:** Macroscale problem.

The two-scale nonlinear boundary value problems summarized in Box 1 and Box 2 can be solved using direct computational homogenization procedures (see for instance [11] and [16]). Instead, we proceed by formulating a mesomechanical approach based on the generalization of the mathematical homogenization theory with eigendeformation. We start by introducing the decomposition of the microscale displacement field [25, 26, 27]

$$u_i^1(\mathbf{x}, \mathbf{y}, t) = H_{ikl}(\mathbf{y})\,\bar{\epsilon}_{kl}(\mathbf{x}, t) + \tilde{u}_i(\mathbf{x}, \mathbf{y}, t) \tag{3.25}$$

where, $H_{ikl}$ is a $\Theta$-periodic function, and $\tilde{u}_i$ is the displacement field induced by damage process within the microconstituents and interfaces. The microscale displacement field decomposition given by Eq. 3.25 is valid for arbitrary damage state. We first consider the state in which microconstituents are free of damage with perfect bonding along the interfaces (i.e., $\omega_{\text{ph}} = 0$, $\delta_i = 0$). In this case, the damage induced displacement field vanishes and the equilibrium of the unit cell reduces to:

**Elastic Influence Function (EIF) Problem**:

Given $L_{ijmn}(\mathbf{y})$, find $H_{ikl}(\mathbf{y}) : \bar{\Theta} \to \mathbb{R}$ such that:

$$\begin{gathered}
\{L_{ijmn}(\mathbf{y})\, A_{mnkl}(\mathbf{y})\}_{,y_j} = 0; \quad \mathbf{y} \in \Theta \\
A_{ijkl}(\mathbf{y}) = I_{ijkl} + G_{ijkl}(\mathbf{y}); \quad G_{ijkl}(\mathbf{y}) = H_{(i,y_j)kl}(\mathbf{y}) \\
\Theta - \text{periodic boundary conditions on } \mathbf{y} \in \Gamma_\Theta
\end{gathered}$$

where, $I_{ijkl}$ is the fourth order identity tensor. The elastic influence function (EIF) problem is solved for $H_{ikl}$. For a comprehensive treatment of the linear unit cell problem see [10, 38].

Next, consider the case when $\bar{\epsilon}_{ij} = 0$ and arbitrary damage variables $\omega_{\text{ph}}$ and $\omega_{\text{int}}$. Equation 3.14 then reduces to

$$\left\{L_{ijkl}\left(\mathbf{y}\right)\left[\tilde{\epsilon}_{kl}\left(\mathbf{x},\mathbf{y},t\right)-\mu_{kl}\left(\mathbf{x},\mathbf{y},t\right)\right]\right\}_{,y_j}=0 \tag{3.26}$$

Equation 3.26 constitutes an elasticity problem with eigenstrains, $\mu_{ij}$, within the microconstituents and eigendisplacements, $\delta_i$, along the interface. The solution may be expressed by means of damage influence functions as

$$\tilde{u}_i\left(\mathbf{x},\mathbf{y},t\right)=\int\limits_{\theta} h^{\text{ph}}_{ikl}\left(\mathbf{y},\hat{\mathbf{y}}\right)\mu_{kl}\left(\mathbf{x},\hat{\mathbf{y}},t\right)d\hat{y}+\int\limits_{S} h^{\text{int}}_{im}\left(\mathbf{y},\hat{\mathbf{y}}\right)\delta_m\left(\mathbf{x},\hat{\mathbf{y}},t\right)d\hat{y} \tag{3.27}$$

in which, $h^{\text{ph}}_{ikl}$ and $h^{\text{int}}_{im}$ are the influence functions for damage within the microconstituents and along the interfaces, respectively. Expressions similar to the first term in Eq. 3.27 can be found in [31, 32, 39, 40]. The phase influence function, $h^{\text{ph}}_{ikl}$, is computed by solving the so-called Phase Damage Influence Function (PDIF) problem defined below.

**Phase Damage Influence Function (PDIF) Problem**:

Given $L_{ijmn}\left(\mathbf{y}\right)$, find $h^{\text{ph}}_{ikl}\left(\mathbf{y},\hat{\mathbf{y}}\right):\bar{\Theta}\times\bar{\Theta}\rightarrow\mathbb{R}$ such that:

$$\left\{L_{ijmn}\left(\mathbf{y}\right)\left(g^{\text{ph}}_{mnkl}\left(\mathbf{y},\hat{\mathbf{y}}\right)+I_{mnkl}d\left(\mathbf{y}-\hat{\mathbf{y}}\right)\right)\right\}_{,y_j}=0;\quad \mathbf{y},\hat{\mathbf{y}}\in\Theta$$

$$g^{\text{ph}}_{ijkl}\left(\mathbf{y},\hat{\mathbf{y}}\right)=h^{\text{ph}}_{(i,y_j)kl}\left(\mathbf{y},\hat{\mathbf{y}}\right)$$

$$\Theta-\text{periodic boundary conditions on }\mathbf{y}\in\Gamma_{\Theta}$$

$$\left[\!\left[h^{\text{ph}}_{ikl}\right]\!\right]\left(\mathbf{y},\hat{\mathbf{y}}\right)=0\quad\text{on}\quad\mathbf{y},\hat{\mathbf{y}}\in\Theta$$

where, $g^{\text{ph}}_{ijkl}$ is the polarization function for phase damage; and $d$ the Dirac delta function. The interface influence function, $h^{\text{int}}_{ip}$, satisfies the so-called Interface Damage Influence Function (IDIF) Problem defined below

**Interface Damage Influence Function (IDIF) Problem**:

Given $L_{ijmn}\left(\mathbf{y}\right)$, find $h^{\text{int}}_{ip}\left(\mathbf{y},\hat{\mathbf{y}}\right):\bar{\Theta}\times S\rightarrow\mathbb{R}$ such that:

$$\left\{L_{ijmn}\left(\mathbf{y}\right)g^{\text{int}}_{mnp}\left(\mathbf{y},\hat{\mathbf{y}}\right)\right\}_{,y_j}=0;\quad\mathbf{y}\in\Theta,\quad\hat{\mathbf{y}}\in S$$

$$g^{\text{int}}_{ijp}\left(\mathbf{y},\hat{\mathbf{y}}\right)=h^{\text{int}}_{(i,y_j)p}\left(\mathbf{y},\hat{\mathbf{y}}\right)$$

$$\Theta-\text{periodic boundary conditions on }\mathbf{y}\in\Gamma_{\Theta}$$

$$\left[\!\left[h^{\text{ph}}_{ip}\right]\!\right]\left(\mathbf{y},\hat{\mathbf{y}}\right)=Q_{ip}d\left(\mathbf{y}-\hat{\mathbf{y}}\right)\quad\text{when}\quad\mathbf{y}\in S\text{ or }\hat{\mathbf{y}}\in S$$

in which, $g^{\text{int}}_{ijp}$ is the polarization function for the interface damage; and $Q_{ip}$ denotes transformation from the local interface to the global Cartesian coordinate system.

We now proceed to constructing a unit cell problem that incorporates the influence functions. Based on Eq. 3.25, the $O(\zeta^{-1})$ equilibrium equation takes the form

$$\left\{L_{ijmn}(\mathbf{y})\left[A_{mnkl}(\mathbf{y})\bar{\epsilon}_{kl}(\mathbf{x},t)+\tilde{\epsilon}_{kl}(\mathbf{x},\mathbf{y},t)-\mu_{kl}\left(\mathbf{x},\mathbf{y},t\right)\right]\right\}_{,y_j}=0 \tag{3.28}$$

where, the damage induced strain, $\tilde{\epsilon}_{ij}$, is given as

$$\tilde{\epsilon}_{ij}(\mathbf{x},\mathbf{y},t)=\tilde{u}_{(i,y_j)}(\mathbf{x},\mathbf{y},t)=\int\limits_{\theta} g^{\text{ph}}_{ijkl}\left(\mathbf{y},\hat{\mathbf{y}}\right)\mu_{kl}\left(\mathbf{x},\hat{\mathbf{y}},t\right)d\hat{y}+\int_{S} g^{\text{int}}_{ijm}\left(\mathbf{y},\hat{\mathbf{y}}\right)\delta_m\left(\mathbf{x},\hat{\mathbf{y}},t\right)d\hat{y} \tag{3.29}$$

Premultiplying Eq. 3.28 by the interface damage influence function, $h_{ip}^{\text{int}}$, integrating by parts over the unit cell $\Theta$, using Green's theorem and considering the periodicity as well as the symmetry conditions on $L_{ijkl}$, the relation between the interface tractions and phase stresses are obtained

$$t_p\left(\mathbf{x},\hat{\mathbf{y}},t\right) = -\int_{\Theta} g_{ijp}^{\text{int}}\left(\mathbf{y},\hat{\mathbf{y}}\right) L_{ijmn}\left(\mathbf{y}\right)\left[A_{mnkl}\left(\mathbf{y}\right)\bar{\epsilon}_{kl}(\mathbf{x},t) + \tilde{\epsilon}_{mn}(\mathbf{x},\mathbf{y},t) - \mu_{mn}(\mathbf{x},\mathbf{y},t)\right] dy \tag{3.30}$$

Equations 3.15, 3.29, 3.30 along with the interface conditions summarized in Box 1 and damage evolution equations constitute a series of integral equations with inequality constraints. This system is summarized in Box 3.

*Given*: material properties, $L_{ijkl}$, $k_N$, $k_T$, $\mu_F$; influence functions, $H_{ikl}$, $h_{ikl}^{\text{ph}}$, $h_{ip}^{\text{int}}$, and macroscopic strains, $\bar{\epsilon}_{ij}$
*Find*: $\mu_{ij} \in \bar{\Omega}\times\bar{\Theta}\times[0,t_0]\rightarrow\mathbb{R}$ and $\delta_i \in \bar{\Omega}\times S\times[0,t_0]\rightarrow\mathbb{R}$ which satisfy on $\mathbf{x}\in\Omega$ and $t\in[0,t_0]$

- Kinetics ($\hat{\mathbf{y}}\in S$):

$$t_p\left(\mathbf{x},\hat{\mathbf{y}},t\right) = -\int_{\Theta} g_{ijp}^{\text{int}}\left(\mathbf{y},\hat{\mathbf{y}}\right) L_{ijmn}\left[A_{mnkl}\left(\mathbf{y}\right)\bar{\epsilon}_{kl}(\mathbf{x},t) + \tilde{\epsilon}_{mn}(\mathbf{x},\mathbf{y},t) - \mu_{mn}(\mathbf{x},\mathbf{y},t)\right] dy$$

- Kinematics ($\mathbf{y}\in\Theta$):

$$\begin{aligned}
\tilde{\epsilon}_{ij}(\mathbf{x},\mathbf{y},t) &= \int_{\theta} g_{ijkl}^{\text{ph}}\left(\mathbf{y},\hat{\mathbf{y}}\right)\mu_{kl}\left(\mathbf{x},\hat{\mathbf{y}},t\right)d\hat{y} + \int_{S} g_{ijm}^{\text{int}}\left(\mathbf{y},\hat{\mathbf{y}}\right)\delta_m\left(\mathbf{x},\hat{\mathbf{y}},t\right)d\hat{y}\\
\mu_{ij}\left(\mathbf{x},\mathbf{y},t\right) &= \omega_{\text{ph}}\left(\mathbf{x},\mathbf{y},t\right)\left[A_{ijkl}\left(\mathbf{y}\right)\bar{\epsilon}_{kl}\left(\mathbf{x},t\right) + \tilde{\epsilon}_{ij}\left(\mathbf{x},\mathbf{y},t\right)\right]
\end{aligned}$$

- Unilateral contact and adhesion conditions in the normal direction ($\mathbf{y}\in S$):

$$\begin{aligned}
t^N\left(\mathbf{x},\mathbf{y},t\right) &- \left[1-\omega_{\text{int}}\left(\mathbf{x},\mathbf{y},t\right)\right]k_N\left(\mathbf{y}\right)\delta^N\left(\mathbf{x},\mathbf{y},t\right)\leq 0;\quad \delta^N\left(\mathbf{x},\mathbf{y},t\right)\geq 0\\
\{t^N\left(\mathbf{x},\mathbf{y},t\right) &- \left[1-\omega_{\text{int}}\left(\mathbf{x},\mathbf{y},t\right)\right]k_N\left(\mathbf{y}\right)\delta^N\left(\mathbf{x},\mathbf{y},t\right)\}\delta^N\left(\mathbf{x},\mathbf{y},t\right) = 0
\end{aligned}$$

- Friction and adhesion conditions in the tangential direction ($\mathbf{y}\in S$):

$$\begin{aligned}
t_\rho^T\left(\mathbf{x},\mathbf{y},t\right) &= t_\rho^{Ta}\left(\mathbf{x},\mathbf{y},t\right) + t_\rho^{Tf}\left(\mathbf{x},\mathbf{y},t\right)\\
t_\rho^{Ta}\left(\mathbf{x},\mathbf{y},t\right) &- \left[1-\omega_{\text{int}}\left(\mathbf{x},\mathbf{y},t\right)\right]k_T\left(\mathbf{y}\right)\delta_\rho^T\left(\mathbf{x},\mathbf{y},t\right) = 0\\
\left\|\mathbf{t}^{Tf}\right\|\left(\mathbf{x},\mathbf{y},t\right) &\leq t_{\text{crit}}\left(\mathbf{x},\mathbf{y},t\right)\\
\left\|\mathbf{t}^{Tf}\right\|\left(\mathbf{x},\mathbf{y},t\right) &< t_{\text{crit}}\left(\mathbf{x},\mathbf{y},t\right)\Rightarrow\dot{\delta}_\rho^T\left(\mathbf{x},\mathbf{y},t\right) = 0\\
\left\|\mathbf{t}^{Tf}\right\|\left(\mathbf{x},\mathbf{y},t\right) &= t_{\text{crit}}\left(\mathbf{x},\mathbf{y},t\right)\Rightarrow\dot{\delta}_\rho^T\left(\mathbf{x},\mathbf{y},t\right) = \kappa t_\rho^{Tf}\left(\mathbf{x},\mathbf{y},t\right);\ \ \kappa\geq 0\\
t_{\text{crit}}\left(\mathbf{x},\mathbf{y},t\right) &= \mu_F\left|t^N\left(\mathbf{x},\mathbf{y},t\right) - \left[1-\omega_{\text{int}}\left(\mathbf{x},\mathbf{y},t\right)\right]k_N\left(\mathbf{y}\right)\delta^N\left(\mathbf{x},\mathbf{y},t\right)\right|
\end{aligned}$$

- Evolution equations for $\omega_{\text{ph}}\left(\mathbf{x},\mathbf{y},t\right)$ and $\omega_{\text{int}}\left(\mathbf{x},\mathbf{y},t\right)$

**Box 3:** Unit cell problem based on the generalized mathematical homogenization with eigenstrains.

# 4 A Reduced Order Model

To reduce the computational cost of direct homogenization method, the integral equations in Box 3 are decomposed using separation of variables for the interface damage, damage induced strain, phase

damage and inelastic strain fields

$$\omega_{\text{ph}}(\mathbf{x},\mathbf{y},t)=\sum_{\gamma}N_{\text{ph}}^{(\gamma)}(\mathbf{y})\,\omega_{\text{ph}}^{(\gamma)}(\mathbf{x},t);\quad \mu_{ij}(\mathbf{x},\mathbf{y},t)=\sum_{\gamma}N_{\text{ph}}^{(\gamma)}(\mathbf{y})\,\mu_{ij}^{(\gamma)}(\mathbf{x},t) \tag{4.1}$$

$$\omega_{\text{int}}(\mathbf{x},\mathbf{y},t)=\sum_{\beta}N_{\text{int}}^{(\beta)}(\mathbf{y})\,\omega_{\text{int}}^{(\beta)}(\mathbf{x},t);\quad \hat{\delta}_i(\mathbf{x},\mathbf{y},t)=\sum_{\beta}N_{\text{int}}^{(\beta)}(\mathbf{y})\,\hat{\delta}_i^{(\beta)}(\mathbf{x},t) \tag{4.2}$$

$$\gamma=1,2,\ldots;\quad \beta=1,2,\ldots$$

The phase shape functions, $N_{\text{ph}}^{(\gamma)}$, are assumed to be $C^{-1}(\Theta)$ continuous matching the continuity of the displacement derivatives. On the other hand, the interface shape functions, $N_{\text{int}}^{(\beta)}$, are taken to be $C^0(S)$ due to $C^0(S)$ continuity of the displacement jumps at the interface, i.e. $\hat{\delta}_i\in C^0(S)$. In Eq. 4.2, displacement jumps are decomposed into opening/sliding components in the local coordinate system, $\hat{\boldsymbol{\delta}}^{(\beta)}=\left[\delta^{N(\beta)}\quad\left(\boldsymbol{\delta}^{T(\beta)}\right)^{\text{T}}\right]^{\text{T}}$.

Both $N_{\text{ph}}^{(\gamma)}$ and $N_{\text{int}}^{(\beta)}$ are assumed to satisfy the partition of unity property

$$\sum_{\gamma}N_{\text{ph}}^{(\gamma)}(\mathbf{y})=1;\quad \sum_{\beta}N_{\text{int}}^{(\beta)}(\mathbf{y})=1 \tag{4.3}$$

In the following, superscripts, $\eta$ and $\gamma$ are reserved for functions denoting phase fields, whereas, $\alpha$ and $\beta$ are reserved for the interfaces fields.

We further define weighted average fields as

$$\omega_{\text{ph}}^{(\gamma)}(\mathbf{x},t)=\int_{\Theta}\varphi_{\text{ph}}^{(\gamma)}(\mathbf{y})\,\omega_{\text{ph}}(\mathbf{x},\mathbf{y},t)\,dy;\quad \mu_{ij}^{(\gamma)}(\mathbf{x},t)=\int_{\Theta}\varphi_{\text{ph}}^{(\gamma)}(\mathbf{y})\,\mu_{ij}(\mathbf{x},\mathbf{y},t)\,dy \tag{4.4}$$

$$\omega_{\text{int}}^{(\beta)}(\mathbf{x},t)=\int_{S}\varphi_{\text{int}}^{(\beta)}(\mathbf{y})\,\omega_{\text{int}}(\mathbf{x},\mathbf{y},t)\,dy;\quad \hat{\delta}_i^{(\beta)}(\mathbf{x},t)=\int_{S}\varphi_{\text{int}}^{(\beta)}(\mathbf{y})\,\hat{\delta}_i(\mathbf{x},\mathbf{y},t)\,dy \tag{4.5}$$

in which, the phase and interface weight functions, $\varphi_{\text{ph}}^{(\gamma)}$ and $\varphi_{\text{int}}^{(\beta)}$ satisfy positivity

$$\varphi_{\text{ph}}^{(\gamma)}(\mathbf{y})\geq 0;\quad \varphi_{\text{int}}^{(\beta)}(\mathbf{y})\geq 0 \tag{4.6}$$

and normalization

$$\int_{\Theta}\varphi_{\text{ph}}^{(\gamma)}(\mathbf{y})\,dy=1;\quad \int_{S}\varphi_{\text{int}}^{(\beta)}(\mathbf{y})\,dy=1 \tag{4.7}$$

conditions. It can be easily shown that Eqs 4.1, 4.2, 4.4, and 4.5 imply orthonormality of the shape and weight functions for arbitrary damage state within the phases and interfaces

$$\int_{\Theta}\varphi_{\text{ph}}^{(\gamma)}(\mathbf{y})\,N_{\text{ph}}^{(\eta)}(\mathbf{y})\,dy=\delta_{\gamma\eta}^{\text{K}} \tag{4.8}$$

$$\int_{S}\varphi_{\text{int}}^{(\beta)}(\mathbf{y})\,N_{\text{int}}^{(\alpha)}(\mathbf{y})\,dy=\delta_{\beta\alpha}^{\text{K}} \tag{4.9}$$

in which, $\delta_{\gamma\eta}^{\text{K}}$ is the Kronecker delta.

We now focus on various choices of the weight and shape functions satisfying orthonormality (Eqs. 4.8 and 4.9), partition of unity (Eq. 4.3), positivity (Eq. 4.6) and normalization (Eq. 4.7) conditions.

Consider a two-scale heterogeneous material composed of $n_{\text{ph}}$ phases and $n_{\text{int}}$ interfaces (e.g., for fibrous or woven composites, $n_{\text{ph}}$ is typically 2 with matrix and fiber phases occupying domains, $\Theta^{(M)}$ and $\Theta^{(F)}$, respectively, and $n_{\text{int}}=1$). The microstructure is further partitioned into $n$ subdomains denoted by $\Theta^{(\eta)}$, $\eta=1,2,\ldots,n$. The partitioning is constructed so that each subdomain belongs to

a single phase ($\Theta^{(\eta)} \bigcap \Theta^{(M)} \equiv \Theta^{(\eta)}$ or $\Theta^{(\eta)} \bigcap \Theta^{(F)} \equiv \Theta^{(\eta)}$), $\Theta \equiv \bigcup_{\eta=1}^{n} \Theta^{(\eta)}$ and $\Theta^{(\eta)} \bigcap \Theta^{(\gamma)} \equiv \emptyset$ for $\eta \neq \gamma$. The phase shape and weight functions ($N_{\text{ph}}^{(\eta)}$ and $\varphi_{\text{ph}}^{(\eta)}$, respectively) are selected to be piecewise constant in $\Theta$ with nonzero values within their corresponding partitions, $\Theta^{(\eta)}$, only

$$N_{\text{ph}}^{(\gamma)}(\mathbf{y}) = \begin{cases} 1 \text{ if } \mathbf{y} \in \Theta^{(\eta)} \\ 0 \text{ elsewhere} \end{cases} \tag{4.10}$$

$$\varphi_{\text{ph}}^{(\gamma)}(\mathbf{y}) = \frac{1}{\left|\Theta^{(\eta)}\right|} N_{\text{ph}}^{(\gamma)}(\mathbf{y}) \tag{4.11}$$

where, $\left|\Theta^{(\eta)}\right|$ is the volume of partition $\Theta^{(\eta)}$. It is a trivial exercise to verify that the above phase shape functions satisfy the orthonormality (Eq. 4.8) and partition of unity (Eq. 4.3) conditions, whereas the weight functions satisfy the normalization and positivity conditions. It is important to note that the local supports, $\Theta^{(\eta)}$, are arbitrary noncontiguous domains. This choice proves to be valuable in devising an adaptive partitioning strategy discussed in Section 4.3.

The interface is divided into $m$ partitions such that $S \equiv \bigcup_{\alpha=1}^{m} \bar{S}^{(\alpha)}$. In contrast to the phase partitioning, interface partitions overlap as schematically shown in Fig. 3.

$$\bar{S}^{(\alpha)} = S^{(\alpha)} \bigcup \sum_{\substack{\beta=1 \\ \beta \neq \alpha}}^{m} O^{(\alpha\beta)} \tag{4.12}$$

where $S^{(\alpha)}$ is the nonoverlapping region in $\bar{S}^{(\alpha)}$; and $O^{(\alpha\beta)}$ is the overlap between neighboring partitions $\bar{S}^{(\alpha)}$ and $\bar{S}^{(\beta)}$. The interface shape functions, $N_{\text{int}}^{(\alpha)}$, are constructed by a linear combination of finite element shape functions corresponding to the nodes in the interface partition, $S^{(\alpha)}$

$$N_{\text{int}}^{(\alpha)}(\mathbf{y}) = \sum_{a \in S^{(\alpha)}} N_a(\mathbf{y}); \quad \mathbf{y} \in S \tag{4.13}$$

in which, $N_a$ are standard finite element shape functions associated with the microscopic finite element mesh node $a$. The interface weight functions are chosen to be piecewise constant

$$\varphi_{\text{int}}^{(\alpha)}(\mathbf{y}) = \begin{cases} 1/\left|S^{(\alpha)}\right| & \text{if } \mathbf{y} \in S^{(\alpha)} \\ 0 & \text{elsewhere} \end{cases} \tag{4.14}$$

where $\left|S^{(\alpha)}\right|$ is the area of interface partition, $S^{(\alpha)}$. Again, it is a trivial exercise to verify that the interface shape and weight functions satisfy the aforementioned four conditions (Eqs. 4.3, 4.6, 4.7, and 4.9).

Employing the above definitions of the phase and interface weight functions, Eqs. 4.4 and 4.5 reduce to

$$\begin{aligned} \omega_{\text{ph}}^{(\eta)}(\mathbf{x},t) &= \frac{1}{\left|\Theta^{(\eta)}\right|} \int_{\Theta^{(\eta)}} \omega_{\text{ph}}(\mathbf{x},\mathbf{y},t)\, dy \quad \mu_{ij}^{(\eta)}(\mathbf{x},t) = \frac{1}{\left|\Theta^{(\eta)}\right|} \int_{\Theta^{(\eta)}} \mu_{ij}(\mathbf{x},\mathbf{y},t)\, dy \\ \omega_{\text{int}}^{(\alpha)}(\mathbf{x},t) &= \frac{1}{\left|S^{(\alpha)}\right|} \int_{S^{(\alpha)}} \omega_{\text{int}}(\mathbf{x},\mathbf{y},t)\, dy \quad \hat{\delta}_i^{(\alpha)}(\mathbf{x},t) = \frac{1}{\left|S^{(\alpha)}\right|} \int_{S^{(\alpha)}} \hat{\delta}_i(\mathbf{x},\mathbf{y},t)\, dy \end{aligned} \tag{4.15}$$

Substituting Eqs. 4.1-4.2 into Eqs. 3.15 and 3.29, premultiplying the resulting equation by $\varphi_{\text{ph}}^{(\eta)}$, and integrating over the unit cell yields

$$\begin{aligned} \sum_{\gamma=1}^{n} \left[\delta_{\eta\gamma}^{\text{K}} I_{ijkl} - P_{ijkl}^{(\eta\gamma)} \omega_{\text{ph}}^{(\eta)}(\mathbf{x},t)\right] \mu_{kl}^{(\gamma)}(\mathbf{x},t) - \omega_{\text{ph}}^{(\eta)}(\mathbf{x},t) \sum_{\beta=1}^{m} \left[\hat{\mathbf{R}}_{ij}^{(\eta\beta)} \cdot \hat{\boldsymbol{\delta}}^{(\beta)}(\mathbf{x},t)\right] \\ = \omega_{\text{ph}}^{(\eta)}(\mathbf{x},t)\, A_{ijkl}^{(\eta)} \bar{\epsilon}_{kl}(\mathbf{x},t) \end{aligned} \tag{4.16}$$

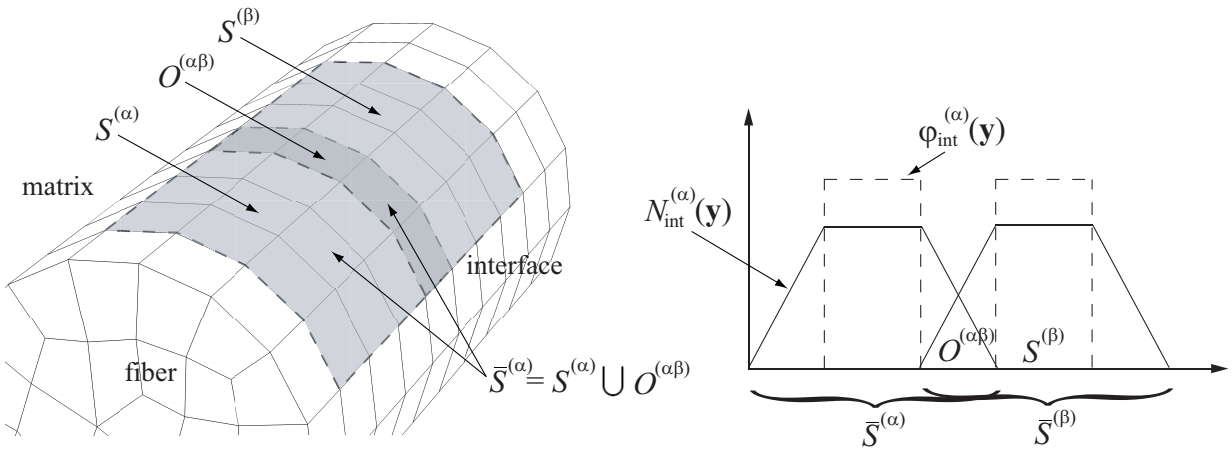


Figure 3: The interface shape and weight functions: (a) Interface partitions in multidimensions, (b) Interface shape and weight function in one dimension.

where

$$P_{ijkl}^{(\eta\gamma)} = \frac{1}{\left|\Theta^{(\eta)}\right|} \int_{\Theta^{(\eta)}} \tilde{P}_{ijkl}^{(\gamma)}(\mathbf{y})\, dy \tag{4.17}$$

$$A_{ijkl}^{(\eta)} = \frac{1}{\left|\Theta^{(\eta)}\right|} \int_{\Theta^{(\eta)}} A_{ijkl}(\mathbf{y})\, dy \tag{4.18}$$

$$\hat{\mathbf{R}}_{ij}^{(\eta\beta)} = \frac{1}{\left|\Theta^{(\eta)}\right|} \int_{\Theta^{(\eta)}} \tilde{\mathbf{R}}_{ij}^{(\beta)}(\mathbf{y})\, dy \tag{4.19}$$

$$\tilde{P}_{ijkl}^{(\eta)}(\mathbf{y}) = \int_{\Theta^{(\eta)}} g_{ijkl}^{\text{ph}}(\mathbf{y}, \hat{\mathbf{y}})\, d\hat{y} \tag{4.20}$$

$$\tilde{\mathbf{R}}_{ij}^{(\alpha)}(\mathbf{y}) = \int_{\bar{S}^{(\alpha)}} g_{ijp}^{\text{int}}(\mathbf{y}, \hat{\mathbf{y}})\, N_{\text{int}}^{(\alpha)}(\hat{\mathbf{y}})\, \hat{\mathbf{e}}_p(\hat{\mathbf{y}})\, d\hat{y} \tag{4.21}$$

where, $\hat{\mathbf{e}}_p$ are the basis vectors in the local normal and tangential directions along the interface. Summation convention is not applied for the repeated superscripts.

Substituting Eqs. 4.1-4.2 into Eq. 3.30, premultiplying the result by $\varphi_{\text{int}}^{(\alpha)}$, and integrating over the interface gives

$$\hat{\mathbf{t}}^{(\alpha)}(\mathbf{x}, t) + \sum_{\beta=1}^{M} \hat{\mathbf{D}}^{(\alpha\beta)} \cdot \hat{\boldsymbol{\delta}}^{(\beta)}(\mathbf{x}, t) + \sum_{\gamma=1}^{n} \hat{\mathbf{F}}_{ij}^{(\alpha\gamma)} \mu_{ij}^{(\gamma)}(\mathbf{x}, t) = -\hat{\mathbf{C}}_{ij}^{(\alpha)} \bar{\epsilon}_{ij}(\mathbf{x}, t) \tag{4.22}$$

where,

$$\hat{\mathbf{t}}^{(\alpha)}(\mathbf{x}, t) \equiv \frac{1}{\left|S^{(\alpha)}\right|} \int_{S^{(\alpha)}} \hat{\mathbf{t}}(\mathbf{x}, \mathbf{y}, t)\, dy \tag{4.23}$$

in which, $\hat{\mathbf{t}} = \left[t^N \quad \left(\mathbf{t}^T\right)^{\mathrm{T}}\right]^{\mathrm{T}}$ is the traction vector in local coordinates; and

$$\hat{\mathbf{C}}_{ij}^{(\alpha)} = \frac{1}{\left|S^{(\alpha)}\right|} \int\limits_{S^{(\alpha)}} \int\limits_{\Theta} g_{mnp}^{\mathrm{int}}\left(\mathbf{y}, \hat{\mathbf{y}}\right) L_{mnkl}\left(\mathbf{y}\right) A_{klij}\left(\mathbf{y}\right) \hat{\mathbf{e}}_p\left(\hat{\mathbf{y}}\right) dyd\hat{y} \tag{4.24}$$

$$\hat{\mathbf{D}}^{(\alpha\beta)} = \frac{1}{\left|S^{(\alpha)}\right|} \int\limits_{S^{(\alpha)}} \int\limits_{\Theta} g_{mnp}^{\mathrm{int}}\left(\mathbf{y}, \hat{\mathbf{y}}\right) L_{mnkl}\left(\mathbf{y}\right) \tilde{\mathbf{R}}_{kl}^{(\beta)}\left(\mathbf{y}\right) \otimes \hat{\mathbf{e}}_p\left(\hat{\mathbf{y}}\right) dyd\hat{y} \tag{4.25}$$

$$\hat{\mathbf{F}}_{ij}^{(\alpha\gamma)} = \frac{1}{\left|S^{(\alpha)}\right|} \int\limits_{S^{(\alpha)}} \int\limits_{\Theta} g_{mnp}^{\mathrm{int}}\left(\mathbf{y}, \hat{\mathbf{y}}\right) L_{mnkl}\left(\mathbf{y}\right) \left(\tilde{P}_{klij}^{(\gamma)}\left(\mathbf{y}\right) - I_{klij} N_{\mathrm{ph}}^{(\gamma)}\left(\mathbf{y}\right)\right) \hat{\mathbf{e}}_p\left(\hat{\mathbf{y}}\right) dyd\hat{y} \tag{4.26}$$

We now turn our attention to the contact, adhesion and friction conditions along the interfaces. The adhesion conditions in the normal direction are expressed in terms of $t^{N(\alpha)}$ and $\delta^{N(\alpha)}$ by employing Eqs. 4.2, integrating with respect to $\varphi_{\mathrm{int}}^{(\alpha)}$, using the orthonormality, and positivity of the weight functions give

$$t^{N(\alpha)}\left(\mathbf{x}, t\right) - \left[1 - \omega_{\mathrm{int}}^{(\alpha)}\left(\mathbf{x}, t\right)\right] k_N^{(\alpha)} \delta^{N(\alpha)}\left(\mathbf{x}, t\right) \leqslant 0; \quad \delta^{N(\alpha)}\left(\mathbf{x}, t\right) \geqslant 0 \tag{4.27}$$

where

$$k_N^{(\alpha)} = \frac{1}{\left|S^{(\alpha)}\right|} \int_S k_N\left(\mathbf{y}\right) dy \tag{4.28}$$

and the consistency condition is given as

$$\left\{t^{N(\alpha)}\left(\mathbf{x}, t\right) - \left[1 - \omega_{\mathrm{int}}^{(\alpha)}\left(\mathbf{x}, t\right)\right] k_N^{(\alpha)} \delta^{N(\alpha)}\left(\mathbf{x}, t\right)\right\} \delta^{N(\alpha)}\left(\mathbf{x}, t\right) = 0 \tag{4.29}$$

In the tangential direction, the adhesion condition may be obtained similarly to the expressions in the normal direction.

$$\mathbf{t}^{Ta(\alpha)} = \left[1 - \omega_{\mathrm{int}}^{(\alpha)}\left(\mathbf{x}, t\right)\right] k_T^{(\alpha)} \boldsymbol{\delta}^{T(\alpha)}\left(\mathbf{x}, t\right) \tag{4.30}$$

where, $k_T^{(\alpha)}$ is defined analogous to $k_N^{(\alpha)}$. The friction condition along the interfaces is given by

$$\left\|\mathbf{t}^{Tf(\alpha)}\right\| \leqslant \mu_F \left|t^{N(\alpha)}\left(\mathbf{x}, t\right) - \left[1 - \omega_{\mathrm{int}}^{(\alpha)}\left(\mathbf{x}, t\right)\right] k_N^{(\alpha)} \delta^{N(\alpha)}\left(\mathbf{x}, t\right)\right| \tag{4.31}$$

$$\left\|\mathbf{t}^{Tf(\alpha)}\right\| < \mu_F \left|t^{N(\alpha)}\left(\mathbf{x}, t\right) - \left[1 - \omega_{\mathrm{int}}^{(\alpha)}\left(\mathbf{x}, t\right)\right] k_N^{(\alpha)} \delta^{N(\alpha)}\left(\mathbf{x}, t\right)\right| \Rightarrow \dot{\boldsymbol{\delta}}^{T(\alpha)}\left(\mathbf{x}, t\right) = 0 \tag{4.32}$$

$$\left\|\mathbf{t}^{Tf(\alpha)}\right\| = \mu_F \left|t^{N(\alpha)}\left(\mathbf{x}, t\right) - \left[1 - \omega_{\mathrm{int}}^{(\alpha)}\left(\mathbf{x}, t\right)\right] k_N^{(\alpha)} \delta^{N(\alpha)}\left(\mathbf{x}, t\right)\right| \Rightarrow \dot{\boldsymbol{\delta}}^{T(\alpha)} = \kappa \mathbf{t}^{Tf(\alpha)}, \ \kappa \geqslant 0 \tag{4.33}$$

Equations 4.16, 4.22, 4.27, 4.29, and Eqs. 4.30-4.33 constitute a discrete system of equations in terms of $\mu_{ij}^{(\gamma)}$ and $\hat{\delta}_i^{(\beta)}$, with contact constraints. The resulting reduced order model is termed thereafter as $(m+n)$ point model, in which $m$ and $n$ denote the number of interface and phase partitions, respectively. The $(m+n)$ point model is summarized in Box 4.

*Given*: coefficient tensors and material parameters: $P^{(\eta\gamma)}_{ijkl}$, $A^{(\eta)}_{ijkl}$, $\hat{\mathbf{R}}^{(\eta\beta)}_{ij}$, $\hat{\mathbf{C}}^{(\alpha)}_{ij}$, $\hat{\mathbf{D}}^{(\alpha\beta)}$, $\hat{\mathbf{F}}^{(\alpha\gamma)}_{ij}$, $k^{(\alpha)}_N$, $k^{(\alpha)}_T$, $\mu_F$ and the macroscopic strain, $\bar{\epsilon}_{ij}$
*Find*: $\mu^{(\gamma)}_{ij}$; $\gamma = 1, 2, \ldots, n$ and $\delta^{(\alpha)}_i$; $\alpha = 1, 2, \ldots, m$ which satisfy on $\mathbf{x} \in \Omega$ and $t \in [0, t_0]$

- Kinetics:

$$\hat{\mathbf{t}}^{(\alpha)}(\mathbf{x}, t) + \sum_{\beta=1}^{m} \hat{\mathbf{D}}^{(\alpha\beta)} \cdot \hat{\boldsymbol{\delta}}^{(\beta)}(\mathbf{x}, t) + \sum_{\gamma=1}^{n} \hat{\mathbf{F}}^{(\alpha\gamma)}_{ij} \mu^{(\gamma)}_{ij}(\mathbf{x}, t) = -\hat{\mathbf{C}}^{(\alpha)}_{ij} \bar{\epsilon}_{ij}(\mathbf{x}, t)$$

- Kinematics:

$$\sum_{\gamma=1}^{n} \left[ \delta^{\mathrm{K}}_{\eta\gamma} I_{ijkl} - P^{(\eta\gamma)}_{ijkl} \omega^{(\eta)}_{\mathrm{ph}}(\mathbf{x}, t) \right] \mu^{(\gamma)}_{kl}(\mathbf{x}, t) - \omega^{(\eta)}_{\mathrm{ph}}(\mathbf{x}, t) \sum_{\beta=1}^{m} \left[ \hat{\mathbf{R}}^{(\eta\beta)}_{ij} \cdot \hat{\boldsymbol{\delta}}^{(\beta)}(\mathbf{x}, t) \right] = \omega^{(\eta)}_{\mathrm{ph}}(\mathbf{x}, t) A^{(\eta)}_{ijkl} \bar{\epsilon}_{kl}(\mathbf{x}, t)$$

- Unilateral contact and adhesion conditions in the normal direction:

$$t^{N(\alpha)}(\mathbf{x}, t) - \left(1 - \omega^{(\alpha)}_{\mathrm{int}}(\mathbf{x}, t)\right) k^{(\alpha)}_N \delta^{N(\alpha)}(\mathbf{x}, t) \leqslant 0; \quad \delta^{N(\alpha)}(\mathbf{x}, t) \geqslant 0$$
$$\left\{ t^{N(\alpha)}(\mathbf{x}, t) - \left(1 - \omega^{(\alpha)}_{\mathrm{int}}(\mathbf{x}, t)\right) k^{(\alpha)}_N \delta^{N(\alpha)}(\mathbf{x}, t) \right\} \delta^{N(\alpha)}(\mathbf{x}, t) = 0$$

- Friction and adhesion conditions in the tangential direction:

$$\begin{aligned}
\mathbf{t}^{T(\alpha)}(\mathbf{x}, t) &= \mathbf{t}^{Ta(\alpha)}(\mathbf{x}, t) + \mathbf{t}^{Tf(\alpha)}(\mathbf{x}, t) \\
\mathbf{t}^{Ta(\alpha)}(\mathbf{x}, t) &= \left(1 - \omega^{(\alpha)}_{\mathrm{int}}(\mathbf{x}, t)\right) k^{(\alpha)}_T \boldsymbol{\delta}^{T(\alpha)}(\mathbf{x}, t) \\
\left\| \mathbf{t}^{Tf(\alpha)} \right\| &\leqslant t^{(\alpha)}_{\mathrm{crit}}(\mathbf{x}, t) \\
\left\| \mathbf{t}^{Tf(\alpha)} \right\| &< t^{(\alpha)}_{\mathrm{crit}}(\mathbf{x}, t) \;\Rightarrow\; \dot{\boldsymbol{\delta}}^{T(\alpha)}(\mathbf{x}, t) = 0 \\
\left\| \mathbf{t}^{Tf(\alpha)} \right\| &= t^{(\alpha)}_{\mathrm{crit}}(\mathbf{x}, t) \;\Rightarrow\; \dot{\boldsymbol{\delta}}^{T(\alpha)}(\mathbf{x}, t) = \kappa \mathbf{t}^{Tf(\alpha)}(\mathbf{x}, t), \; \kappa \geqslant 0 \\
t^{(\alpha)}_{\mathrm{crit}}(\mathbf{x}, t) &= \mu_F \left| t^{N(\alpha)}(\mathbf{x}, t) - \left(1 - \omega^{(\alpha)}_{\mathrm{int}}(\mathbf{x}, t)\right) k^{(\alpha)}_N \delta^{N(\alpha)}(\mathbf{x}, t) \right|
\end{aligned}$$

- Evolution equations for $\omega^{(\gamma)}_{\mathrm{ph}}(\mathbf{x}, t)$ and $\omega^{(\alpha)}_{\mathrm{int}}(\mathbf{x}, t)$

**Box 4:** $(m + n)$ point model.

The constitutive relation for the macroscopic problem is obtained by substituting Eq. 3.9 into Eq. 3.11, and using the decompositions given by Eqs. 4.1-4.2

$$\bar{\sigma}_{ij}(\mathbf{x}, t) = \bar{L}_{ijkl} \bar{\epsilon}_{kl}(\mathbf{x}, t) + \sum_{\beta=1}^{m} \bar{\mathbf{R}}^{(\beta)}_{ij} \cdot \hat{\boldsymbol{\delta}}^{(\beta)}(\mathbf{x}, t) + \sum_{\gamma=1}^{n} \bar{M}^{(\gamma)}_{ijkl} \mu^{(\gamma)}_{kl}(\mathbf{x}, t) \tag{4.34}$$

in which,

$$\bar{L}_{ijkl} = \frac{1}{|\Theta|}\int_{\Theta} L_{ijmn}(\mathbf{y})\, A_{mnkl}(\mathbf{y})\, dy \tag{4.35}$$

$$\bar{\mathbf{R}}^{(\beta)}_{ij} = \frac{1}{|\Theta|}\int_{\Theta} L_{ijkl}(\mathbf{y})\, \tilde{\mathbf{R}}^{(\beta)}_{kl}(\mathbf{y})\, dy \tag{4.36}$$

$$\bar{M}^{(\gamma)}_{ijkl} = \frac{1}{|\Theta|}\int_{\Theta} L_{ijmn}(\mathbf{y})\left(\tilde{P}^{(\gamma)}_{klij}(\mathbf{y}) - I_{klij} N^{(\gamma)}_{\mathrm{ph}}(\mathbf{y})\right) dy \tag{4.37}$$

The formulation of homogenized tangent moduli $\mathcal{L}_{ijkl} = \partial\bar{\sigma}_{ij}/\partial\bar{\epsilon}_{kl}$ is given in Section 5.2.

## 4.1 A nonlocal damage evolution

It is well known [41, 42] that strain softening caused by evolution of damage gives rise to loss ellipticity and consequently discrete solutions are mesh-dependent. This deficiency of the CDM model can be alleviated using nonlocal formulation [43] (among several other methods), a variant of which is adopted here.

We start by defining the nonlocal strain and stress fields over partition $\Theta^{(\gamma)}$ as

$$\epsilon^{(\eta)}_{ij}(\mathbf{x},t) = \int_{\Theta^{(\eta)}} \varphi^{(\eta)}_{\mathrm{ph}}(\mathbf{y})\, \epsilon^{0}_{ij}(\mathbf{x},\mathbf{y},t)\, dy = \frac{1}{\left|\Theta^{(\eta)}\right|}\int_{\Theta^{(\eta)}} \epsilon^{0}_{ij}(\mathbf{x},\mathbf{y},t)\, dy \tag{4.38}$$

$$\sigma^{(\eta)}_{ij}(\mathbf{x},t) = \int_{\Theta^{(\eta)}} \varphi^{(\eta)}_{\mathrm{ph}}(\mathbf{y})\, \sigma^{0}_{ij}(\mathbf{x},\mathbf{y},t)\, dy = \frac{1}{\left|\Theta^{(\eta)}\right|}\int_{\Theta^{(\eta)}} \sigma^{0}_{ij}(\mathbf{x},\mathbf{y},t)\, dy \tag{4.39}$$

The nonlocality of the above fields requires that the phase partitions be constructed such that the characteristic nonlocal volume, $\Theta_{\mathrm{C}}$, is fully encompassed by the corresponding smallest partitions, i.e., $\Theta_{\mathrm{C}} \subset \Theta^{(\gamma)}$ for each $\gamma = 1, 2, \ldots, n$. This formalism was originally proposed by Fish and Yu [44].

We proceed by approximating stresses and strains at any point in a unit cell in terms of the phase shape functions and nonlocal phase stress and strain values as

$$\epsilon^{0}_{ij}(\mathbf{x},\mathbf{y},t) = \sum_{\gamma} N^{(\gamma)}_{\mathrm{ph}}(\mathbf{y})\, \epsilon^{(\gamma)}_{ij}(\mathbf{x},t)\,; \quad \sigma^{0}_{ij}(\mathbf{x},\mathbf{y},t) = \sum_{\gamma} N^{(\gamma)}_{\mathrm{ph}}(\mathbf{y})\, \sigma^{(\gamma)}_{ij}(\mathbf{x},t) \tag{4.40}$$

Substituting Eq. 4.40 into Eq.3.16 yields

$$\omega^{0}_{\mathrm{ph}}(\mathbf{x},\mathbf{y},t) = \omega^{0}_{\mathrm{ph}}\left(\sum_{\gamma} N^{(\gamma)}_{\mathrm{ph}}(\mathbf{y})\, \epsilon^{(\gamma)}_{ij}(\mathbf{x},t), \sum_{\gamma} N^{(\gamma)}_{\mathrm{ph}}(\mathbf{y})\, \sigma^{(\gamma)}_{ij}(\mathbf{x},t), \sum_{\gamma} N^{(\gamma)}_{\mathrm{ph}}(\mathbf{y})\, \mathbf{s}^{(\gamma)}_{\mathrm{ph}}(\mathbf{x},t)\right) \tag{4.41}$$

Premultiplying Eq. 4.41 by the phase weight functions and integrating over the unit cell yields

$$\omega^{(\eta)}_{\mathrm{ph}}(\mathbf{x},t) = \int_{\Theta} \varphi^{(\eta)}_{\mathrm{ph}}(\mathbf{y})\, \omega^{0}_{\mathrm{ph}}\left(\sum_{\gamma} N^{(\gamma)}_{\mathrm{ph}}(\mathbf{y})\, \epsilon^{(\gamma)}_{ij}(\mathbf{x},t), \sum_{\gamma} N^{(\gamma)}_{\mathrm{ph}}(\mathbf{y})\, \sigma^{(\gamma)}_{ij}(\mathbf{x},t), \sum_{\gamma} N^{(\gamma)}_{\mathrm{ph}}(\mathbf{y})\, \mathbf{s}^{(\gamma)}_{\mathrm{ph}}(\mathbf{x},t)\right) dy \tag{4.42}$$

Note that $\varphi^{(\eta)}_{\mathrm{ph}}$ is equal to $1/\left|\Theta^{(\eta)}\right|$ over $\Theta^{(\eta)}$ and 0 elsewhere. Over $\Theta^{(\eta)}$, the only nonzero phase shape function is $N^{(\eta)}_{\mathrm{ph}}$ and its value over this partition is equal to one. Therefore, Eq. 4.42 reduces to

$$\omega^{(\eta)}_{\mathrm{ph}}(\mathbf{x},t) = \omega^{(\eta)}_{\mathrm{ph}}\left(\epsilon^{(\eta)}_{ij}(\mathbf{x},t), \sigma^{(\eta)}_{ij}(\mathbf{x},t), \mathbf{s}^{(\eta)}_{\mathrm{ph}}(\mathbf{x},t)\right) \tag{4.43}$$

which is identical to Eq. 3.16 except that the evolution equation is defined with respect to nonlocal quantities. We now describe the model in detail.

The nonlocal phase damage variable, $\omega_{\text{ph}}^{(\eta)}$ is taken to be a monotonically increasing function of nonlocal phase deformation function $\kappa_{\text{ph}}^{(\eta)}$. The evolution of phase damage may be expressed as

$$\omega_{\text{ph}}^{(\eta)}\left(\mathbf{x},t\right)=\Phi_{\text{ph}}\left(\kappa_{\text{ph}}^{(\eta)}\left(\mathbf{x},t\right)\right);\quad\frac{\partial\Phi_{\text{ph}}\left(\kappa_{\text{ph}}^{(\eta)}\right)}{\partial\kappa_{\text{ph}}^{(\eta)}}\geq0 \tag{4.44}$$

The nonlocal phase deformation function, $\kappa_{\text{ph}}^{(\eta)}$ is a function of phase damage equivalent strain

$$\kappa_{\text{ph}}^{(\eta)}\left(\mathbf{x},t\right)=\max\left\{\left\langle\upsilon_{\text{ph}}^{(\eta)}\left(\mathbf{x},\tau\right)-\upsilon_{\text{ini}}^{(\eta)}\right\rangle_{+}\middle|\,\tau\leq t\right\} \tag{4.45}$$

where, $\upsilon_{\text{ph}}^{(\eta)}$ is nonlocal phase damage equivalent strain; and $\upsilon_{\text{ini}}^{(\eta)}$ the threshold value of $\upsilon_{\text{ph}}^{(\eta)}$ below which no damage in $\Theta^{(\eta)}$ is allowed to occur. The nonlocal phase damage equivalent strain is defined based on the strain-based damage theory [45] as

$$\upsilon_{\text{ph}}^{(\eta)}\left(\mathbf{x},t\right)=\sqrt{\frac{1}{2}\left(\mathbf{F}^{(\eta)}\hat{\boldsymbol{\epsilon}}^{(\eta)}\right)^{\text{T}}\hat{\mathbf{L}}^{(\eta)}\left(\mathbf{F}^{(\eta)}\hat{\boldsymbol{\epsilon}}^{(\eta)}\right)} \tag{4.46}$$

in which, $\hat{\boldsymbol{\epsilon}}^{(\eta)}$ is the vector of principal components of the average strains,$\epsilon_{ij}^{(\eta)}$, in $\Theta^{(\eta)}$; $\hat{\mathbf{L}}^{(\eta)}$ the tensor of elastic moduli in principal directions of $\boldsymbol{\epsilon}^{(\eta)}$; $\mathbf{F}^{(\eta)}$ denotes the weighting matrix. The purpose of the weighting matrix is to differentiate between the damage accumulation in tensile and compressive loading directions

$$\mathbf{F}^{(\eta)}\left(\mathbf{x},t\right)=\begin{bmatrix}h_1^{(\eta)}&0&0\\0&h_2^{(\eta)}&0\\0&0&h_3^{(\eta)}\end{bmatrix}\quad\text{when }\ n_{sd}=3 \tag{4.47}$$

$$h_{\xi}^{(\eta)}\left(\mathbf{x},t\right)=\frac{1}{2}+\frac{1}{\pi}\text{atan}\left[c_1^{(\eta)}\left(\hat{\epsilon}_{\xi}^{(\eta)}-c_2^{(\eta)}\right)\right] \tag{4.48}$$

where $c_1^{(\eta)}$ and $c_2^{(\eta)}$ represent the contribution of tensile and compressive loadings in the principal directions.

The nonlocal strain in a phase partition $\Theta^{(\eta)}$ is given as

$$\epsilon_{ij}^{(\eta)}\left(\mathbf{x},t\right)=A_{ijkl}^{(\eta)}\bar{\epsilon}_{kl}\left(\mathbf{x},t\right)+\tilde{\epsilon}_{ij}^{(\eta)}\left(\mathbf{x},t\right) \tag{4.49}$$

where,

$$\tilde{\epsilon}_{ij}^{(\eta)}\left(\mathbf{x},t\right)=\sum_{\beta=1}^{m}\hat{\mathbf{R}}_{ij}^{(\eta\beta)}\cdot\hat{\boldsymbol{\delta}}^{(\beta)}\left(\mathbf{x},t\right)+\sum_{\gamma=1}^{n}P_{ijkl}^{(\eta\gamma)}\mu_{kl}^{(\gamma)}\left(\mathbf{x},t\right) \tag{4.50}$$

The evolution of phase damage as a function of the phase deformation function follows an arctangent law [28]

$$\Phi_{\text{ph}}^{(\eta)}=\frac{\text{atan}\left(a_{\text{ph}}^{(\eta)}\kappa_{\text{ph}}^{(\eta)}\left(\mathbf{x},t\right)-b_{\text{ph}}^{(\eta)}\right)+\text{atan}\left(b_{\text{ph}}^{(\eta)}\right)}{\pi/2+\text{atan}\left(b_{\text{ph}}^{(\eta)}\right)} \tag{4.51}$$

in which, $a_{\text{ph}}^{(\eta)}$ and $b_{\text{ph}}^{(\eta)}$ are material parameters.

The evolution equations for the interface damage are defined in a similar fashion to those of the phases. The nonlocal interface damage variable, $\omega_{\text{int}}^{(\beta)}$, is given as

$$\omega_{\text{int}}^{(\beta)}\left(\mathbf{x},t\right)=\Phi_{\text{int}}\left(\kappa_{\text{int}}^{(\beta)}\left(\mathbf{x},t\right)\right);\quad\frac{\partial\Phi_{\text{int}}\left(\kappa_{\text{int}}^{(\beta)}\right)}{\partial\kappa_{\text{int}}^{(\beta)}}\geq0 \tag{4.52}$$

The nonlocal interface deformation function, $\kappa_{\text{int}}^{(\beta)}$, is a function of interface damage equivalent displacement jump

$$\kappa_{\text{int}}^{(\beta)}(\mathbf{x},t) = \max\left\{ \upsilon_{\text{int}}^{(\beta)}(\mathbf{x},\tau) \middle| \tau \leq t \right\} \tag{4.53}$$

where, $\upsilon_{\text{int}}^{(\beta)}$ is the nonlocal interface damage equivalent displacements in $S^{(\beta)}$ which is expressed as

$$\upsilon_{\text{int}}^{(\beta)}(\mathbf{x},t) = k_N^{(\beta)} \delta^{N(\beta)}(\mathbf{x},t) + k_T^{(\beta)} \left\| \boldsymbol{\delta}^{T(\beta)}(\mathbf{x},t) \right\| \tag{4.54}$$

The evolution of interface damage as a function of the interface deformation function is given by the following law

$$\Phi_{\text{int}}^{(\beta)} = \frac{\operatorname{atan}\left( a_{\text{int}}^{(\beta)} \kappa_{\text{ph}}^{(\beta)}(\mathbf{x},t) / b_{\text{int}}^{(\beta)} \right)}{\operatorname{atan}\left( a_{\text{int}}^{(\beta)} \right)}; \quad \Phi_{\text{int}}^{(\beta)} \leq 1 \tag{4.55}$$

in which, $a_{\text{int}}^{(\beta)}$ and $b_{\text{int}}^{(\beta)}$ are material parameters.

## 4.2 Influence functions

The coefficient tensors of the $(m+n)$ point model are functions of the elastic ($H_{ikl}$), phase ($h_{ikl}^{\text{ph}}$), and interface ($h_{im}^{\text{int}}$) influence functions. The influence functions are obtained by numerically solving the three unit cell problems: (i) elastic influence function (EIF), (ii) phase damage influence function (PDIF), and, (iii) interface damage influence function (IDIF) problems defined in Section 3. Guedes and Kikuchi [10] provides a comprehensive treatise on the solution of the EIF problem. In this section, numerical approximations of the PDIF and IDIF problems are discussed.

Let $\hat{\Theta}$ be an arbitrary subdomain of $\Theta$ (i.e., $\hat{\Theta} \subset \Theta$), and define

$$\hat{d}_{\hat{\Theta}}(\mathbf{y}) = \begin{cases} \dfrac{1}{|\hat{\Theta}|} & \mathbf{y} \in \hat{\Theta} \\ 0 \text{ elsewhere} \end{cases} \tag{4.56}$$

In the limit

$$\lim_{|\hat{\Theta}| \to 0} \hat{d}_{\hat{\Theta}}(\mathbf{y}) = d(\mathbf{y} - \hat{\mathbf{y}}); \quad \hat{\mathbf{y}} \in \hat{\Theta} \tag{4.57}$$

The unit cell PDIF problem is approximated by replacing the Dirac delta function in the PDIF problem box by $\hat{d}_{\hat{\Theta}}$ which gives

**Discrete Phase Damage Influence Function (Discrete PDIF) Problem** :

Given $L_{ijmn}(\mathbf{y})$, find $h_{ikl}^{\text{ph}}(\mathbf{y},\hat{\mathbf{y}}) : \bar{\Theta} \times \bar{\Theta} \to \mathbb{R}$ such that:

$$\left\{ L_{ijmn}(\mathbf{y}) \left( g_{mnkl}^{\text{ph}}(\mathbf{y},\hat{\mathbf{y}}) + I_{mnkl} \hat{d}_{\hat{\Theta}}(\mathbf{y}) \right) \right\}_{,y_j} = 0; \quad \mathbf{y}, \hat{\mathbf{y}} \in \Theta$$

$$\Theta - \text{periodic boundary conditions on } \mathbf{y} \in \Gamma_\Theta$$

$$[\![ h_{ikl}^{\text{ph}} ]\!](\mathbf{y},\hat{\mathbf{y}}) = 0 \quad \text{on} \quad \mathbf{y}, \hat{\mathbf{y}} \in \Theta$$

The approximation to the phase influence function (solution of Discrete PDIF problem) and the exact solution of PDIF problem are both denoted by $h_{ikl}^{\text{ph}}$ for conciseness of the presentation. The weak form of the PDIF problem states

$$\int_\Theta w_{(i,y_j)}(\mathbf{y}) L_{ijmn}(\mathbf{y}) g_{mnkl}^{\text{ph}}(\mathbf{y},\hat{\mathbf{y}}) \, dy + \frac{1}{|\hat{\Theta}|} \int_{\hat{\Theta}} w_{(i,y_j)}(\mathbf{y}) L_{ijkl}(\mathbf{y}) \, dy = 0; \quad \hat{\mathbf{y}} \in \hat{\Theta} \tag{4.58}$$

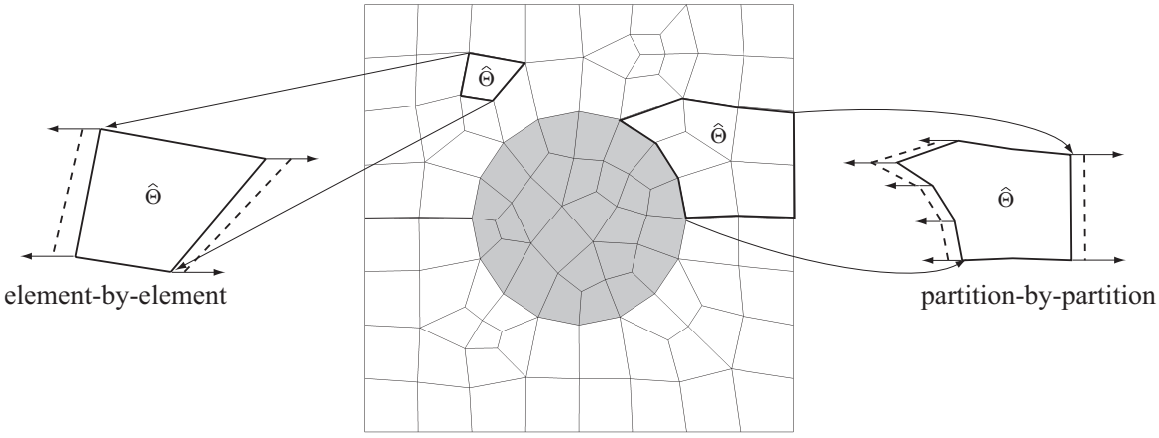


Figure 4: Evaluation of the phase influence function using element-by-element and partition-by-partition methods.

where, $w_i \in \mathcal{V}$ is the weight function; and $\mathcal{V} = \{w_i \in H^1(\Theta) \mid w_i\ \Theta - \text{periodic}\}$. The above equation is discretized and solved using the finite element method. $\hat{\Theta}$ in Eq. 4.56 is selected either as a domain of a single finite element or a group of elements in the microscopic mesh. In view of the definition of $\hat{d}_{\hat{\Theta}}$ provided in Eq. 4.56, $h^{\text{ph}}_{ikl}$ may be fully computed by dividing the microstructure into $n_{\text{patch}}$ patches and solving the weak form of PDIF problem (Eq. 4.58) $n_{\text{patch}}$ times. $n_{\text{patch}}$ is typically selected as the number of finite elements, $n_{\text{el}}$, or number of phase partitions, $n$. The evaluation of the phase influence function based on element-by-element and partition-by-partition methods is schematically illustrated in Fig 4. When $n_{\text{patch}} = n_{\text{el}}$, the phase influence functions can be computed *a-priori* and only coefficient tensors need to be recomputed in the case of the dynamic partitioning scheme discussed in the next section. When $n_{\text{patch}} = n$, the phase influence functions are recomputed when the model order is updated. Figure 5 illustrates the components of the phase influence function evaluated within one element of a 2-phase unit cell.

The interface influence function is numerically approximated by considering an analogous formulation to the evaluation of phase influence function discussed above. Let $\hat{d}_{\hat{S}}$ be an approximation to the Dirac delta function to be subsequently defined, then the IDIF unit cell problem is replaced by

**Discrete Interface Damage Influence Function (Discrete IDIF) Problem**:

Given $L_{ijmn}(\mathbf{y})$, find $h^{\text{int}}_{ip}(\mathbf{y}, \hat{\mathbf{y}}) : \bar{\Theta} \times S \to \mathbb{R}$ such that:

$$\left\{L_{ijmn}(\mathbf{y})\, g^{\text{int}}_{mnp}(\mathbf{y}, \hat{\mathbf{y}})\right\}_{,y_j} = 0; \quad \mathbf{y} \in \Theta, \quad \hat{\mathbf{y}} \in S$$

$$\Theta - \text{periodic boundary conditions on } \mathbf{y} \in \Gamma_\Theta$$

$$[\![h^{\text{ph}}_{ip}]\!](\mathbf{y}, \hat{\mathbf{y}}) = Q_{ip}\hat{d}_{\hat{S}} \quad \text{when} \quad \mathbf{y} \in S \text{ or } \hat{\mathbf{y}} \in S$$

The interface influence function is approximated using standard finite element shape functions, $N_a(\mathbf{y})$; $a = 1, 2, \ldots, n_{nd}$; and $n_{nd}$ is the total number of nodes in the microscopic finite element mesh. The interface displacement jumps are modeled by placing double nodes along the interfaces. $\hat{d}_{\hat{S}}$ is then expressed in terms of shape functions as

$$\hat{d}_{\hat{S}}(\hat{\mathbf{y}}) = \frac{N_a(\hat{\mathbf{y}})}{\int_{\hat{S}} N_a(\hat{\mathbf{y}})\, d\hat{y}}; \quad \hat{\mathbf{y}} \in S \tag{4.59}$$

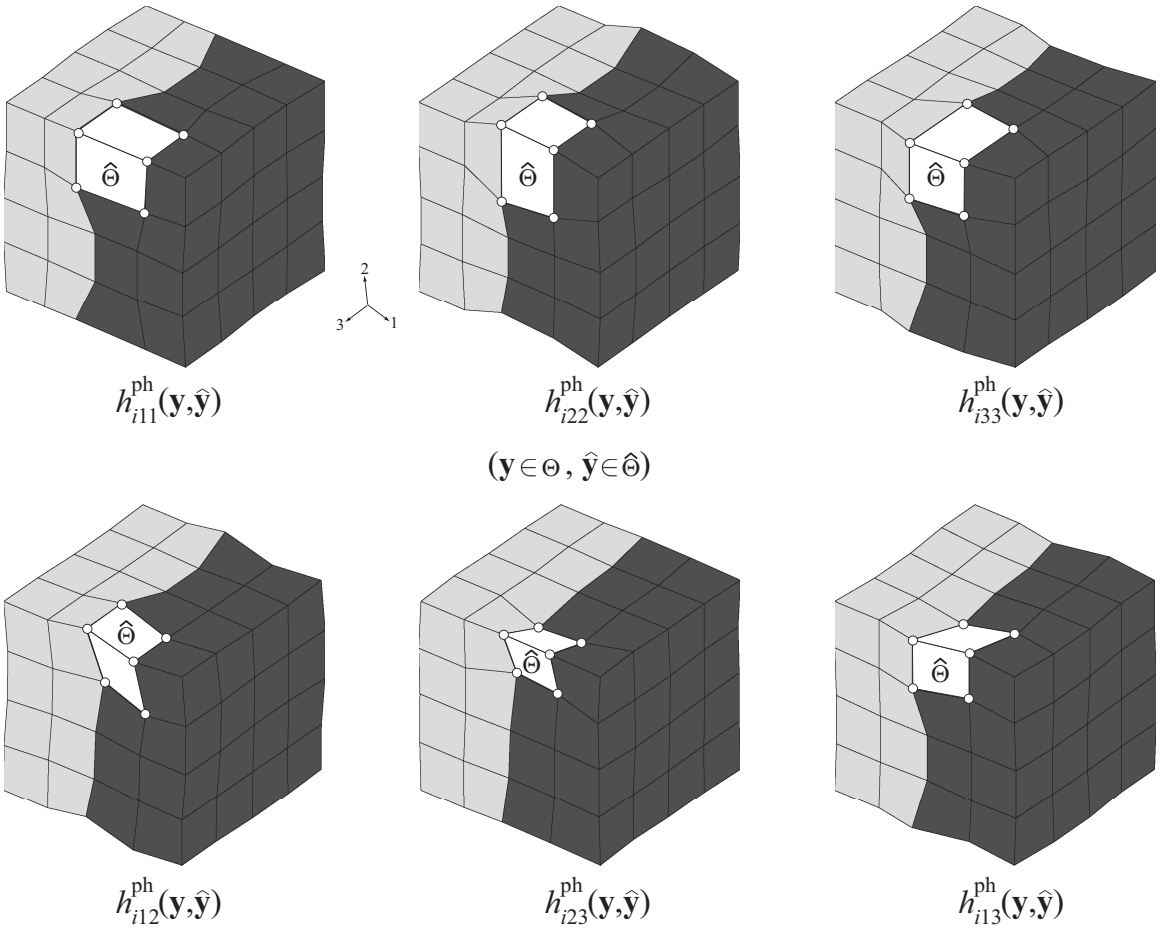


Figure 5: Components of the phase influence function using element-by-element approach.

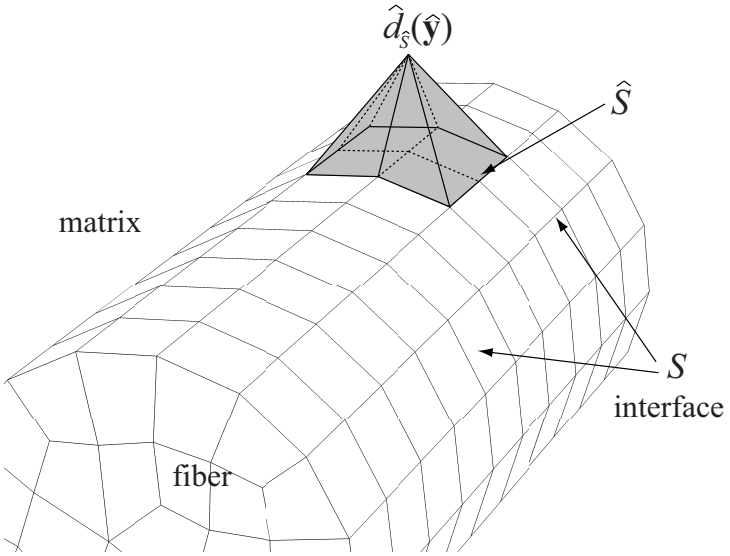


Figure 6: Approximation of the Dirac delta function for computation of the interface influence function.

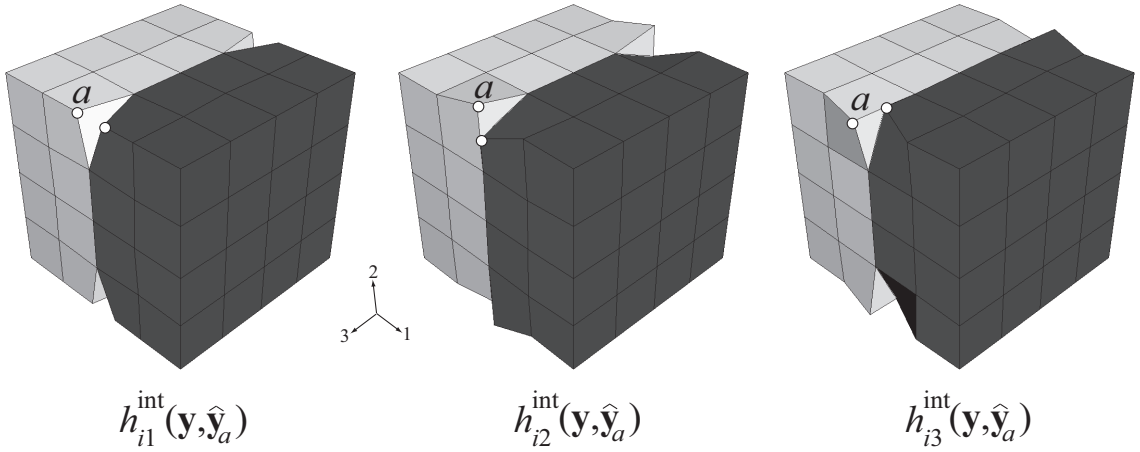


Figure 7: Components of the interface influence function.

where, $\hat{S}$ is the local support of $N_a$ along the interface. The function, $\hat{d}_{\hat{S}}$, is schematically illustrated in Fig. 6. $h_{ip}^{\text{int}}$ may be computed by solving the Discrete IDIF problem $n_{in}$ times, where, $n_{in}$ is the number of double nodes placed along the interface. Figure 7 depicts the components of the interface influence function evaluated for a pair of interface nodes.

## 4.3 Model improvement strategies

The $(m+n)$ point model results in nonlinear system of $3m + 6n$ equations. Selection of $m$ and $n$ is crucial to the accuracy and computational efficiency. Clearly, larger values of $m$ and $n$ lead to a superior accuracy at the expense of increased computational cost. In addition to the selection of the model degree, proper partitioning of the microconstituents affects the accuracy of the proposed models.

Much like the discretizations in the finite element method, the optimal strategy for the selection of the model degree and domains of each partition depend largely on the specificities of the macroscopic problem in addition to the microstructural details. In this work, we study two partitioning strategies termed as static domain partitioning (SDP) and dynamic domain partitioning (DDP).

In SDP, selection of the model degree ($m$ and $n$) and partitioning of the microstructure is carried out prior to the macroscopic analysis. In this approach, $m$ and $n$, and corresponding microstructural domain partitions, $\Theta^{(\gamma)}$ and $S^{(\alpha)}$ are functions of macroscopic spatial coordinate, $x$, but do not vary in time. In static partitioning coefficient tensors are computed once in the preprocessing stage and remain constant throughout macroscopic analysis. Box 5 summarizes the preprocessing stage for static partitioning. The preprocessing stage consists of the evaluation of the influence functions, partitioning of the microstructural domain, and computation of the corresponding coefficient tensor, given the model order ($m$ and $n$). The computation of the elastic influence function, $H_{ikl}$, interface and phase influence functions, $h^{\text{int}}_{im}$ and $h^{\text{ph}}_{ikl}$, respectively, follows the procedure explained in the previous section. The partitioning of the interface, $S$, and phase, $\Theta$, is based on the elastic macroscopic strains, $\bar{\epsilon}^{\text{el}}_{ij}$, computed in a preliminary linear analysis of the macroscopic problem. At each integration point of the macroscopic mesh, the interface, $S$, is partitioned into $S^{(\alpha)}$, $\alpha = 1, 2, \ldots, m$ based on the magnitude of interface damage strain, $\upsilon_{\text{int}}$. Similarly, the phase damage equivalent strain, $\upsilon_{\text{ph}}$, is computed based on which the microscopic domain, $\Theta$, is partitioned into $\Theta^{(\gamma)}$ , $\gamma = 1, 2, \ldots, n$. The coefficient tensors are evaluated using the integral expressions provided in the previous sections.

The dynamic domain partitioning (DDP) strategy is based on recomputing the microstructural domain partitions as the macroscopic analysis progresses. By this approach, the domain partitioning, as well as the model order vary in time. The number of interface and phase partitions $m$ and $n$ are increased adaptively, as material failure evolves. Figure 8 illustrates the dynamic domain partitioning algorithm. In DDP, the analysis is initiated with minimum number of interface and phase partitions (typically, $m = 1$ and $n = 2$ for a 2-phase material). The model order is increased adaptively as a function of normalized damage

$$f(\omega) = \text{int}\left(\kappa \frac{\omega}{\omega_{\text{crit}}}\right) \tag{4.60}$$

in which, $\omega \in \left\{\omega^{(\alpha)}_{\text{int}}, \omega^{(\gamma)}_{\text{ph}}\right\}$; $\omega_{\text{crit}}$ is the critical damage, above which no more repartitioning can occur; and $\kappa$ is the maximum allowable number of repartitioning; and int denotes the integer operator. The updated numbers of phase and interface partitions are then expressed as:

$$_{t+\Delta t}n = {}_{t}n + \sum_{\gamma=1}^{n} \delta n^{(\gamma)}; \quad \delta n^{(\gamma)} = f\left({}_{t+\Delta t}\omega^{(\gamma)}_{\text{ph}}\right) - f\left({}_{t}\omega^{(\gamma)}_{\text{ph}}\right) \tag{4.61}$$

$$_{t+\Delta t}m = {}_{t}m + \sum_{\alpha=1}^{m} \delta m^{(\alpha)}; \quad \delta m^{(\alpha)} = f\left({}_{t+\Delta t}\omega^{(\alpha)}_{\text{int}}\right) - f\left({}_{t}\omega^{(\alpha)}_{\text{int}}\right) \tag{4.62}$$

in which, the left subscript $t+\Delta t$ and $t$ denote current and previous values, respectively. The updated model order is then used to recompute the coefficient tensors by invoking the algorithm outlined in Box 5. A hierarchical repartitioning is adopted in which, those partitions, $\Theta^{(\gamma)}$ and $S^{(\alpha)}$ with nonzero $\delta n^{(\gamma)}$ and $\delta m^{(\alpha)}$ are repartitioned only. The hierarchical repartitioning is illustrated in Fig. 9.

The DDP strategy offers certain advantages when the number of coefficient tensors recomputations is limited and/or preprocessing cost is substantially lower than the cost of nonlinear iterations. Otherwise, SDP with large $n$ and $m$ might be advantageous both in terms of cost and accuracy.

- Consider the linear elastic unit cell problem:
  - Solve for the elastic influence functions, $H_{ikl}$, and corresponding traction terms along the interface, $\tau_{ikl}$
  - Compute the elastic polarization tensor, $G_{ijkl}$
  - Compute the linear elastic homogenized moduli, $\bar{L}_{ijkl}$ using Eq. 4.35.
- Loop $\hat{a}$ over the nodes along the interface of the unit cell mesh
  - Compute the interface influence function, $h^{\text{int}}_{im}(\mathbf{y}, \hat{\mathbf{y}}_{\hat{a}})$
  - Compute the interface polarization function, $g^{\text{int}}_{ijm}(\mathbf{y}, \hat{\mathbf{y}}_{\hat{a}})$
- Loop $\hat{b}$ over the elements of the unit cell mesh
  - Compute the phase influence function, $h^{\text{ph}}_{ikl}(\mathbf{y}, \hat{\mathbf{y}}_{\hat{b}})$
  - Compute the phase polarization function, $g^{\text{ph}}_{ijkl}(\mathbf{y}, \hat{\mathbf{y}}_{\hat{b}})$
- Preliminary linear analysis of the macroscopic problem to obtain $\bar{\epsilon}^{\text{el}}_{ij}$
- Loop $B$ over each element of the macroscopic mesh
  - Along the interface:

$$\begin{aligned} t^{\text{el}}_i(\mathbf{x}_B, \mathbf{y}) &= \tau_{ikl}(\mathbf{y})\, \bar{\epsilon}^{\text{el}}_{kl}(\mathbf{x}_B); \quad \mathbf{y} \in S \\ \upsilon^{\text{el}}_{\text{int}} &= \|\hat{\mathbf{t}}^{\text{el}}\| / \max_{\mathbf{y}} \|\hat{\mathbf{t}}^{\text{el}}\| \end{aligned}$$

  - Identify $m$ partitions of the interfaces based on $\upsilon^{\text{el}}_{\text{int}}$
  - Within the phases:

$$\begin{aligned} \epsilon^{\text{el}}_{ij}(\mathbf{x}_B, \mathbf{y}) &= A_{ijkl}(\mathbf{y})\, \bar{\epsilon}^{\text{el}}_{kl}(\mathbf{x}_B); \quad \mathbf{y} \in \Theta \\ \upsilon^{\text{el}}_{\text{ph}} &= \left(\mathbf{F}\hat{\boldsymbol{\epsilon}}^{\text{el}}\right)^{\mathrm{T}} \hat{\mathbf{L}} \left(\mathbf{F}\hat{\boldsymbol{\epsilon}}^{\text{el}}\right) / \max_{\mathbf{y}} \left\{ \left(\mathbf{F}\hat{\boldsymbol{\epsilon}}^{\text{el}}\right)^{\mathrm{T}} \hat{\mathbf{L}} \left(\mathbf{F}\hat{\boldsymbol{\epsilon}}^{\text{el}}\right) \right\} \end{aligned}$$

  - Identify $n$ partitions of the phases based on $\upsilon^{\text{el}}_{\text{ph}}$
  - Compute coefficient tensors for macroscopic element, $B$

**Box 5:** Preprocessing.

# 5 Numerical Implementation

## 5.1 Macroscopic stress update procedure

*Given:* Overall strain ${}_t\bar{\epsilon}_{ij}$; phase and interface damage variables, ${}_t\omega^{(\eta)}_{\text{ph}}$, $(\eta = 1, 2, \ldots, n)$ and ${}_t\omega^{(\beta)}_{\text{int}}$, $(\beta = 1, 2, \ldots, m)$, respectively; increment of overall strain, $\Delta\bar{\epsilon}_{ij}$; damage induced displacement jumps in the local coordinate system, ${}_t\hat{\delta}^{(\beta)}_i$; and damage induced inelastic strains, ${}_t\mu_{ij}{}^{(\eta)}$. The left subscript denotes increment step, i.e., ${}_t\Diamond$ and ${}_{t+\Delta t}\Diamond$ are the values at the previous and current increments, respectively. For simplicity, the left subscripts of the current increments are often omitted in the following presentation.

*Compute:* The overall stress, $\bar{\sigma}_{ij}$; current values of damage variables, $\omega^{(\eta)}_{\text{ph}}$ and $\omega^{(\beta)}_{\text{int}}$; damage induced displacement jumps, $\hat{\delta}^{(\beta)}_i$; and inelastic strains, $\mu^{(\eta)}_{ij}$.

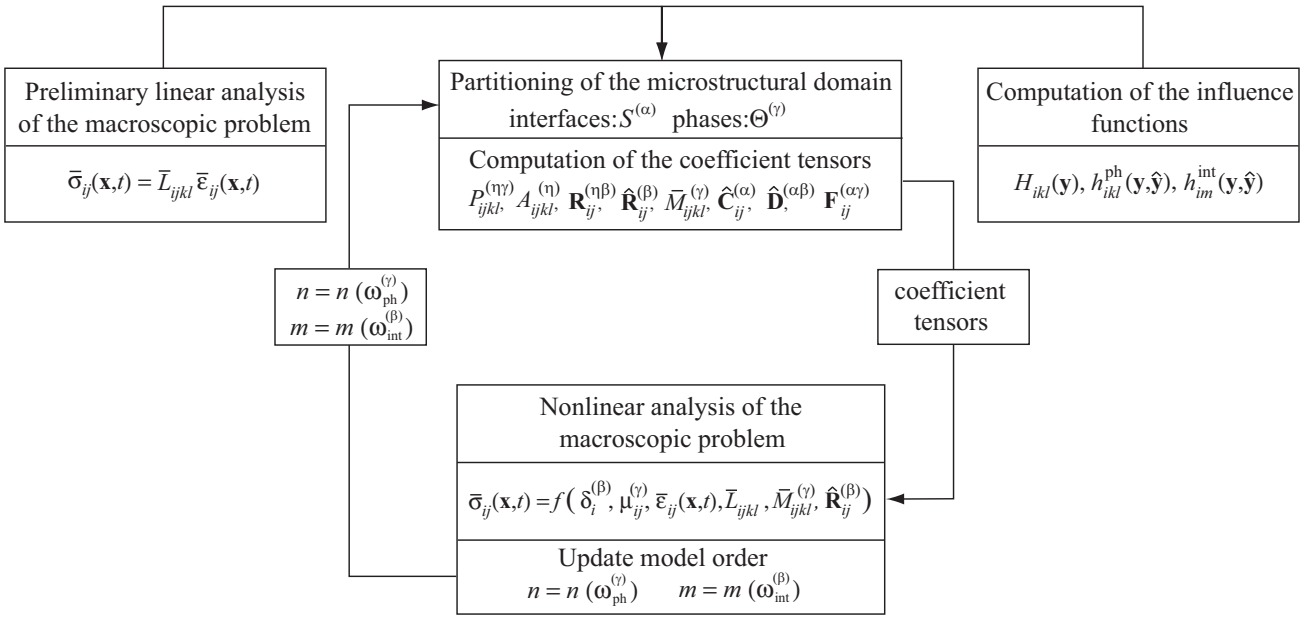


Figure 8: Dynamic domain partitioning (DDP) strategy.

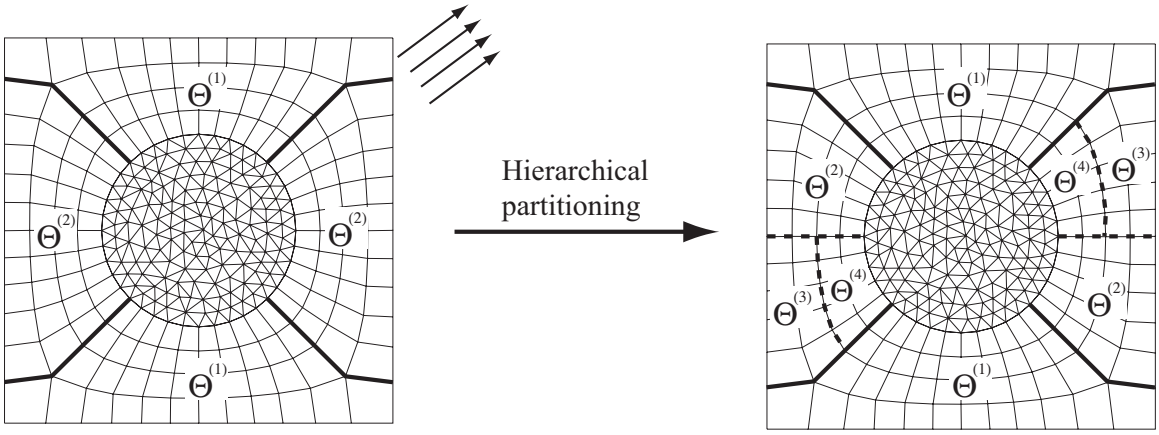


Figure 9: Hierarchical partitioning of the microconstituents in the dynamic domain partitioning strategy.

A vector of state variables, $\mathbf{d}$ is defined such that

$$\mathbf{d} = \left\{ \boldsymbol{\mu}^{(1)}, \boldsymbol{\mu}^{(2)}, \ldots, \boldsymbol{\mu}^{(n)}, \hat{\boldsymbol{\delta}}^{(1)}, \hat{\boldsymbol{\delta}}^{(2)}, \ldots, \hat{\boldsymbol{\delta}}^{(m)} \right\}^{\mathrm{T}} \tag{5.1}$$

in which $\boldsymbol{\mu}^{(\eta)}$ is the vector of inelastic strain components in Voigt notation.

In view of the governing equations of the reduced microscopic problem outlined in Box 4, the damage induced displacement jumps and inelastic strains may be evaluated by invoking a Newton process. The unilateral contact condition is imposed by considering a penalty algorithm. The tangential friction model is implemented using an elastic stick formulation [46] as described below. The resulting nonlinear system is expressed as

$$\boldsymbol{\Psi} = \mathbf{K}(\omega_{\mathrm{ph}}^{(\eta)}, \omega_{\mathrm{int}}^{(\beta)})\mathbf{d} - \mathbf{f}(\omega_{\mathrm{ph}}^{(\eta)}; \bar{\epsilon}_{ij}) + \mathbf{f}^{c}(\mathbf{d}) + \mathbf{f}^{f}(\mathbf{d}) = 0 \tag{5.2}$$

where, $\mathbf{f}^{c}$ is the contribution due to penalty method aimed at enforcing unilateral contact constraint; $\mathbf{f}^{f}$ is the contribution of the friction model; $\mathbf{f}$ is the force vector;

$$\mathbf{K} = \begin{bmatrix} \mathbf{K}_{\mathrm{PP}}(\omega_{\mathrm{ph}}^{(\eta)}) & \mathbf{K}_{\mathrm{PI}}(\omega_{\mathrm{ph}}^{(\eta)}) \\ \mathbf{K}_{\mathrm{IP}} & \mathbf{K}_{\mathrm{II}}(\omega_{\mathrm{int}}^{(\beta)}) \end{bmatrix} \tag{5.3}$$

and,

$$\mathbf{K}_{\mathrm{PP}} = \begin{bmatrix} I_{ijkl} - P_{ijkl}^{(11)}\omega_{\mathrm{ph}}^{(1)} & -P_{ijkl}^{(12)}\omega_{\mathrm{ph}}^{(1)} & \cdots & -P_{ijkl}^{(1n)}\omega_{\mathrm{ph}}^{(1)} \\ -P_{ijkl}^{(21)}\omega_{\mathrm{ph}}^{(2)} & I_{ijkl} - P_{ijkl}^{(22)}\omega_{\mathrm{ph}}^{(2)} & \cdots & -P_{ijkl}^{(2n)}\omega_{\mathrm{ph}}^{(2)} \\ \vdots & \vdots & \ddots & \vdots \\ -P_{ijkl}^{(n1)}\omega_{\mathrm{ph}}^{(n)} & -P_{ijkl}^{(n2)}\omega_{\mathrm{ph}}^{(n)} & \cdots & I_{ijkl} - P_{ijkl}^{(nn)}\omega_{\mathrm{ph}}^{(n)} \end{bmatrix} \tag{5.4}$$

$$\mathbf{K}_{\mathrm{PI}} = \begin{bmatrix} -\hat{\mathbf{R}}_{ij}^{(11)}\omega_{\mathrm{ph}}^{(1)} & -\hat{\mathbf{R}}_{ij}^{(12)}\omega_{\mathrm{ph}}^{(1)} & \cdots & -\hat{\mathbf{R}}_{ij}^{(1m)}\omega_{\mathrm{ph}}^{(1)} \\ -\hat{\mathbf{R}}_{ij}^{(21)}\omega_{\mathrm{ph}}^{(2)} & -\hat{\mathbf{R}}_{ij}^{(22)}\omega_{\mathrm{ph}}^{(2)} & \cdots & -\hat{\mathbf{R}}_{ij}^{(2m)}\omega_{\mathrm{ph}}^{(2)} \\ \vdots & \vdots & \ddots & \vdots \\ -\hat{\mathbf{R}}_{ij}^{(n1)}\omega_{\mathrm{ph}}^{(n)} & -\hat{\mathbf{R}}_{ij}^{(n2)}\omega_{\mathrm{ph}}^{(n)} & \cdots & -\hat{\mathbf{R}}_{ij}^{(nm)}\omega_{\mathrm{ph}}^{(n)} \end{bmatrix} \tag{5.5}$$

$$\mathbf{K}_{\mathrm{IP}} = \begin{bmatrix} \hat{\mathbf{F}}_{ij}^{(11)} & \hat{\mathbf{F}}_{ij}^{(12)} & \cdots & \hat{\mathbf{F}}_{ij}^{(1n)} \\ \hat{\mathbf{F}}_{ij}^{(21)} & \hat{\mathbf{F}}_{ij}^{(22)} & \cdots & \hat{\mathbf{F}}_{ij}^{(2n)} \\ \vdots & \vdots & \ddots & \vdots \\ \hat{\mathbf{F}}_{ij}^{(m1)} & \hat{\mathbf{F}}_{ij}^{(m2)} & \cdots & \hat{\mathbf{F}}_{ij}^{(mn)} \end{bmatrix} \tag{5.6}$$

$$\mathbf{K}_{\mathrm{II}} = \begin{bmatrix} \hat{\mathbf{D}}^{(11)} + \mathbf{E}^{(1)} & \hat{\mathbf{D}}^{(12)} & \cdots & \hat{\mathbf{D}}^{(1m)} \\ \hat{\mathbf{D}}^{(21)} & \hat{\mathbf{D}}^{(22)} + \mathbf{E}^{(2)} & \cdots & \hat{\mathbf{D}}^{(2m)} \\ \vdots & \vdots & \ddots & \vdots \\ \hat{\mathbf{D}}^{(m1)} & \hat{\mathbf{D}}^{(m2)} & \cdots & \hat{\mathbf{D}}^{(mm)} + \mathbf{E}^{(m)} \end{bmatrix} \tag{5.7}$$

where,

$$\mathbf{E}^{(\beta)} = \begin{bmatrix} \left(1 - \omega_{\mathrm{int}}^{(\beta)}\right) k_N^{(\beta)} & 0 & 0 \\ 0 & \left(1 - \omega_{\mathrm{int}}^{(\beta)}\right) k_T^{(\beta)} & 0 \\ 0 & 0 & \left(1 - \omega_{\mathrm{int}}^{(\beta)}\right) k_T^{(\beta)} \end{bmatrix} \tag{5.8}$$

The force vector, $\mathbf{f}$, is expressed as

$$\mathbf{f} = \left[ A_{ijkl}^{(1)}\omega_{\mathrm{ph}}^{(1)}, A_{ijkl}^{(2)}\omega_{\mathrm{ph}}^{(2)}, \ldots, A_{ijkl}^{(n)}\omega_{\mathrm{ph}}^{(n)}, \mathbf{C}_{kl}^{(1)}, \mathbf{C}_{kl}^{(2)}, \ldots, \mathbf{C}_{kl}^{(m)} \right]^{\mathrm{T}} \bar{\epsilon}_{kl} \tag{5.9}$$

The penalty contribution due to unilateral constraint, $\mathbf{f}^c$ is given as

$$\mathbf{f}^c = \frac{1}{\chi}\left[0,\ldots,0,\left\langle \delta^{N(1)}\right\rangle_{-},0,0,\left\langle \delta^{N(2)}\right\rangle_{-},0,0,\ldots,\left\langle \delta^{N(m)}\right\rangle_{-},0,0\right]^{\mathrm{T}} \tag{5.10}$$

in which, $\chi \ll 1$ is the penalty parameter; and $\langle \Diamond \rangle_{-} \equiv (|\Diamond| - \Diamond)/2$.

The friction model is implemented based on the elastic stick formulation, in which the frictional displacement jumps, $\boldsymbol{\delta}^{T(\beta)}$, are decomposed as follows

$$\boldsymbol{\delta}^{T(\beta)} = \boldsymbol{\delta}_{\mathrm{el}}^{T(\beta)} + \boldsymbol{\delta}_{\mathrm{slip}}^{T(\beta)} \tag{5.11}$$

where, $\boldsymbol{\delta}_{\mathrm{el}}^{T(\beta)}$ is the elastic slip which is recoverable upon unloading; and $\boldsymbol{\delta}_{\mathrm{slip}}^{T(\beta)}$ is the plastic slip. The tangential tractions due to friction is then expressed as

$$\mathbf{t}^{Tf(\beta)} = \frac{\mu_F \left| t^{N(\beta)} - \left(1-\omega_{\mathrm{int}}^{(\beta)}\right) k_N^{(\beta)} \delta^{N(\beta)} \right|}{\delta_{\mathrm{crit}}} \boldsymbol{\delta}_{\mathrm{el}}^{T(\beta)} \tag{5.12}$$

in which, $\delta_{\mathrm{crit}}$ is the magnitude of the maximum allowable elastic slip. Equation 5.12 implies that the contribution of the frictional forces along the interface vanishes (i.e., $\mathbf{f}^f = \mathbf{0}$ ) when the normal displacement jumps, $\delta^{N(\beta)} > 0$. Under compression (i.e., $\delta^{N(\beta)} = 0$ )

$$\mathbf{f}^f = \left[0,\ldots,0,0,\mathbf{t}^{Tf(1)},0,\mathbf{t}^{Tf(2)},0,0,\ldots,\mathbf{t}^{Tf(m)}\right]^{\mathrm{T}} \tag{5.13}$$

In the presence of friction, $\boldsymbol{\delta}_{\mathrm{el}}^{T(\beta)}$ is stored as state variable in addition to $\mathbf{d}$ and damage variables.

In view of the definitions above, the stress update procedure consists of the following steps

1. Update the macroscopic strains: $\bar{\epsilon}_{ij} = {}_t\bar{\epsilon}_{ij} + \Delta\bar{\epsilon}_{ij}$
2. Solve Eq. 5.2 by Newton's method

$$^{k+1}\mathbf{d} = {}^{k}\mathbf{d} - \left(\frac{\partial \boldsymbol{\Psi}}{\partial \mathbf{d}}\right)\Bigg|_{{}^{k}\mathbf{d}}^{-1} \boldsymbol{\Psi}|_{{}^{k}\mathbf{d}} \tag{5.14}$$

3. Initialize the Newton procedure by setting $k = 0$, ${}^{k}\mathbf{d} = {}_t\mathbf{d}$, ${}^{k}\omega_{\mathrm{ph}}{}^{(\eta)} = {}_t\omega_{\mathrm{ph}}{}^{(\eta)}$, ${}^{k}\omega_{\mathrm{int}}{}^{(\beta)} = {}_t\omega_{\mathrm{int}}{}^{(\beta)}$, and ${}^{k}\boldsymbol{\delta}_{\mathrm{el}}^{T(\beta)} = {}_t\boldsymbol{\delta}_{\mathrm{el}}^{T(\beta)}$
4. loop until convergence
   (a) Compute ${}^{k}\mathbf{K}$, ${}^{k}\mathbf{f}$, ${}^{k}\mathbf{f}^c$, ${}^{k}\mathbf{f}^f$, and $(\partial\boldsymbol{\Psi}/\partial\mathbf{d})|_{{}^{k}\mathbf{d}}^{-1}$
   (b) Evaluate Eq. 5.14 to obtain ${}^{k+1}\mathbf{d}$
   (c) $k \leftarrow k+1$
5. Compute the macroscopic stress $\bar{\sigma}_{ij}$ using Eq. 4.34.

${}^{k}\mathbf{K}$, ${}^{k}\mathbf{f}$ and ${}^{k}\mathbf{f}^c$ may be obtained directly using Eqs. 5.3-5.10. Derivation of $(\partial\boldsymbol{\Psi}/\partial\mathbf{d})$ is given in Section 5.2. The update of frictional contribution, ${}^{k}\mathbf{f}^f$, may be summarized as follows

*Given:* Displacement jumps, ${}^{k}\hat{\boldsymbol{\delta}}^{(\beta)}$, elastic part of the tangential displacement jumps, ${}^{k}\boldsymbol{\delta}_{\mathrm{el}}^{T(\beta)}$, and normal tractions, ${}^{k}t^{N(\beta)}$

*Compute:* ${}^{k}\boldsymbol{\delta}_{\mathrm{el}}^{T(\beta)}$, ${}^{k}\mathbf{t}^{Tf(\beta)}$ and ${}^{k}\mathbf{f}^f$

1. Separation along the interface: ${}^{k}\delta^{N(\beta)} > 0 \Rightarrow {}^{k}\mathbf{t}^{Tf(\beta)} = 0$
2. Compression along the interface: ${}^{k}\delta^{N(\beta)} = 0$

(a) Compute predictor tangential displacement jumps

$$\boldsymbol{\delta}_{\mathrm{pr}}^{(\beta)} = {}_t\boldsymbol{\delta}_{\mathrm{el}}^{T(\beta)} + {}^k\Delta\boldsymbol{\delta}^{T(\beta)} \tag{5.15}$$

in which, ${}^k\Delta\boldsymbol{\delta}^{T(\beta)}$ is the tangential displacement jump increment at iteration $k$.

3. Elastic stick:

$$\frac{\left\|\boldsymbol{\delta}_{\mathrm{pr}}^{(\beta)}\right\|}{\delta_{\mathrm{crit}}} < 1 \Rightarrow {}^k\mathbf{t}^{Tf(\beta)} = \frac{\mu_F {}^k t^{N(\beta)}}{\delta_{\mathrm{crit}}}\boldsymbol{\delta}_{\mathrm{pr}}^{(\beta)} \tag{5.16}$$

$${}^k\boldsymbol{\delta}_{\mathrm{el}}^{T(\beta)} = \boldsymbol{\delta}_{\mathrm{pr}}^{(\beta)} \tag{5.17}$$

4. Plastic slip:

$$\frac{\left\|\boldsymbol{\delta}_{\mathrm{pr}}^{(\beta)}\right\|}{\delta_{\mathrm{crit}}} \geq 1 \Rightarrow {}^k\mathbf{t}^{Tf(\beta)} = \frac{\mu_F {}^k t^{N(\beta)}}{\left\|\boldsymbol{\delta}_{\mathrm{pr}}^{(\beta)}\right\|}\boldsymbol{\delta}_{\mathrm{pr}}^{(\beta)} \tag{5.18}$$

$${}^k\boldsymbol{\delta}_{\mathrm{el}}^{T(\beta)} = \boldsymbol{\delta}_{\mathrm{pr}}^{(\beta)} - \frac{{}^k\mathbf{t}^{Tf(\beta)}}{\mu_F {}^k t^{N(\beta)}}\left(\left\|\boldsymbol{\delta}_{\mathrm{pr}}^{(\beta)}\right\| - \delta_{\mathrm{crit}}\right) \tag{5.19}$$

5. Construct ${}^k\mathbf{f}^f$ using ${}^k\mathbf{t}^{Tf(\beta)}$ as shown in Eq, 5.13

## 5.2 Macroscopic tangent moduli

In this section a closed form expression for the macroscopic tangent moduli, $\mathcal{L}_{ijkl}$, is derived. We follow the notation introduced in Section 5.1 for the representation of the values of the fields at the current and previous time steps. Recall that the macroscopic stress is expressed as

$$\bar{\sigma}_{ij}(\mathbf{x},t) = \bar{L}_{ijkl}\bar{\epsilon}_{kl}(\mathbf{x},t) + \sum_{\beta=1}^{m}\bar{\mathbf{R}}_{ij}^{(\beta)}\cdot\hat{\boldsymbol{\delta}}^{(\beta)}(\mathbf{x},t) + \sum_{\gamma=1}^{n}\bar{M}_{ijkl}^{(\gamma)}\mu_{kl}^{(\gamma)}(\mathbf{x},t) \tag{5.20}$$

The coefficient tensors, $\bar{L}_{ijkl}$, $\bar{\mathbf{R}}_{ij}^{(\beta)}$, and $\bar{M}_{ijkl}^{(\gamma)}$ are independent of the macroscopic strain, $\bar{\epsilon}_{kl}(\mathbf{x},t)$. Differentiating Eq. 5.20 with respect to $\bar{\epsilon}_{kl}$ yields

$$\mathcal{L}_{ijkl} = \frac{\bar{\sigma}_{ij}}{\bar{\epsilon}_{kl}} = \bar{L}_{ijkl} + \sum_{\beta=1}^{m}\bar{\mathbf{R}}_{ij}^{(\beta)}\cdot\frac{\partial\hat{\boldsymbol{\delta}}^{(\beta)}}{\partial\bar{\epsilon}_{kl}} + \sum_{\gamma=1}^{n}\bar{M}_{ijmn}^{(\gamma)}\frac{\partial\mu_{mn}^{(\gamma)}}{\partial\bar{\epsilon}_{kl}} \tag{5.21}$$

It remains to evaluate $\partial\mathbf{d}/\partial\bar{\epsilon}_{kl}$. We proceed by recalling the nonlinear system of equations to be solved

$$\hat{\boldsymbol{\Psi}} = \mathbf{K}(\mathbf{d})\mathbf{d} - \mathbf{f}(\mathbf{d};\bar{\epsilon}_{ij}) + \mathbf{f}^c(\mathbf{d}) + \mathbf{f}^f(\mathbf{d}) = 0 \tag{5.22}$$

Differentiating Eq. 5.22 with respect to $\bar{\epsilon}_{kl}$ and using the chain rule leads to

$$\frac{\partial\mathbf{d}}{\partial\bar{\epsilon}_{kl}} = \mathcal{C}^{-1}\frac{\partial\mathbf{f}}{\partial\bar{\epsilon}_{kl}} \tag{5.23}$$

where,

$$\mathcal{C} \equiv \frac{\partial\hat{\boldsymbol{\Psi}}}{\partial\mathbf{d}} = \frac{\partial\mathbf{K}}{\partial\mathbf{d}}\mathbf{d} + \mathbf{K} - \frac{\partial\mathbf{f}}{\partial\mathbf{d}} + \frac{\partial\mathbf{f}^c}{\partial\mathbf{d}} + \frac{\partial\mathbf{f}^f}{\partial\mathbf{d}} \tag{5.24}$$

$\partial\mathbf{f}/\partial\bar{\epsilon}_{kl}$ may be obtained directly from Eq. 5.9

$$\frac{\partial\mathbf{f}}{\partial\bar{\epsilon}_{kl}} = \left[A_{ijkl}^{(1)}\omega_{\mathrm{ph}}^{(1)}, A_{ijkl}^{(2)}\omega_{\mathrm{ph}}^{(2)}, \ldots, A_{ijkl}^{(n)}\omega_{\mathrm{ph}}^{(n)}, \mathbf{C}_{kl}^{(1)}, \mathbf{C}_{kl}^{(2)}, \ldots, \mathbf{C}_{kl}^{(m)}\right]^{\mathrm{T}} \tag{5.25}$$

Derivative of the force vector, $\mathbf{f}$, with respect to $\mathbf{d}$ may be obtained using the chain rule

$$\frac{\partial \mathbf{f}}{\partial \mathbf{d}} = \sum_{\gamma=1}^{n} \frac{\partial \mathbf{f}}{\partial \omega_{\text{ph}}^{(\gamma)}} \frac{\partial \omega_{\text{ph}}^{(\gamma)}}{\partial \mathbf{d}} \tag{5.26}$$

$$\frac{\partial \omega_{\text{ph}}^{(\gamma)}}{\partial \mathbf{d}} = \frac{\partial \omega_{\text{ph}}^{(\gamma)}}{\partial \kappa_{\text{ph}}^{(\gamma)}} \frac{\partial \kappa_{\text{ph}}^{(\gamma)}}{\partial \upsilon_{\text{ph}}^{(\gamma)}} \frac{\partial \upsilon_{\text{ph}}^{(\gamma)}}{\partial \hat{\boldsymbol{\epsilon}}^{(\gamma)}} \frac{\partial \hat{\boldsymbol{\epsilon}}^{(\gamma)}}{\partial \boldsymbol{\epsilon}^{(\gamma)}} \frac{\partial \boldsymbol{\epsilon}^{(\gamma)}}{\partial \tilde{\boldsymbol{\epsilon}}^{(\gamma)}} \frac{\partial \tilde{\boldsymbol{\epsilon}}^{(\gamma)}}{\partial \mathbf{d}} \tag{5.27}$$

$\partial \mathbf{f} / \partial \omega_{\text{ph}}^{(\gamma)}$ may be obtained by differentiating Eq. 5.9 with respect to the phase damage variable, $\omega_{\text{ph}}^{(\gamma)}$

$$\frac{\partial \mathbf{f}}{\partial \omega_{\text{ph}}^{(\gamma)}} = \left[0, \ldots, 0, A_{IJ}^{(\gamma)} \bar{\epsilon}_J, 0, \ldots, 0\right]^{\text{T}} \tag{5.28}$$

$\partial \omega_{\text{ph}}^{(\gamma)} / \partial \kappa_{\text{ph}}^{(\gamma)}$ is evaluated by differentiating Eq. 4.51

$$\frac{\partial \omega_{\text{ph}}^{(\gamma)}}{\partial \kappa_{\text{ph}}^{(\gamma)}} = \frac{a_{\text{ph}}^{(\gamma)}}{\left[\pi/2 + \text{atan}\left(b_{\text{ph}}^{(\gamma)}\right)\right]\left[1 + \left(a_{\text{ph}}^{(\gamma)} \kappa_{\text{ph}}^{(\gamma)} - b_{\text{ph}}^{(\gamma)}\right)^2\right]} \tag{5.29}$$

$\partial \kappa_{\text{ph}}^{(\gamma)} / \partial \upsilon_{\text{ph}}^{(\gamma)} = 1$ for damage process and vanishes if no damage is accumulated at the current time step. From Eqs. 4.46 and 4.47 follows

$$\frac{\partial \upsilon_{\text{ph}}^{(\gamma)}}{\partial \hat{\boldsymbol{\epsilon}}^{(\gamma)}} = \frac{1}{2\upsilon_{\text{ph}}^{(\gamma)}} \left(\mathbf{F}^{(\gamma)} \hat{\boldsymbol{\epsilon}}^{(\gamma)}\right)^{\text{T}} \hat{\mathbf{L}}^{(\gamma)} \frac{\partial \left(\mathbf{F}^{(\gamma)} \hat{\boldsymbol{\epsilon}}^{(\gamma)}\right)}{\partial \hat{\boldsymbol{\epsilon}}^{(\gamma)}} \tag{5.30}$$

where,

$$\frac{\partial \left(\mathbf{F}^{(\gamma)} \hat{\boldsymbol{\epsilon}}^{(\gamma)}\right)}{\partial \hat{\boldsymbol{\epsilon}}^{(\gamma)}} = \begin{bmatrix} \dfrac{\partial \left(h_1^{(\gamma)} \hat{\epsilon}_1^{(\gamma)}\right)}{\partial \hat{\epsilon}_1^{(\gamma)}} & 0 & 0 \\ 0 & \dfrac{\partial \left(h_2^{(\gamma)} \hat{\epsilon}_2^{(\gamma)}\right)}{\partial \hat{\epsilon}_2^{(\gamma)}} & 0 \\ 0 & 0 & \dfrac{\partial \left(h_3^{(\gamma)} \hat{\epsilon}_3^{(\gamma)}\right)}{\partial \hat{\epsilon}_3^{(\gamma)}} \end{bmatrix} \tag{5.31}$$

and,

$$\frac{\partial \left(h_\xi^{(\gamma)} \hat{\epsilon}_\xi^{(\gamma)}\right)}{\partial \hat{\epsilon}_\xi^{(\gamma)}} = \frac{c_1^{(\gamma)}/\pi}{1 + \left[c_1^{(\gamma)}\left(\hat{\epsilon}_\xi^{(\gamma)} - c_2^{(\gamma)}\right)\right]^2} \hat{\epsilon}_\xi^{(\gamma)} + h_\xi^{(\gamma)} \tag{5.32}$$

No summation is implied for superscripts and for Greek indices. The derivative of the principal strain, $\hat{\boldsymbol{\epsilon}}^{(\gamma)}$, with respect to total strain, $\boldsymbol{\epsilon}^{(\gamma)}$ is evaluated by considering the Hamilton's Theorem

$$\left(\hat{\epsilon}_i^{(\gamma)}\right)^3 - I_1 \left(\hat{\epsilon}_i^{(\gamma)}\right)^2 + I_2 \hat{\epsilon}_i^{(\gamma)} - I_3 = 0 \tag{5.33}$$

in which, $I_1$, $I_2$, and $I_3$ are the three strain invariants. Differentiating Eq. 5.33 with respect to total strain yields

$$\frac{\partial \hat{\epsilon}_i^{(\gamma)}}{\partial \epsilon_{kl}^{(\gamma)}} = \left[3\left(\hat{\epsilon}_i^{(\gamma)}\right)^2 - 2I_1 \hat{\epsilon}_i^{(\gamma)} + I_2\right]^{-1} \left[\frac{\partial I_1}{\partial \epsilon_{kl}^{(\gamma)}} \left(\hat{\epsilon}_i^{(\gamma)}\right)^2 - \frac{\partial I_2}{\partial \epsilon_{kl}^{(\gamma)}} \left(\hat{\epsilon}_i^{(\gamma)}\right) + \frac{\partial I_3}{\partial \epsilon_{kl}^{(\gamma)}}\right] \tag{5.34}$$

The derivatives of the invariants are obtained as

$$\frac{\partial I_1}{\partial \epsilon_{ij}^{(\gamma)}} = \delta_{ij}^{\mathrm{K}} \tag{5.35}$$

$$\frac{\partial I_2}{\partial \epsilon_{ij}^{(\gamma)}} = \mathrm{trace}\left(\boldsymbol{\epsilon}^{(\gamma)}\right)\delta_{ij}^{\mathrm{K}} - \epsilon_{ij}^{(\gamma)} \tag{5.36}$$

$$\frac{\partial I_3}{\partial \epsilon_{ij}^{(\gamma)}} = \epsilon_{ik}^{(\gamma)}\epsilon_{kj}^{(\gamma)} - \mathrm{trace}\left(\boldsymbol{\epsilon}^{(\gamma)}\right)\epsilon_{ij}^{(\gamma)} - \frac{1}{2}\epsilon_{kl}^{(\gamma)}\epsilon_{lk}^{(\gamma)}\delta_{ij}^{\mathrm{K}} + \frac{1}{2}\left(\mathrm{trace}\left(\boldsymbol{\epsilon}^{(\gamma)}\right)\right)^2\delta_{ij}^{\mathrm{K}} \tag{5.37}$$

In view of Eq. 3.4 and the derivative of Eq. 3.25, $\partial\boldsymbol{\epsilon}^{(\gamma)}/\partial\tilde{\boldsymbol{\epsilon}}^{(\gamma)}$ is equal to the identity tensor.

It is easy to show that phase average damage induced strains, $\tilde{\boldsymbol{\epsilon}}^{(\gamma)}$ may be expressed in terms of the damage induced strains and displacements jumps

$$\tilde{\epsilon}_{ij}^{(\gamma)} = \sum_{\beta=1}^{m}\hat{\mathbf{R}}_{ij}^{(\gamma\beta)}\cdot\hat{\boldsymbol{\delta}}^{(\beta)} + \sum_{\eta=1}^{n}P_{ijkl}^{(\gamma\eta)}\mu_{kl}^{(\eta)} \tag{5.38}$$

Differentiating $\tilde{\boldsymbol{\epsilon}}^{(\gamma)}$ with respect to $\mathbf{d}$

$$\frac{\partial\tilde{\boldsymbol{\epsilon}}^{(\gamma)}}{\partial\mathbf{d}} = \left[\begin{array}{cccccccc} P_{ijkl}^{(\gamma 1)} & P_{ijkl}^{(\gamma 2)} & \cdots & P_{ijkl}^{(\gamma n)} & \hat{\mathbf{R}}_{ij}^{(\gamma 1)} & \hat{\mathbf{R}}_{ij}^{(\gamma 2)} & \cdots & \hat{\mathbf{R}}_{ij}^{(\gamma m)} \end{array}\right] \tag{5.39}$$

which completes the evaluation of $\partial\mathbf{f}/\partial\mathbf{d}$.

The derivative of the contact constraint penalty contribution $\mathbf{f}^c$ with respect to $\mathbf{d}$ may be evaluated directly from Eq. 5.10 in the form

$$\frac{\partial\mathbf{f}^c}{\partial\mathbf{d}} = -\frac{1}{2\chi}\left[\begin{array}{cc}\mathbf{0} & \mathbf{0}\\ \mathbf{0} & d\mathbf{f}^c\end{array}\right] \tag{5.40}$$

where,

$$d\mathbf{f}^c = \left[\begin{array}{ccccccccccc}
1-\mathrm{sgn}(\delta^{N(1)}) & 0 & 0 & 0 & 0 & 0 & \dots & 0 & 0 & 0\\
0 & 0 & 0 & 0 & 0 & 0 & \dots & 0 & 0 & 0\\
0 & 0 & 0 & 0 & 0 & 0 & \dots & 0 & 0 & 0\\
0 & 0 & 0 & 1-\mathrm{sgn}(\delta^{N(2)}) & 0 & 0 & \dots & 0 & 0 & 0\\
0 & 0 & 0 & 0 & 0 & 0 & \dots & 0 & 0 & 0\\
0 & 0 & 0 & 0 & 0 & 0 & \dots & 0 & 0 & 0\\
\vdots & \vdots & \vdots & \vdots & \vdots & \vdots & \ddots & \vdots & \vdots & \vdots\\
0 & 0 & 0 & 0 & 0 & 0 & \dots & 1-\mathrm{sgn}(\delta^{N(m)}) & 0 & 0\\
0 & 0 & 0 & 0 & 0 & 0 & \dots & 0 & 0 & 0\\
0 & 0 & 0 & 0 & 0 & 0 & \dots & 0 & 0 & 0
\end{array}\right] \tag{5.41}$$

in which $\mathrm{sgn}\left(\Diamond\right) = |\Diamond|/\Diamond$ is the sign operator.

$\mathbf{K}$ is a function of phase and interface damage variables, $\omega_{\mathrm{ph}}^{(\gamma)}$ and $\omega_{\mathrm{int}}^{(\beta)}$ as shown in Eqs. 5.2-5.8. Using the chain rule

$$\frac{\partial\mathbf{K}}{\partial\mathbf{d}} = \sum_{\gamma=1}^{n}\frac{\partial\mathbf{K}}{\partial\omega_{\mathrm{ph}}^{(\gamma)}}\frac{\partial\omega_{\mathrm{ph}}^{(\gamma)}}{\partial\mathbf{d}} + \sum_{\beta=1}^{m}\frac{\partial\mathbf{K}}{\partial\omega_{\mathrm{int}}^{(\beta)}}\frac{\partial\omega_{\mathrm{int}}^{(\beta)}}{\partial\mathbf{d}} \tag{5.42}$$

Equation 5.3 reveals that the nonzero components of the derivatives of $\mathbf{K}$ with respect to damage

variables are $\partial \mathbf{K}_{\rm PP}/\partial\omega_{\rm ph}^{(\gamma)}$; $\partial \mathbf{K}_{\rm PI}/\partial\omega_{\rm ph}^{(\gamma)}$; and $\partial \mathbf{K}_{\rm II}/\partial\omega_{\rm int}^{(\beta)}$

$$\frac{\partial \mathbf{K}_{\rm PP}}{\partial \omega_{\rm ph}^{(\gamma)}} = \begin{bmatrix} 0 & 0 & \dots & 0 \\ \vdots & \vdots & \ddots & \vdots \\ 0 & 0 & \dots & 0 \\ -P_{ijkl}^{(\gamma 1)} & -P_{ijkl}^{(\gamma 2)} & \dots & -P_{ijkl}^{(\gamma n)} \\ 0 & 0 & \dots & 0 \\ \vdots & \vdots & \ddots & \vdots \\ 0 & 0 & \dots & 0 \end{bmatrix} \tag{5.43}$$

$$\frac{\partial \mathbf{K}_{\rm PI}}{\partial \omega_{\rm ph}^{(\gamma)}} = \begin{bmatrix} 0 & 0 & \dots & 0 \\ \vdots & \vdots & \ddots & \vdots \\ 0 & 0 & \dots & 0 \\ -\hat{\mathbf{R}}_{ij}^{(\gamma 1)} & -\hat{\mathbf{R}}_{ij}^{(\gamma 2)} & \dots & -\hat{\mathbf{R}}_{ij}^{(\gamma n)} \\ 0 & 0 & \dots & 0 \\ \vdots & \vdots & \ddots & \vdots \\ 0 & 0 & \dots & 0 \end{bmatrix} \tag{5.44}$$

The only nonzero component in $\partial \mathbf{K}_{\rm II}/\partial\omega_{\rm int}^{(\beta)}$ is $\partial \mathbf{E}^{(\beta)}/\partial\omega_{\rm int}^{(\beta)}$, given by

$$\frac{\partial \mathbf{E}^{(\beta)}}{\partial \omega_{\rm int}^{(\beta)}} = \begin{bmatrix} -k_N^{(\beta)} & 0 & 0 \\ 0 & -k_T^{(\beta)} & 0 \\ 0 & 0 & -k_T^{(\beta)} \end{bmatrix} \tag{5.45}$$

The derivative of the interface damage variables,$\omega_{\rm int}^{(\beta)}$, with respect to $\mathbf{d}$ may be expanded using the chain rule

$$\frac{\partial \omega_{\rm int}^{(\beta)}}{\partial \mathbf{d}} = \frac{\partial \omega_{\rm int}^{(\beta)}}{\partial \kappa_{\rm int}^{(\beta)}} \frac{\partial \kappa_{\rm int}^{(\beta)}}{\partial \upsilon_{\rm int}^{(\beta)}} \frac{\partial \upsilon_{\rm int}^{(\beta)}}{\partial \mathbf{d}} \tag{5.46}$$

where,

$$\frac{\partial \omega_{\rm int}^{(\beta)}}{\partial \kappa_{\rm int}^{(\beta)}} = \frac{b_{\rm int}^{(\beta)2}}{\left[\operatorname{atan}\left(a_{\rm int}^{(\beta)}\right)\right]\left[b_{\rm int}^{(\beta)2} + \left(a_{\rm int}^{(\beta)}\kappa_{\rm int}^{(\beta)}\right)^2\right]} \tag{5.47}$$

$\partial \kappa_{\rm int}^{(\beta)}/\partial \upsilon_{\rm int}^{(\beta)} = 1$ for damage process and vanishes if no damage is accumulated at the time step.

$$\frac{\partial \upsilon_{\rm int}^{(\beta)}}{\partial \mathbf{d}} = \left[0, \dots, 0, k_N^{(\beta)}, \frac{\delta_1^{T(\beta)}}{\left\|\boldsymbol{\delta}^{T(\beta)}\right\|} k_T^{(\beta)}, \frac{\delta_2^{T(\beta)}}{\left\|\boldsymbol{\delta}^{T(\beta)}\right\|} k_T^{(\beta)}, 0, \dots, 0\right] \tag{5.48}$$

We now turn our attention to the last term in $\mathcal{C}$. When the elastic stick condition is in effect, consistent linearization of the friction algorithm presented in Section 5.1 leads to

$$\partial \mathbf{t}^{Tf(\beta)} = \frac{\mu_F t^{N(\beta)}}{\delta_{\rm crit}} \partial \boldsymbol{\delta}^{T(\beta)} + \mathbf{n} \frac{\mu_F}{2\chi} \left[1 - \operatorname{sgn}\left(\delta^{N(\beta)}\right)\right] \partial \delta^{N(\beta)} \tag{5.49}$$

in which, $\mathbf{n} = \mathbf{t}^{Tf(\beta)}/t^{N(\beta)}$. In the presence of plastic slip the final result is

$$\partial \mathbf{t}^{Tf(\beta)} = \left(\boldsymbol{\delta}^{\rm K} - \mathbf{n} \otimes \mathbf{n}\right) \frac{\mu_F t^{N(\beta)}}{\left\|\boldsymbol{\delta}_{\rm pr}^{(\beta)}\right\|} \partial \boldsymbol{\delta}^{T(\beta)} + \mathbf{n} \frac{\mu_F}{2\chi} \left[1 - \operatorname{sgn}\left(\delta^{N(\beta)}\right)\right] \partial \delta^{N(\beta)} \tag{5.50}$$

Equations 5.49 and 5.50 are sufficient to evaluate the derivative of $\mathbf{f}^f$ with respect to $\mathbf{d}$ in view of Eq. 5.13.

## 5.3 Extension to large macro-deformation

In Section 5.1 it was assumed that stress at the current increment $\bar{\sigma}_{ij}$ can be computed from strain ${}_t\bar{\epsilon}_{ij}$ and state of damage ${}_t\mathbf{d}$ in the previous increment as well as the current strain increment, $\Delta\bar{\epsilon}_{ij}$ that drives the evolution of eigenstrains and interface decohesion. In other words, only material response was accounted for, while the effect of large deformation has been neglected. In this section we discuss the effect of large deformation. For this purpose it is convenient to split the effect of large deformation into two parts. One is due to large deformation within a local coordinate system attached to a unit cell. The second is due to large rotation of the entire unit cell as a rigid body. The former gives rise to unit cell distortion, while the latter, termed as macromechanical rotation, does not affect stresses in the material or so-called co-rotational frame. While in principle, the proposed model reduction approach can handle the two sources of deformation, accounting for unit cell distortion requires repeated calculation of the influence functions. This in turn requires solution of the unit cell problems at every increment and at every iteration, making the computational cost comparable to that of the direct homogenization method.

On the other hand, accounting for macromechanical rotation increment, denoted as $\Delta\bar{R}$, can be easily accommodated within the existing computational framework either by using a two-step stress update approach or by utilizing co-rotational formulation [47, 48]. For instance, in the two-step approach, stresses are first rotated to the material frame using macro-rotation increment, $\Delta\bar{R}$. This is followed by material stress update as described in Section 5.1. Finally, updated stresses are rotated back to the global Cartesian frame. For microstructures with obvious definition of material coordinate system, such as in the case of fibrous composites, $\Delta\bar{R}$ is an incremental rotation of the specific material coordinate system. On the other hand, in case of particles randomly distributed in the microstructure, the incremental rotation, $\Delta\bar{R}$ can be computed from either the incremental vorticity [49] or from polar decomposition.

# 6 Verification and Validation

Our numerical experimentation agenda includes three test problems: (i) verification for a single scale (one unit cell) problem; (ii) verification for a two-scale problem, and; (iii) validation problem. For verification, comparison is made to direct homogenization, while, for validation, comparison is made to physical experiment.

## 6.1 Single-scale verification studies

We consider a single fibrous unit cell subjected to static loading. The geometry of the microstructure is illustrated in Fig. 10. The unit cell consists of a fiber with a circular cross section. The volume fraction of the fiber in the unit cell is 19.6%. The finite element mesh of the unit cell, depicted in Fig. 10, consists of 930 hexahedral elements. The fiber phase consists of 270 elements and the material properties are taken to be Young's Modulus = 200 GPa and Poisson's ratio = 0.3. The fiber material is assumed to be isotropic elastic with no damage accumulation. The elastic properties of the matrix material are taken as Young's Modulus = 60 GPa and Poisson's ratio = 0.3. The phase damage evolution parameters of the matrix material are $a_{\text{ph}} = 32$, and $b_{\text{ph}} = 16.3$. The compressive principal strain components do not contribute to damage accumulation. The weighting matrix (Eq. 4.48) parameters are therefore chosen as $c_1 = 1 \times 10^5$ and $c_2 = 0$. The interface between the fiber and the matrix phase consists of 176 double nodes. The interface damage evolution parameters are $a_{\text{int}} = 6.67$, and $b_{\text{int}} = 6.67 \times 10^{-4}$.

The macroscopic finite element mesh consists of a single 8 node hexahedral element. The coefficient tensors are computed *a-priori* based on the elastic properties of the matrix and fiber materials. The finite element analysis of the unit cell configuration using the original system of equations provided by

Eqs. 2.4-2.6, 2.10-2.13, and 2.15-2.24 are evaluated as the reference solution for verification purposes. Verification simulations consist of:

C1. Biaxial expansion in the directions orthogonal to the fiber in the presence of interface damage only

C2. Uniaxial expansion in a direction orthogonal to the fiber in the presence of interface damage only

C3. Biaxial expansion in the directions orthogonal to the fiber in the presence of interface and matrix damage

C4. Uniaxial expansion in the directions orthogonal to the fiber in the presence of interface and matrix damage

C5. Uniaxial expansion along the fiber direction in the presence of interface and matrix damage

In C1, The matrix and the fiber are assumed to be linear and elastic with damage accumulation only along the interfaces. The simulations were conducted until full separation along the matrix-fiber interface as shown in Fig. 11a. Figure 11b displays the force-displacement curves as computed using the reference and a 1+0 point model. Note that number of phase partitions, $n$, is set to zero since damage is not allowed to accumulate within phases and does not contribute to damage induced fields. The force-displacement curves show an excellent agreement between the reference solution and the 1+0 point model. Next, failure under uniaxial loading is considered (C2). Similar to C1, the phase materials are assumed to be elastic. Figure 12a displays a nonuniform loading along the interface. Therefore, characterization of the interface calls for multiple partitions. Figure 12b shows the force-displacement comparison of the 1+0 and 2+0 point models against the reference solution. Improved results can be seen as the model is refined. Simulations C3 and C4 employ identical loading conditions with C1 and C2, respectively. In the present simulations, the matrix material is allowed to accumulate damage in addition to interface debonding. The force displacement curves (Figs. 13, 14) in both configurations are in reasonable agreement with the reference configurations for low point models such as 1+1, 2+2 and 2+5 point models. In the last series of simulations (C5), uniaxial loading is applied in the direction of the elastic fibers. Upon degradation of the phase materials, loading is expected to be transferred by the fibers only. Figure 15 shows the force-displacement diagram for configuration C5. The 1+1 point model successfully predicts the failure in the matrix and the post failure stiffness.

## 6.2 Two scale verification study

We consider a crack propagation problem in a square panel with a blunt notch. Figure 16 illustrates the macroscopic geometry and the finite element mesh of the composite panel. An initial notch of length, $a_0$, is introduced such that $a_0/l = 0.5$, where $l$ is the width of the panel. The thickness to width ratio of the panel is $t/l = 0.125$ The macroscopic mesh is composed of 509 hexahedral reduced integration elements. Finite elements far away from the crack tip are modeled as elastic with homogenized properties computed using classical linear elastic homogenization theory. The inelastic zone shown in Fig. 16 is composed of 320 elements. The composite material fibrous microstructure is shown in Fig. 17. The fiber is assumed to be elastic with Young's modulus, $E = 200$ GPa and Poisson's ratio, $\nu = 0.3$. The matrix material is assumed to behave according to nonlocal damage model presented in Section 4.1. The initial elastic properties of the matrix materials are: $E = 60$ GPa and Poisson's ratio, $\nu = 0.3$. The phase damage evolution parameters of the matrix material are $a_{\text{ph}} = 32$, and $b_{\text{ph}} = 16.3$. The weighting matrix parameters are chosen such that no damage is accumulated when the material is under pure compression: $c_1 = 1 \times 10^5$ and $c_2 = 0$. The fiber volume fraction of the microstructure is 28.2%. The interface between the matrix and fiber is assumed to be perfect. The microscale mesh is composed of 351 tetrahedral elements.

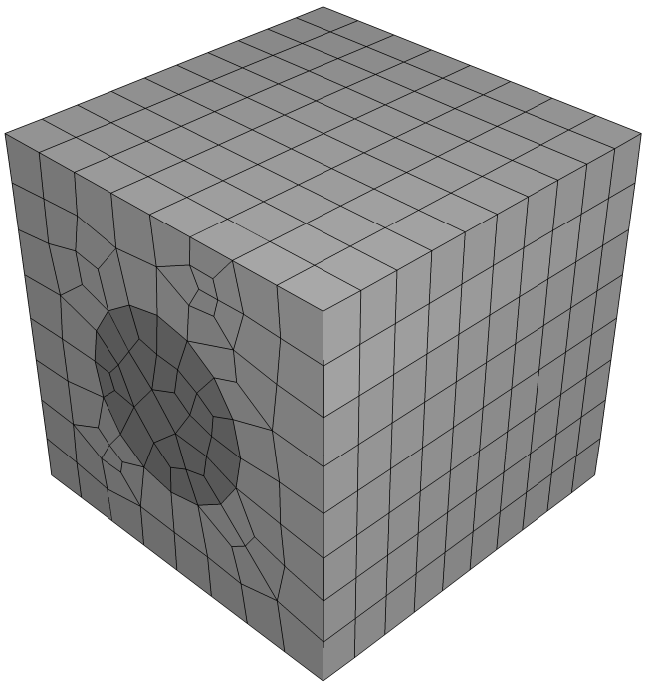

Figure 10: Geometry and the finite element mesh of the fibrous unit cell.

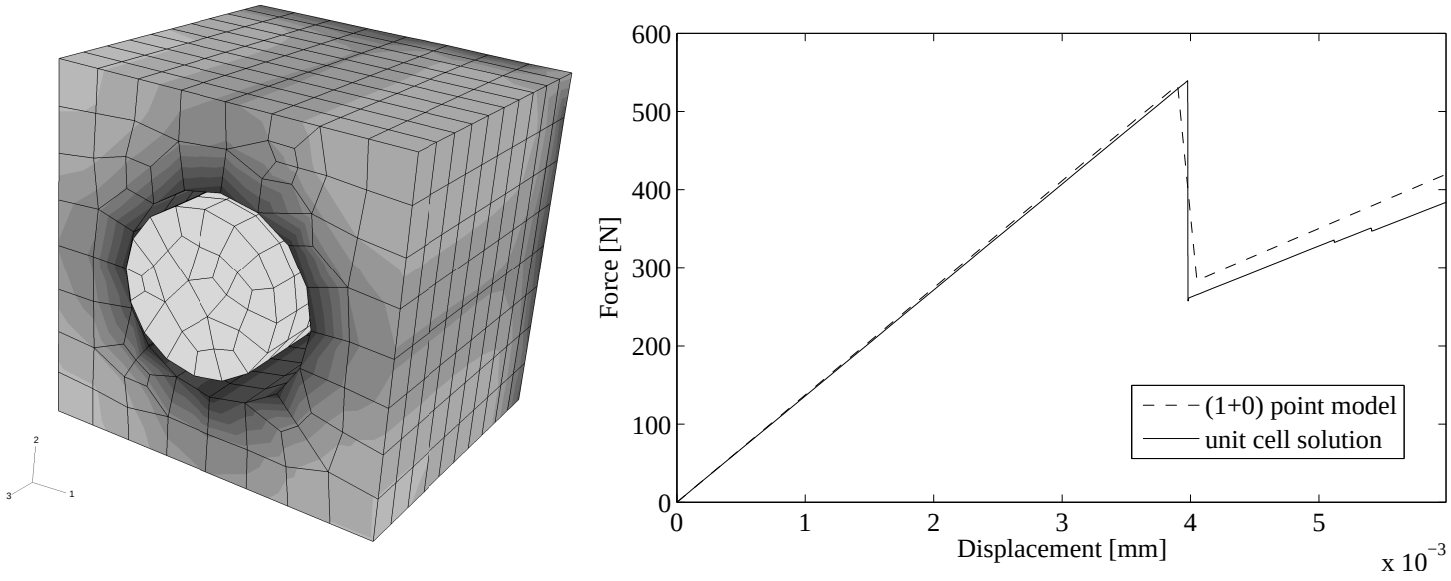


Figure 11: Interface debonding in the fibrous unit cell under biaxial expansion (C1).

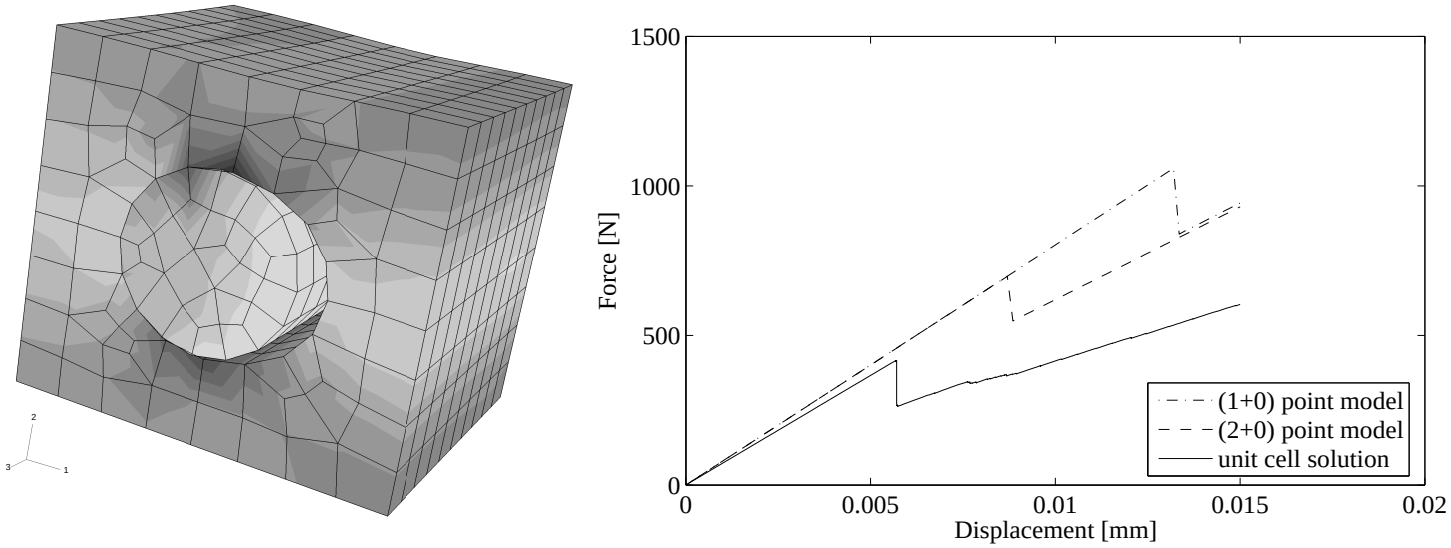


Figure 12: Interface debonding in the fibrous unit cell under uniaxial tension (C2).

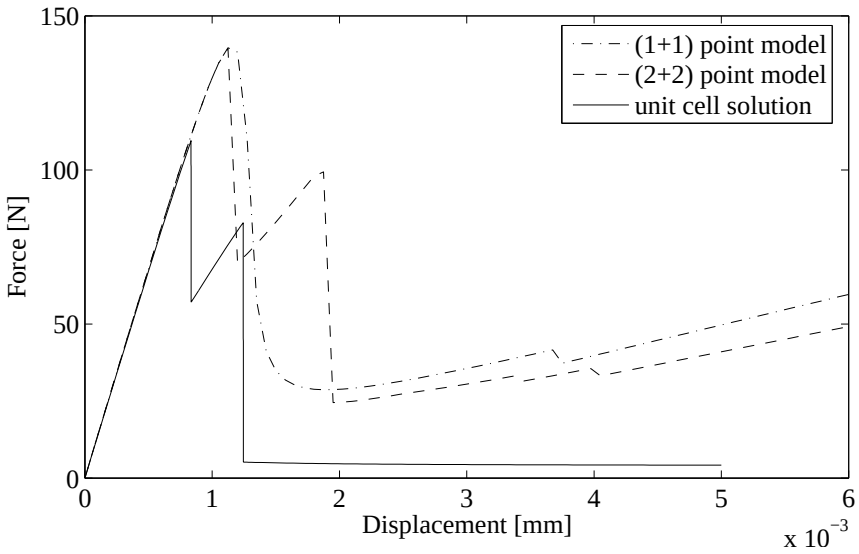


Figure 13: Force displacement curve under biaxial expansion orthogonal to the fiber direction (C3).

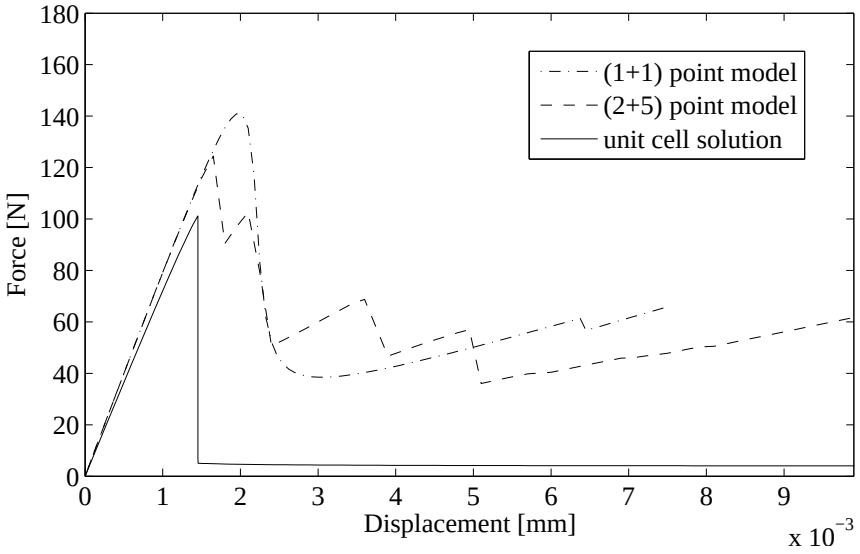


Figure 14: Force displacement curve under uniaxial tension orthogonal to the fiber direction (C4).

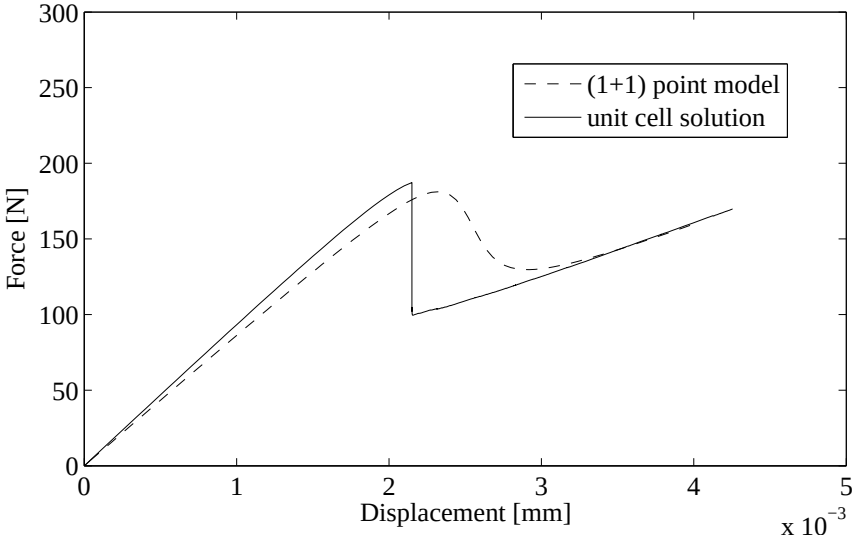


Figure 15: Force displacement curve under uniaxial tension along the fiber direction (C5).

Table 1: Performance of the $(m+n)$ point models and direct homogenization method

| Model | # of incr. | # of iter. | incr. / iter | CPU time |
|---|---|---|---|---|
| (0+1) point | 32 | 57 | 1.78 | $\sim$ 1 min. |
| (0+5) point | 32 | 122 | 3.81 | $\sim$ 3 min. |
| variable point | 32 | 109 | 3.41 | $\sim$ 5 min. |
| (0+10) point | 32 | 112 | 3.50 | $\sim$ 25 min. |
| reference | 9 | 81 | 9.00 | $\sim$ 6 days |

A number of $(0+n)$ point models were verified against the direct homogenization method for the notched panel problem. In the direct homogenization method, the entire unit cell problem as outlined in Box 1 is repeatedly solved at every increment and at every integration point of the macroscopic finite element mesh (see for instance [11] and [16]). In the limit, as the $(3n+2m)$ approach the number of degrees of freedom in the direct homogenization approach the results of the two methods will provide comparable results. Therefore, the direct homogenization approach is used as a reference solution. The errors associated with the direct homogenization approach are well documented (see for instance [10]) and the discussion on this subject is outside the scope of this manuscript.

In the first set of simulations, the $90^0$ degree lay-up (i.e., fibers lie in the direction perpendicular to the notch) of the microstructure is considered. The panel is subjected to uniform loading along the fiber direction. Figure 18 depicts the crack propagation paths as calculated using $(0+1)$, $(0+5)$, and (0+10) point models, in comparison to the direct homogenization method. It can be seen that the crack tends to propagate close to the fiber direction with elastic fibers serving as "barriers" against mode I propagation. Figure 19 illustrates crack propagation paths computed using a variable point model and dynamic domain partitioning strategy. In the variable point model, damage zone is divided into 3 zones, and modeled with (0+10) point model immediately around the notch, (0+5) point model in the intermediate zone, and (0+1) point model away from the notch using the static partitioning technique (Fig. 19). In the dynamic domain partitioning, the highest order model is chosen to be $(0+10)$. The crack length versus loading (time) plots, illustrated in Fig. 20, indicates that $(0+5)$ and $(0+10)$ point models, in addition to the variable point and dynamic domain partitioning are in reasonable agreement with the direct homogenization method. Table 1 summarizes the computational cost of various models in terms of total CPU time, number of iterations and average number of iterations per increment. The computational cost of the $(0+5)$ point model is roughly 3000 times lower than that of direct homogenization, and the crack growth is within 85% accuracy which is acceptable from the engineering standpoint.

In the second set of simulations, we consider a $0^0$ lay-up, in which the fibers are parallel to the notch. The panel is loaded orthogonal to the fiber direction. Figure 21 displays the snapshots of the simulations conducted using $(0+1)$, $(0+2)$, and $(0+5)$ point models compared to the direct homogenization method. It can be seen that all models predict crack propagation in mode I. Figure 22 illustrates the crack length-versus load comparison for various $(0+n)$ point models and the direct homogenization method. As in the previous example, the $(0+5)$ point model was found to be in excellent agreement with the reference solution.

# 7 Validation study

For model validation, we study fragmentation failure of a composite tube subjected to impact loading. The tube crush experiment was conducted by Starbuck *et al.* [50]. The experiment is concerned with the characterization of the energy absorption capabilities of carbon fiber reinforced composite tubes under intermediate rate crushing loads. The specimen is a 10 cm-by-10 cm square tube with a 2 mm thickness. The composite material consists of 0-90 woven T300B carbon fiber tows (with a tow size

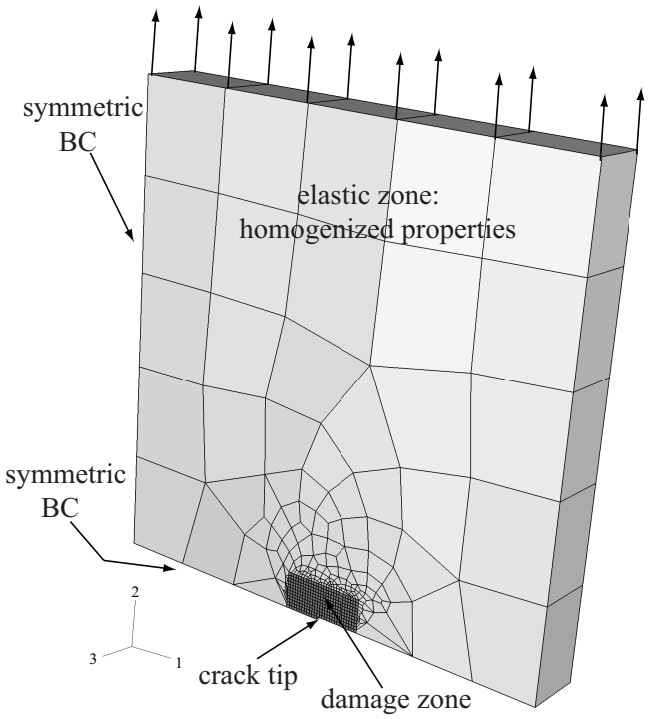


Figure 16: Geometry and the finite element mesh of the panel with a blunt notch.

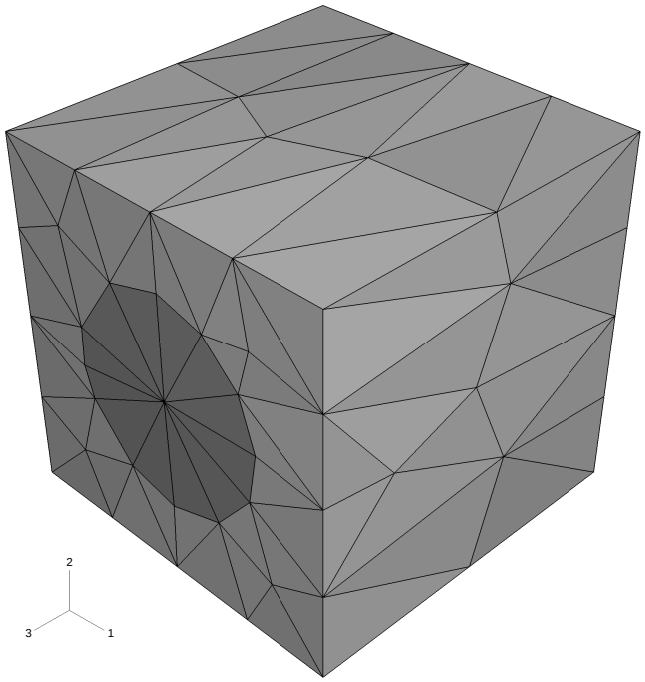


Figure 17: Fibrous microstructure of the panel with a blunt notch.

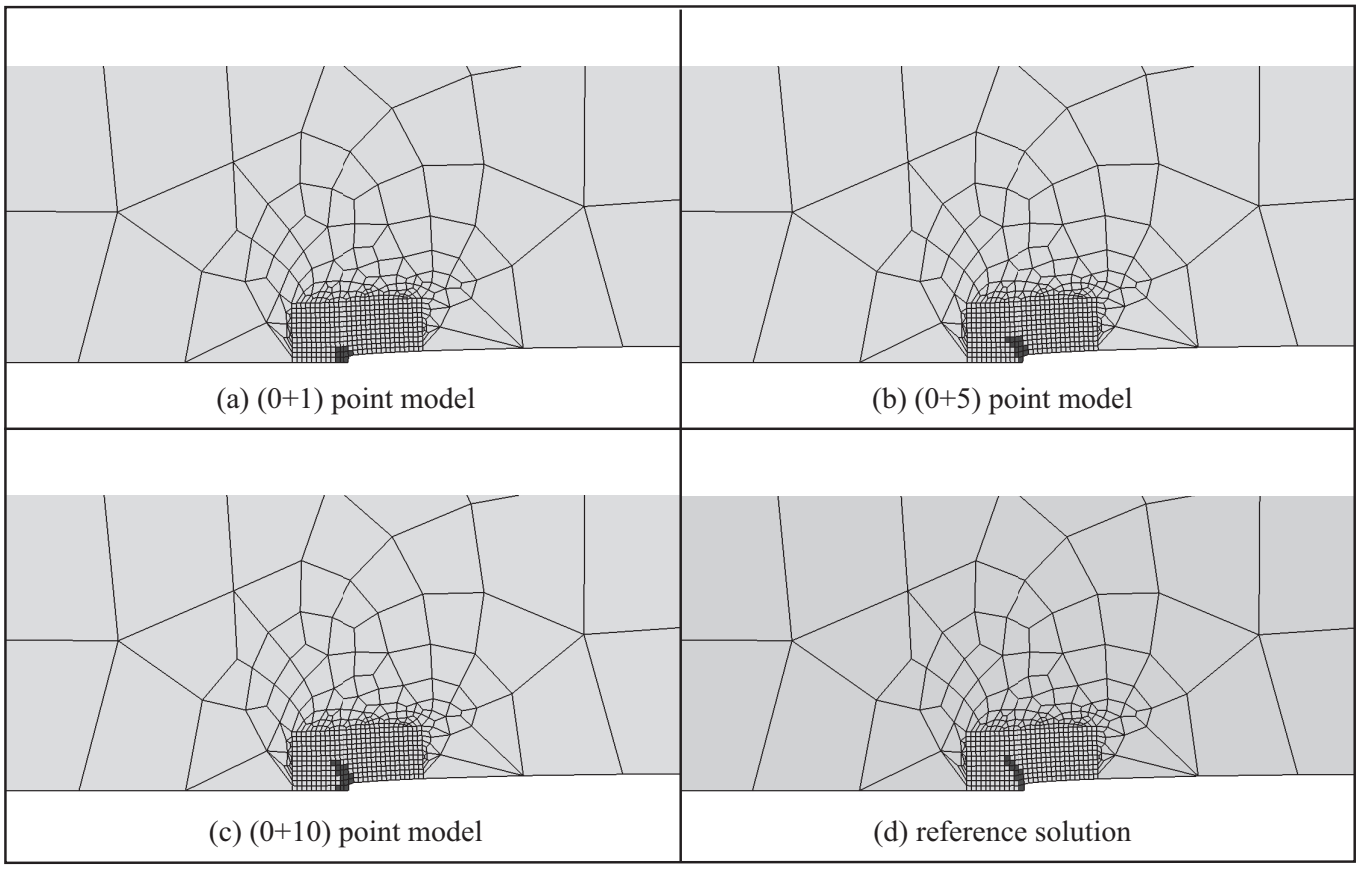


Figure 18: Crack paths of the $(0+n)$ point models and the reference solution for $90^0$ lay-up.

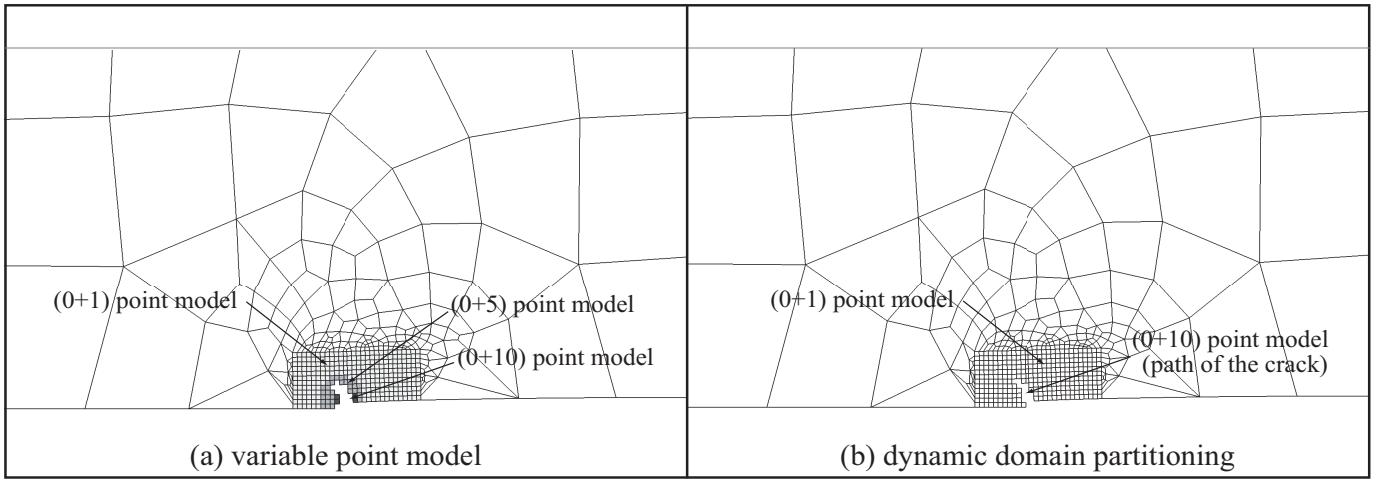


Figure 19: Crack paths by the variable point model and dynamic domain partitioning method.

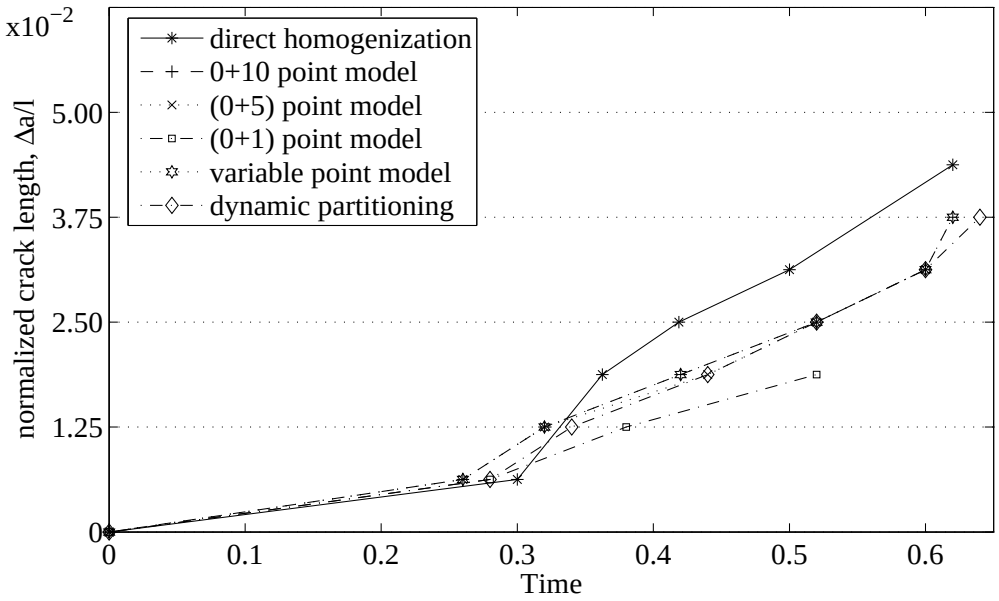


Figure 20: Crack growth curves for $90^0$ lay-up.

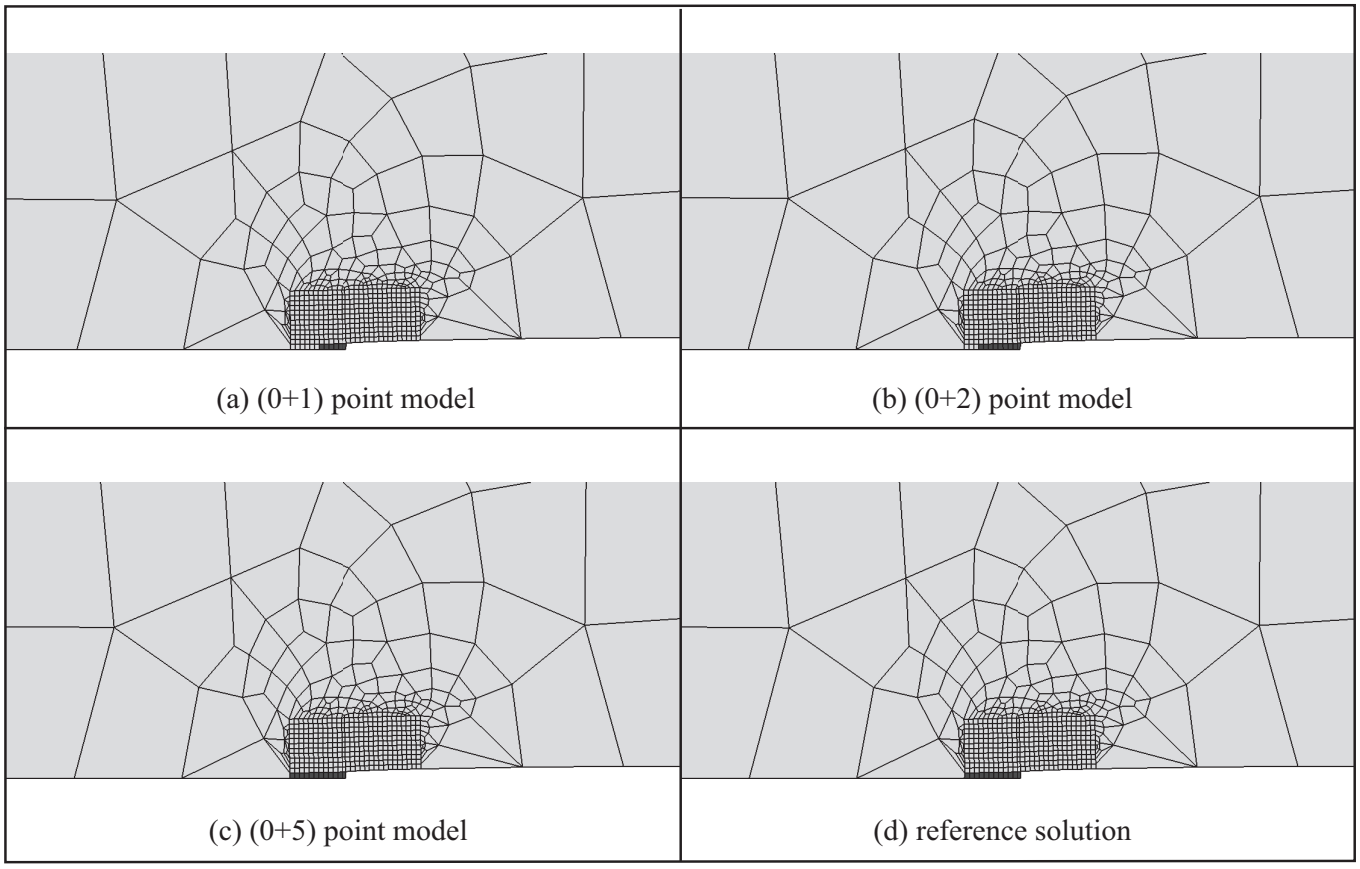


Figure 21: Crack paths of the $(0 + n)$ point models and the reference solution for $0^0$ lay-up.

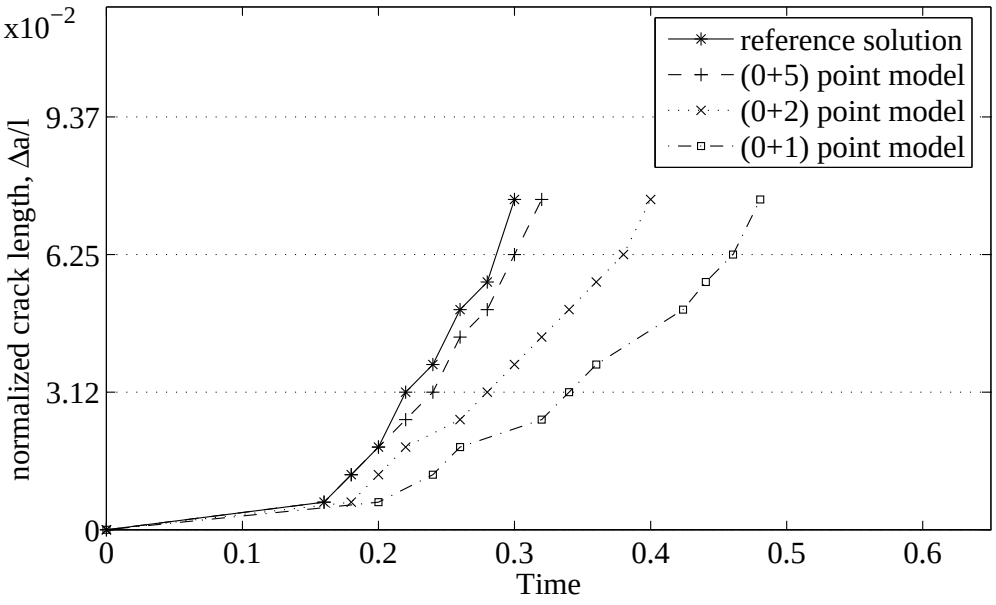


Figure 22: Crack growth curves for $0^0$ lay-up.

Table 2: Material property values used in the tube crush simulation

| $E^{(F)}$ | $\nu^{(F)}$ | $E^{(M)}$ | $\nu^{(M)}$ | |
|---|---|---|---|---|
| 235 GPa | 0.26 | 3.2 GPa | 0.35 | |
| $k_N$ | $k_T$ | $a_{\text{int}}$ | $b_{\text{int}}$ | |
| 1.E5 GPa/mm | 1.E5 GPa/mm | 6.67 | 1.7E3 | |
| $a_{\text{ph}}^{(FT)}$ | $a_{\text{ph}}^{(FT)}$ | $c_1^{(FT)}$ | $c_2^{(FT)}$ | $\upsilon_{\text{ini}}^{(FT)}$ |
| 0.5 | 1.0 | -100.0 | 0.0 | 0.0 |
| $a_{\text{ph}}^{(M)}$ | $a_{\text{ph}}^{(M)}$ | $c_1^{(M)}$ | $c_2^{(M)}$ | $\upsilon_{\text{ini}}^{(M)}$ |
| 4.0 | 1.0 | -100.0 | 0.0 | 0.0 |

of 3000 individual fibers) and epoxy resin. The weight percentage of the fiber tows is 58%. The tube specimen was subjected to 4 m/s constant velocity compressive loading and crushing behavior was monitored. Figure 23 shows snapshots of the specimen at the beginning, during, and at the end of the loading.

The microstructure of the carbon fiber composite is idealized using the finite element mesh depicted in Fig. 24. The microstructural mesh of the woven composite system includes 370 and 1196 tedrahedra in the fiber and matrix phases, respectively. The discretization of the 0-90 woven carbon fiber is shown in Fig. 24b. We consider a $(1+3)$ point model where the matrix-fiber interface is represented with a single point; one point for matrix phase, and two points for fiber phase, one in each direction. The $(1+3)$ point model is considered throughout the tube geometry and no adaptivity is employed in this simulation.

Static tension and compression coupon test data, provided by Starbuck *et al.* [50], is employed to calibrate the failure properties of the interface and phase materials. The material properties used in the simulation is summarized in Table 2. The total number of material parameters is 19, which include the elastic properties of the matrix and the fiber, interface and phase failure parameters. The provided coupon tests fail to adequately span all possible failure modes the material may exhibit. Therefore, a number of assumptions were made for some of the material parameters. The elastic properties of the fiber tows are obtained by considering them as fibrous composite. (Fig. 25). The Young's modulus

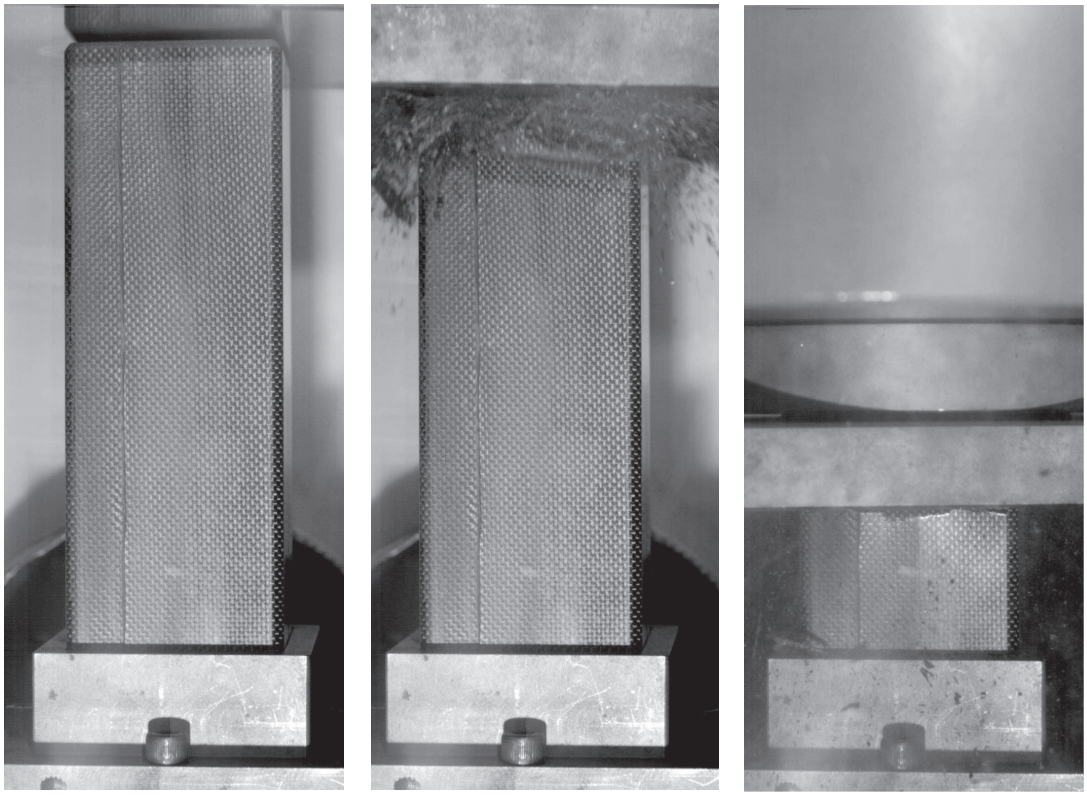

Figure 23: Snapshots of the tube specimen at the beginning, during and at the end of loading. Experiment conducted by Starbuck *et al.* [50]

.

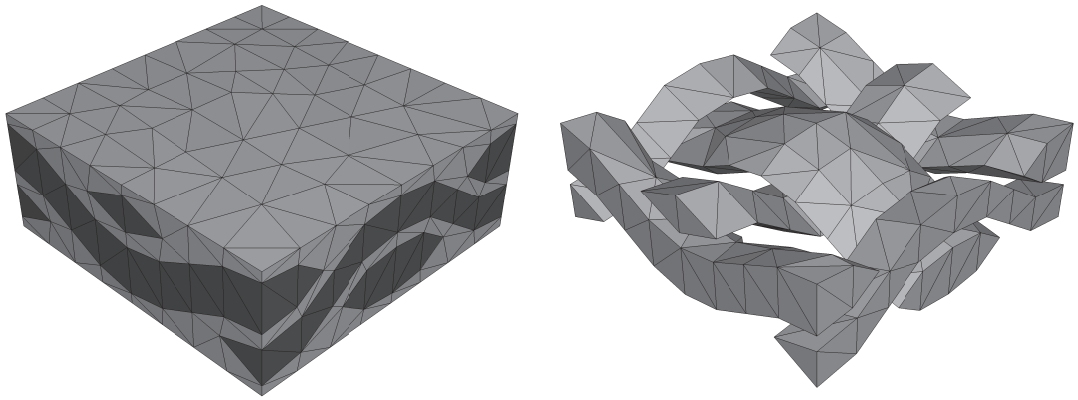

Figure 24: The finite element mesh of the woven carbon fiber composite microstructure of the tube specimen

.

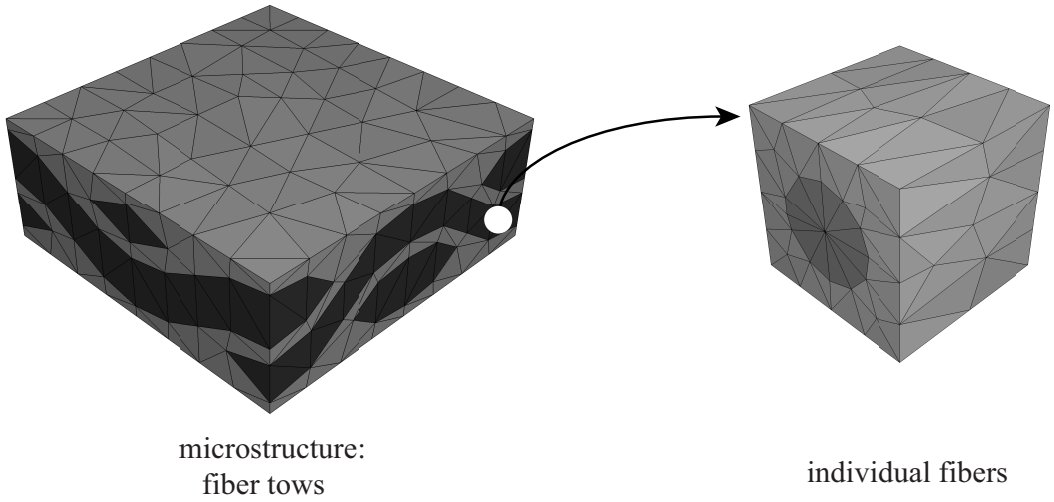


Figure 25: Calibration of the elastic properties by modeling elastic homogenization of the fiber tows

.

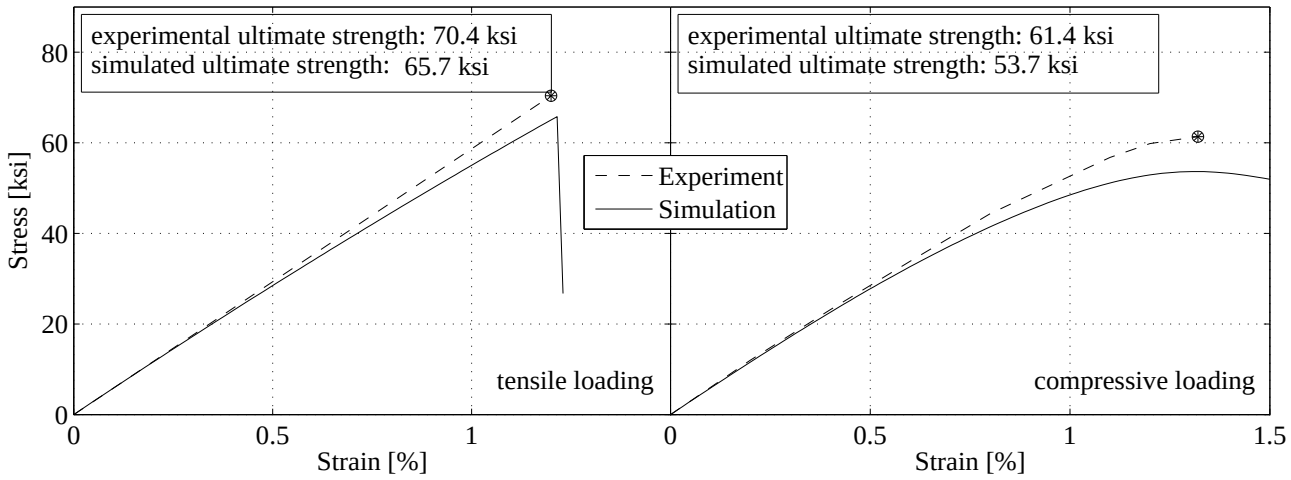


Figure 26: Stress-strain curves provided by the experiments and calibrated multiscale model

.

and Poisson's ratio of the individual fibers ($E^{(F)}$, $\nu^{(F)}$) as well as the matrix material ($E^{(M)}$, $\nu^{(M)}$) were calibrated based on the elastic properties provided by the coupon tests and the virgin properties of the fiber tows. The interface behavior is assumed to be isotropic ($k_N = k_T$). The frictional forces in the tangential direction are assumed to be due to adhesion only ($\mu_F = 0$). Within phases, the damage is set to accumulate at the onset of loading: $\upsilon_{\text{ini}}^{(FT)} = \upsilon_{\text{ini}}^{(M)} = 0$, where, $\upsilon_{\text{ini}}^{(FT)}$ and $\upsilon_{\text{ini}}^{(M)}$ are threshold values for the damage equivalent strains in the fiber tows and matrix phases, respectively. The failure parameters were then set by minimizing the discrepancy between the experimental and simulated stress-strain curves. Figure 26 illustrates the stress-strain curves provided by the experiments and calibrated multiscale model.

The tube mesh consists of 17908 quadrilateral shell elements. Plane stress conditions were imposed. The proposed model is incorporated into ABAQUS EXPLICIT finite element code. Fragmentation of the composite tube was modeled using element deletion technique. By this approach, the elements were set to vanish provided that one of the two criteria is satisfied: (a) full damage within the matrix phase and in the circumferential fiber direction; (b) full damage within the matrix phase and debonding

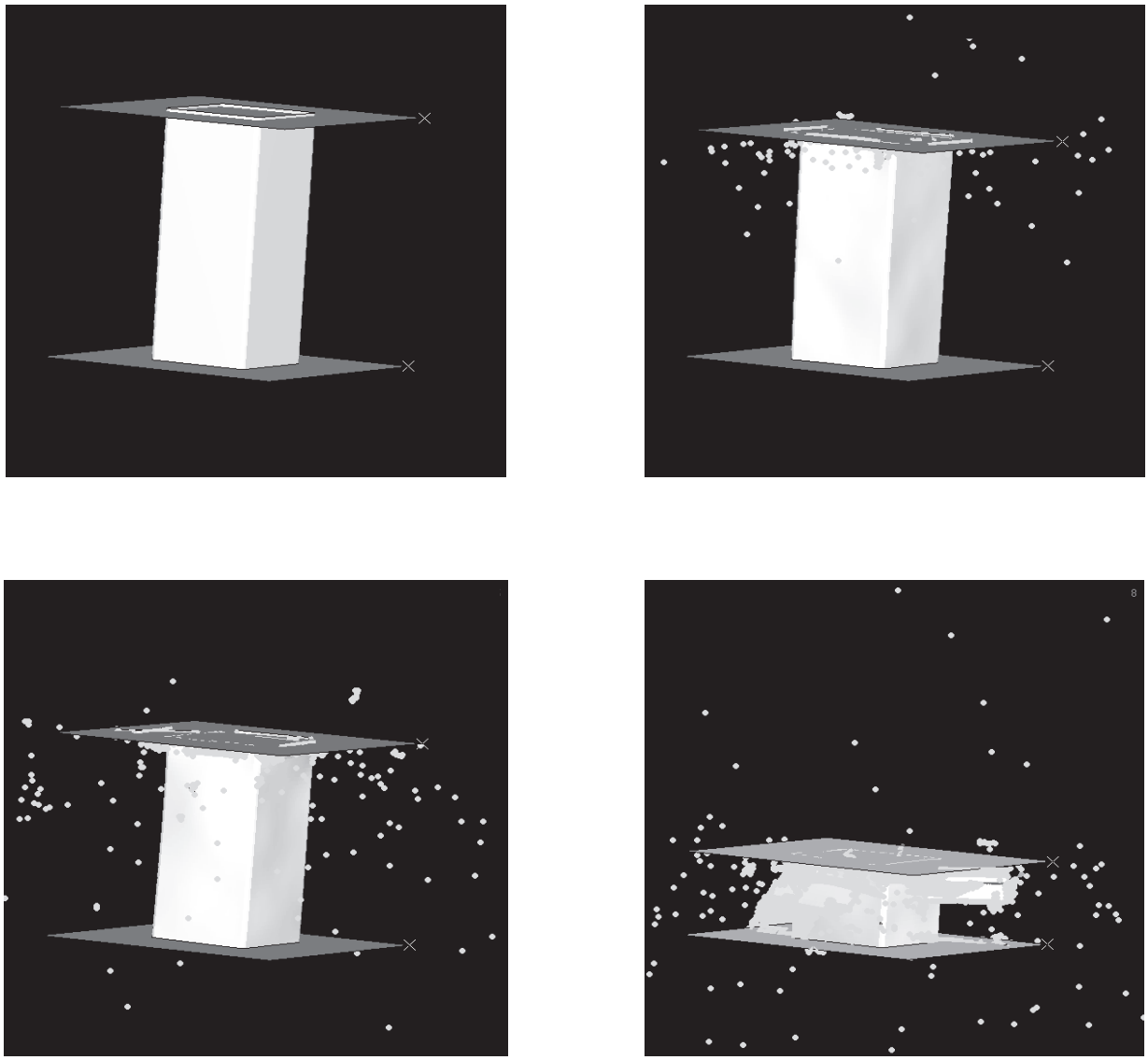

Figure 27: Snapshots of the tube simulation at the beginning, during and at the end of loading.

.

along the matrix fiber interface.

Figure 27 illustrates the snapshots of the tube crush simulation prior to, during, and at the end of the loading. Comparison of the experimental and simulated snapshots reveals a similar fragmentation and failure pattern. Force-displacement curves are presented in Fig. 28. The simulated and the experimental curves were found to be reasonable agreement; energy absorption (area under force-displacement curve) predicted by the simulation was approximately 20% lower than in the actual experiment. This discrepancy can be attributed to variety of factors including: uncertainty in material data, material calibration error, strain rate sensitivity and others. The computational cost of the tube crush simulations with the $(1+3)$ point model is approximately 14 days using a single 3.16GHz Pentium 4 processor. In view of the performance results of the two-scale verification study presented in Section 6.2, tube crush simulation using the direct homogenization method is clearly computationally exhaustive with the allocated computational resources.

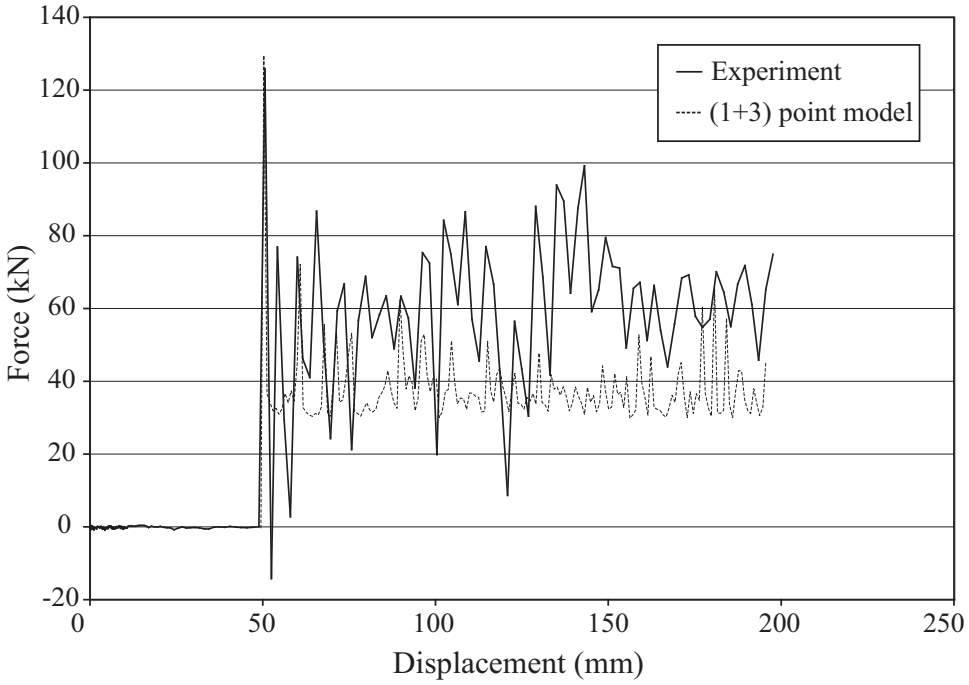


Figure 28: Experimental and simulated force-displacement curves of the tube specimen

.

# 8 Summary and Future Research Directions

We presented a new mesomechanical homogenization approach, which combines salient features of multiple scale asymptotic expansion method with the transformation field analysis in attempt to reduce the computational cost of a direct homogenization approach without significantly compromising on solution accuracy. The method avoids repeated consideration of unit cell equilibrium equations by means of residual-free influence functions computed at the preprocessing stage. The basic idea is that residual-free deformation is expressed in terms of eigendeformation, which is subsequently expressed in terms of state variables. The reduced model is obtained by defining average or nonlocal state variables. It is effective because of two main reasons. First and the principal one is that the quantities of interest are at a macroscopic level, which in turn depend on fine scale averages. Secondly, the averages are anyway needed due to loss of ellipticity of governing equations stated on the fine scale. Adaptivity is employed to control the accuracy of the reduced order model. We presented a heuristic approach to adaptivity, but certainly a more rigorous framework based on error analysis in quantities of interest would be advantageous [51]. Several challenges, however, remain. First is the experimental calibration issue. Should the material properties of the direct homogenization model be calibrated or that of reduced order model? In the present manuscript we have done the latter. The second is with respect to the generality of the proposed approach; how to account for unit cell distortion, the strain rate sensitivity and the multiplicative decomposition of deformation tensor into elastic and inelastic parts? And finally, how is the existing framework can be extended to more than two scales? A 3-scale mathematical homogenized approach with eigenstrains was developed in [44], but the lingering issue of multiple scale model calibration requires further investigation.

# Acknowledgement

The financial supports of National Science Foundation under grants CMS-0310596, 0303902, 0408359, Rolls-Royce contract 0518502, Automotive Composite Consortium contract 606-03-063L, and AFRL/MNAC MNK-BAA-04-0001 contract are gratefully acknowledged.

# References

[1] J. D. Eshelby. The determination of the field of an ellipsoidal inclusion and related problems. *Proc. R. Soc. Lond. A*, 241:376–396, 1957.

[2] Z. Hashin. The elastic moduli of heterogeneous materials. *J. Appl. Mech.*, 29:143–150, 1962.

[3] T. Mori and K. Tanaka. Average stress in the matrix and average elastic energy of materials with misfitting inclusions. *Acta. Metall.*, 21:571–574, 1973.

[4] R. Hill. A self-consistent mechanics of composite materials. *J. Mech. Phys. Solids*, 13:357–372, 1965.

[5] R. M. Christensen and K. H. Lo. Solution for effective shear properties in three phase sphere and cylinder models. *J. Mech. Phys. Solids*, 27:315–330, 1979.

[6] I. Babuska. Homogenization and application. mathematical and computational problems. In B. Hubbard, editor, *Numerical Solution of Partial Differential Equations - III, SYNSPADE*. Academic Press, 1975.

[7] A. Benssousan, J. L. Lions, and G. Papanicolaou. *Asymptotic Analysis for Periodic Structures*. North-Holland, Amsterdam, 1978.

[8] P. M. Suquet. Elements of homogenization for inelastic solid mechanics. In E. Sanchez-Palencia and A. Zaoui, editors, *Homogenization Techniques for Composite Media*. Springer-Verlag, 1987.

[9] E. Sanchez-Palencia. *Non-homogeneous media and vibration theory*, volume 127 of *Lecture notes in physics*. Springer-Verlag, Berlin, 1980.

[10] J. M. Guedes and N. Kikuchi. Preprocessing and postprocessing for materials based on the homogenization method with adaptive finite element methods. *Comput. Meth. Appl. Mech. Engng.*, 83:143–198, 1990.

[11] K. Terada and N. Kikuchi. Nonlinear homogenization method for practical applications. In S. Ghosh and M. Ostoja-Starzewski, editors, *Computational Methods in Micromechanics*, volume AMD-212/MD-62, pages 1–16. ASME, 1995.

[12] M. Jardak and R. Ghanem. Spectral stochastic homogenization of divergence-type pdes. *Comput. Meth. Appl. Mech. Engng.*, 193(6-8):429–447, 2004.

[13] S. Ghosh, K. Lee, and P. Raghavan. A multi-level computational model for multi-scale damage analysis in composite and porous materials. *Int. J. Solids Structures*, 38:2335–2385, 2001.

[14] T. I. Zohdi, J. T. Oden, and G. J. Rodin. Hierachical modeling of heterogeneous bodies. *Comput. Meth. Appl. Mech. Engng.*, 138:273–298, 1996.

[15] M. G. D. Geers, V. Kouznetsova, and W. A. M. Brekelmans. Gradient-enhanced computational homogenization for the micro-macro scale transition. *J. Phys. IV*, 11:145–152, 2001.

[16] F. Feyel and J.-L. Chaboche. Fe2 multiscale approach for modelling the elastoviscoplastic behavior of long fiber sic/ti composite materials. *Comput. Methods Appl. Mech. Engrg.*, 183:309–330, 2000.

[17] E. Giladi and H. B. Keller. Space-time domain decomposition for parabolic problems. *Numerische Mathematik*, 93(2), 2002.

[18] H. Waisman and J. Fish. Space-time multigrid method for molecular dynamics simulations. *Comp. Meth. Appl. Mech. Engng.*, 2006. to appear.

[19] M. Gosz, B. Moran, and J. D. Achenbach. Matrix cracking in transversely loaded fiber composites with compliant interphases. In AMD-150/AD-32, editor, *Damage Mechanics in Composites*. ASME, 1992.

[20] S. Ghosh and S. Moorthy. Elastic-plastic analysis of arbitrary heterogeneous materials with the voronoi cell finite element method. *Comput. Methods Appl. Mech. Engng.*, 121(1-4):373–409, 1995.

[21] J. Aboudi. A continuum theory for fiber-reinforced elastic-viscoplastic composites. *J. Eng. Sci.*, 20(55):605–621, 1982.

[22] G. J. Dvorak. Transformation field analysis of inelastic composite materials. *Proc. R. Soc. Lond. A*, 437:311–327, 1992.

[23] Y. A. Bahei-El-Din, A. M. Rajendran, and M. A. Zikry. A micromechanical model for damage progression in woven composite systems. *Int. J. Solids Structures*, 41:2307–2330, 2004.

[24] H. Moulinec and P. Suquet. A fast numerical method for computing the linear and nonlinear properties of composites. *C. R. Acad. Sc. Paris II*, 318:1417–1423, 1994.

[25] H. Moulinec and P. Suquet. A numerical method for computing the overall response of nonlinear composites with complex microstructure. *Comput. Meth. Appl. Mech. Engng*, 157:69–94, 1998.

[26] L. V. Berlyand and A. G. Kolpakov. Network approximation in the limit of small interparticle distance of the effective properties of a high-contrast random dispersed composite. *Archive for Rational Mechanics and Analysis*, 159:179–227, 2001.

[27] J. Fish, K. L. Shek, and Shephard M. S. Pandheeradi, M. Computational plasticity for composite structures based on mathematical homogenization: Theory and practice. *Comput. Meth. Appl. Mech. Engng.*, 148:53–73, 1997.

[28] Q. Fish, J. Yu and K. L. Shek. Computational damage mechanics for composite materials based on mathematical homogenization. *Int. J. Numer. Meth. Engng.*, 45:1657–1679, 1999.

[29] J. Fish and K. L. Shek. Finite deformation plasticity of composite structures: Computational models and adaptive strategies. *Comput. Meth. Appl. Mech. Engng.*, 172:145–174, 1999.

[30] J. L. Chaboche, S. Kruch, J. F. Maire, and T. Pottier. Towards a micromechanics based inelastic and damage modeling of composites. *Int. J. Plasticity*, 17:411–439, 2001.

[31] J. C. Michel and P. Suquet. Computational analysis of nonlinear composite structures using the nonuniform transformation field analysis. *Comput. Meth. Appl. Mech. Engng*, 193:5477–5502, 2004.

[32] G. J. Dvorak and Y. Benveniste. On transformation strains and uniform fields in multiphase elastic media. *Proc. R. Soc. Lond. A*, 437:291–310, 1992.

[33] N. Laws. On the thermostatics of composite materials. *J. Mech. Phys. Solids*, 21:9–17, 1973.

[34] J. Willis. Variational and related methods for the overall properties of composites. In C. S. Yih, editor, *Advances in Applied Mechanics*, volume 21, pages 1–78. Academic Press, New York, 1981.

[35] G. J. Dvorak. On uniform fields in heterogeneous media. *Proc. R. Soc. Lond. A*, 431:89–110, 1990.

[36] M. Raous, L. Cangemi, and M. Cocu. A consistent model coupling adhesion, friction, and unilateral contact. *Comput. Meth. Appl. Mech. Engng.*, 177:383–399, 1999.

[37] D. Krajcinovic. *Damage Mechanics*, volume 41 of *North Holland Series in Applied Mathematics and Mechanics*. Elsevier Science, 1996.

[38] J. Fish and A. Wagiman. Multiscale finite element method for a locally nonperiodic heterogeneous medium. *Comp. Mech.*, 12:164–180, 1993.

[39] V. Levin. Determination of the thermoelastic constants of composite materials. *Mekh. Tverdogo Tels, Trans. Soviet Acad. Sciences (Mech. of Solids)*, 6:137–145, 1976.

[40] J. Willis. Variational principles and bounds for the overall properties of composites. In J. W. Provan, editor, *Continuum Models of Discrete Systems*, pages 185–215. University Waterloo Press, 1978.

[41] Z. P. Bazant. Instability, ductility, and size effect in strain-softening concrete. *J. Engng. Mech. Div.*, 102:331–344, 1976.

[42] J. C. Simo. Strain softening and dissipation: A unification of approaches. In J. Mazars and Z. P. Bazant, editors, *Cracking and Damage: Strain Localization and Size Effect*, pages 440–461. Elsevier, New York, 1989.

[43] G. Pijaudier-Cabot and Z. P. Bazant. Nonlocal damage theory. *J. Eng. Mech.*, 113:1512–1533, 1987.

[44] J. Fish and Q. Yu. Multiscale damage modelling for composite materials: Theory and computational framework. *Int. J. Numer. Meth. Engng.*, 52:161–191, 2001.

[45] J. C. Simo and J. W. Ju. Strain- and stress-based continuum damage models - i. formulation. *Int. J. Solids Structures*, 23(7):821–840, 1987.

[46] J. T. Oden and E. B. Pires. Nonlocal and nonlinear friction laws and variational principals for contact problems in elasticity. *J. Appl. Mech.*, 50:67–76, 1983.

[47] T. Belytschko, W. K. Liu, and B. Moran. *Nonlinear Finite Elements for Continua and Structures*. John Wiley and Sons, 2003.

[48] J. C. Simo and T. J. R. Hughes. *Computational Inelasticity*. Springer, New York, 1998.

[49] T. J. R. Hughes and J. Winget. Finite rotation effects in numerical integration of rate constitutive equations arising in large-deformation analysis. *Int. J. Numer. Meth. Engng.*, 15:1862–1867, 1980.

[50] J. M. Starbuck, R. G. Boeman, N. Rastogi, C. D. Warren, J. A. Carpenter, and P. S. Sklad. Crash analysis of adhesively bonded structures. In E. J. Wall, R. Sullivan, and J. A. Carpenter, editors, *FY 2004 Progress Report for Automotive Lightweighting Materials*, pages 221–227. US Department of Energy, 2004.

[51] J. T. Oden and K. S. Vemaganti. Estimation of local modeling error and goal-oriented adaptive modeling of heterogeneous materials i. error estimates and adaptive algorithms. *J. Computational Physics*, 164(1):22–47, 2000.